Aqueous-Phase Photochemistry of Organic Acids in the Atmosphere

by

Jéssica Lima Amorim

A thesis submitted in partial fulfillment of the requirements for the degree of

Master of Science

Department of Chemistry

University of Alberta

Abstract

The atmospheric processing of biogenic volatile organic compounds (BVOCs) leading to the formation and evolution of secondary organic aerosols (SOAs) is highly complex, involving "multiphase" chemistry occurring in the gas, particle, and aqueous phases (e.g., cloudwater, fog, aerosol liquid water). Among the many compounds formed upon gas-phase oxidation of BVOCs, the water-soluble fraction of the products can partition to cloudwater or aerosol water and undergo aqueous-phase processing (i.e., chemical reactions). Compared to the gas-phase, the aqueous-phase processing of the water-soluble aerosol components is much less understood; this led to our interest in the fundamental understanding of the chemistry taking place within it. In atmospheric aqueous-phases, the effect of the acid−base chemistry and, by extension, aqueous-phase pH, has been a largely ignored factor.

Chemical reactions are expected to be affected by cloudwater pH, given that the typical pH values vary between 2 and 7 and that atmospheric aqueous phases are becoming less acidic over the past few decades due to reduced emissions of major precursors of acid rain, i.e., of sulfur dioxide (SO_2) and nitrogen oxides (NO_x). The overall objective of this work was to understand the effect of solution pH on the kinetics and mechanisms of organic acids, which undergo acid-dissociation in pH ranges relevant to cloudwater. A fundamental component for the simulation of aqueous-phase reactions occurring in cloud and fog waters is the use of a photoreactor. The wavelength and intensity of UV lights used in the photoreactor were determined carefully by a combination of direct measurement and actinometry. *Cis*-pinonic acid (CPA), a major α-pinene oxidation product, was used as a model compound for the characterization of our photoreactor. Additionally, a kinetic model was developed to assess the OH chemistry within it. The characterized photoreactor was applied for the kinetics investigation of several organic acids under acidic and basic conditions; among which, the water-soluble fraction of α-pinene SOA was targeted. Using a combination of offline and online MS methods, we also investigated the oxidation mechanisms of pinic acid (PA) at pH 2 and pH 8, providing a novel insight into the oxidation products

formed. Among those, major α-pinene SOA tracers, such as norpinic acid and 3-methyl-1,2,3-butanetricarboxylic acid (MBTCA), were identified as primary oxidation products of PA.

Overall, this work represents the first systematic investigation of the effect of cloud and fog water pH on the kinetics and mechanisms of atmospherically relevant organic acids. From the results presented in the chapters of this MSc. thesis, we found that the solution pH did not significantly affect the kinetics of larger organic acids, e.g., PA, CPA, limononic acid with OH radicals, while FA kinetics was largely affected by it. In contrast, the variation in cloud and fog water pH can affect the relative importance of different chemical pathways, as shown in the case of PA. These results contribute to the fundamental understanding of the photochemical processing taking place in atmospheric aqueous phases.

Preface

This thesis is based on manuscripts that have been published in or are in preparation for submission for publication in peer-reviewed journals. Consequently, there may be some overlap in the material that is presented throughout the thesis. All manuscripts included in this thesis were written by Jéssica L. Amorim, with critical comments provided by Ran Zhao. Contributions of any other authors are described below.

Chapter 1: Introduction to Aqueous-phase Organic Chemistry in the Atmosphere

This chapter was written by Jéssica L. Amorim, with critical comments from Ran Zhao.

Chapter 2: Characterization of the Photoreactor Using *cis*-Pinonic Acid as a Model Compound

All experiments in this chapter were performed by Jéssica L. Amorim, with contributions from Chester Lau and Shuang Wu. The characterization of photon flux emitted by the UVB lights in the reactor used for the photo-oxidation experiments was performed by Chester Lau and Shuang Wu, and the kinetic modeling of CPA photochemistry was developed by Shuang Wu, both under the guidance of Ran Zhao. This chapter was written by Jéssica L. Amorim, with critical comments from Ran Zhao.

Chapter 3: pH Dependence of the OH Reactivity of Organic Acids in the Aqueous Phase

All experiments in this chapter were performed by Jéssica L. Amorim, with contributions from Chester Lau on the IC analysis of FA. The flow tube reactor used to generate α-pinene SOA was built by Keifer Klimchuk and Ran Zhao. Pinic acid was synthesized by Florence J. Williams (U of Iowa). The aqueous-phase kinetic box model was originally built by Yuanlong Huang (Caltech) and was modified and adapted to simulate scenarios relevant to our study by Shuang Wu. This chapter was written by Jéssica L. Amorim and Ran Zhao.

Published as: Amorim, J. V.; Wu, S.; Klimchuk, K.; Lau, C.; Williams, F. J.; Huang, Y.; Zhao, R. *Environ. Sci. Technol.* **2020**, *54* (19), 12484–12492.

Chapter 4: Photo-Oxidation of *cis*-Pinic Acid in the Aqueous Phase: A Mechanistic Investigation

All experiments in this chapter were performed by Jéssica L. Amorim, with contributions from Xinyang Guo on the online PILS–ESI–MS measurements. Pinic acid was synthesized by Florence J. Williams (U of Iowa). This chapter was written by Jéssica L. Amorim, with critical comments from Ran Zhao.

Chapter 5: Conclusions and Future Directions

This chapter was written by Jéssica L. Amorim with critical comments from Ran Zhao.

Acknowledgements

First, I would like to thank my supervisor, Dr. Ran Zhao, not only for his contribution to this thesis, but also for his dedicated support and guidance throughout my entire time in his research group. I could not fit in one paragraph the extent to which Ran, in his first year as a supervisor, not only challenged me to sharpen my thinking, but also offered me a safe and supportive environment to deal with my own insecurities as a graduate student. I feel extremely lucky to have been invited to be part of his research team, and to have had such a considerate and encouraging supervisor like him.

I would like to give a special thanks to my supervisory committee members Dr. Xing-Fang Li and Dr. Sarah Styler. In fact, I was fortunate enough to be part of the group of students organizing the first Prairie Environmental Chemistry Colloquium led by Dr. Sarah Styler, Dr. Ran Zhao, and Dr. Tara Kahan. Dr. Styler's leadership and impact on the scientific community is inspiring, and I was honored to have her as such a strong example of the great contributions possible for women in science today. I would also like to thank Dr. Styler, along with Dr. James Harynuk for serving on my final examination committee.

I am particularly grateful for all the assistance given by my research group members, not only during the experiments in which I had to be in two places at the same time, but also during the times I thought I could not persevere. I would like to express my very great appreciation to Tania and Max, especially. You both were always there with a word of encouragement or listening ear. Thank you for reminding me of my strengths every time I felt weak.

I would like to extend my thanks to Bela Reiz and Dr. Randy Whittal from the mass spectrometry facility for all their help during the development and optimization of the LC-MS methods employed in this MSc. thesis. My grateful thanks are also extended to Anna D. Jordan, from the Department of Chemistry, for her constructive editions and recommendations on this thesis.

To my family in Brazil, particularly my parents and brother, thank you for your love, support, and unwavering belief in me throughout these 10 years of academic life. Without you, I would not be the person I am today.

Finally, none of this would be possible without the unconditional love and support from my wife, Morgan. Thank you for all the coffees in the morning, for making me workout to keep my sanity over the past few months, for being my editor and proofreader. But most of all, thank you for being my best friend. I owe you everything.

Contents

Abstract ii
Acknowledgements vi
List of Tables xii
List of Figures xiii
Abbreviations xvi
1. Introduction to Aqueous-phase Organic Chemistry in the Atmosphere 1
1.1 Volatile Organic Compounds in the Atmosphere 1
1.2 Atmospheric Aqueous Phases and Partitioning of Organic Compounds 2
1.2.1 Aqueous Phases in the Atmosphere 2
1.2.2 Partitioning of Organic Compounds to Aqueous Phase 3
1.3 Photochemistry in the Aqueous Phase 4
1.3.1 Direct Photolysis 4
1.3.1.1 Atmospheric Relevant Solar Radiation 5
1.3.1.2 Common Chromophores in Atmospheric Aqueous Phases 6
1.3.1.3 Photolysis Rate of a Compound 7
1.3.2 Indirect Photolysis with a Focus on OH-Oxidation 8
1.3.2.1 Sources of OH Radicals in Atmospheric Aqueous Phases 8
1.3.2.2 Steady-State Concentrations of OH Radical 8
1.3.2.3 OH Reactivity and Reaction Mechanisms 9
1.3.2.4 Unique Radical Chemistry in the Aqueous Phase 10
1.4 Laboratory Approach to Study Aqueous-Phase Chemistry 12
1.4.1 Photoreactors for Bulk Aqueous-Phase Experiments 12
1.4.2 Application of Offline and Online MS Techniques 13
1.5 Summary and Thesis Overview 15
2. Characterization of the Photoreactor Using *cis*-Pinonic Acid as a Model Compound 17
2.1 Introduction 17
2.2 Materials and Methods 19
2.2.1 Chemicals and Materials 19

2.2.2 Experimental Details 19
2.2.2.1 Photochemical Reactor Description 19
2.2.2.2 Determination of UV Flux in the Reactor 20
2.2.2.3 CPA Photo-Oxidation 21
2.2.2.4 Deriving Kinetics Information of CPA Direct Photolysis and OH-Oxidation 21
2.2.2.5 ESI−LC−MS Analysis 22
2.2.3 Kinetic Modeling of CPA Photochemistry 23
2.2.3.1 General Model Description 23
2.2.3.2 Treatment of Direct Photolysis 25
2.2.3.3 Treatment of CPA Products 25
2.2.3.4 Model Scenarios 26
2.3 Results and Discussion 27
2.3.1 Characterization of Wavelength and Flux of UV Light 27
2.3.2 OH Reactivity of CPA 29
2.3.3 Model Simulation for CPA Photochemistry 31
2.4 Summary 33
3. pH Dependence of the OH Reactivity of Organic Acids in the Aqueous Phase[a] 34
3.1 Introduction 34
3.2 Experimental Methods 36
3.2.1 Chemicals and Materials 36
3.2.1.1 Synthesis of Pinic Acid 36
3.2.1.2 Synthesis of Limononic Acid 38
3.2.2 Experimental Apparatus 39
3.2.2.1 SOA Generation and Collection 39
3.2.3 Bulk Photo-Oxidation Experiments 40
3.2.3.1 Aqueous Photoreactor 40
3.2.3.2 Photo-Oxidation Experiments 40
3.2.3.3 Relative Kinetic Method and OH Rate Coefficient Determination 42
3.2.4 Chemical Analysis 43
3.2.4.1 ESI–LC–MS Analysis of PA, CPA, LA and SOA 43

3.2.4.2 IC Analysis of Formic Acid 44
3.2.5 Kinetic Modeling 45
3.2.5.1 Impact of pH 46
3.2.5.2 Potential Impact of Sulfate Radical Formation 46
3.3.1 OH Reactivities of PA, CPA, and LA 47
3.3.2 Model Simulation for CPA Photochemistry 51
3.3.2.1 Impact of pH conditions 52
3.3.2.2 Impact of SO_4^- 52
3.3.3 Comparison between Larger and Smaller OAs 53
3.3.4 OH Reactivities of Other OAs in α-Pinene SOA 55
3.4 Environmental Implications 59
4. Photo-Oxidation of *cis*-Pinic Acid in the Aqueous Phase: A Mechanistic Investigation 61
4.1 Introduction 61
4.2 Experimental Methods 63
4.2.1 Chemicals and Materials 63
4.2.2 PA Aqueous-Phase OH-Oxidation 63
4.2.3 Offline and Online MS Analysis 65
4.2.3.1 Offline LC–MS Analysis of PA 65
4.2.3.2 Online PILS–MS Analysis of PA 65
4.3 Results and Discussion 67
4.3.1 Determination of PA pK_a 67
4.3.2 Offline ESI–LC–MS for Elemental Analysis 68
4.3.3 MS/MS for Further Structural Confirmation 69
4.3.4 Differences Observed at pH 2 and pH 8 72
4.3.5 Online PILS–MS Results 73
4.3.6 Proposed Formation Mechanisms 75
4.4 Summary and Atmospheric Implications 80
5. Conclusions and Future Directions 82
5.1 Photoreactor Characterization using *cis*-Pinonic Acid as a Model Compound 82
5.2 pH Dependence of the OH Reactivity of Organic Acids in the Aqueous Phase 83

5.3 Photo-Oxidation of *cis*-Pinic Acid in the Aqueous Phase: A Mechanistic Investigation..... 84
References..... 87

List of Tables

Table 1. Abbreviations. xvi
Table 2.1 Reactions and Rate Coefficients Used in the CPA Photochemical Model. 23
Table 2.2 Initial Concentrations Used in Model Scenarios. 26
Table 3.1 Experimental Conditions for the Photo-Oxidation Experiments. 42
Table 3.2 Initial Concentrations Used in Model Scenarios. 45
Table 3.3 Calculated Bimolecular Rate Coefficient for OAs Reactions with OH Radicals (k^{II}_{OH} in $\times 10^9\ M^{-1}\ s^{-1}$)..... 50
Table 3.4 Bimolecular Rate Coefficient for α-Pinene SOA WSOC's Reactions with OH Radicals (k^{II}_{OH} in $M^{-1}\ s^{-1}$). 57
Table 4.1 Experimental Parameters Used for Offline and Online LC–MS. 64
Table 4.2 Online ESI–LC–MS Instrument's Parameters for the Analysis of PA OH-Oxidation..... 66
Table 4.3 List of Major PA OH-oxidation Peaks Detected by (-)ESI–LC–MS Under pH 2 and pH 8. 69
Table 4.4 Commonly Observed Loss of Small Fragments in (-)ESI spectra of PA OH-oxidation Products. 70

List of Figures

Figure 1.1. Possible electronic transitions of σ, π, and n electrons.[32] 6
Figure 1.2. Molecular structure of PA and CPA. 7
Figure 1.3. Range of steady-state concentration of OH radicals and O_3 in sunlit surface waters (sw), sunlit cloudwater (cw), drinking-water treatment (dw), and the troposphere (trop(g)). Adapted from Gschwend et al.[29] 9
Figure 2.1. The top view (left) and front view (right) of the photoreactor used in the aqueous-phase photo-oxidation experiments. 20
Figure 2.2. Raw spectral data recorded by the spectroradiometer for the UVB lamps (red) and background lighting in the room (black). 27
Figure 2.3. 2-NB photodecay rate constant calculation. 28
Figure 2.4. Finalized photon flux in the photoreactor. 28
Figure 2.5. Experimental calculation of the first-order rate constant for CPA photodecay. 29
Figure 2.6. OH-oxidation and control experiment for CPA. The signal of CPA is shown as a function of irradiation time and the shaded area presents 1σ from triplicates. 30
Figure 2.7. a) SIM chromatogram of CPA (*m*/*z* 183) and pimelic acid (reference compound, *m*/*z* 159) under 10 min of UVB irradiation. 30
Figure 2.8. Measured OH reaction relative data for aqueous oxidation of CPA. ... 31
Figure 2.9. Simulated and observed CPA concentration in a) direct photolysis, b) OH-oxidation at pH 4.85. The shaded area presents observed data standard deviation range (1 σ). The model result in a) employs the optimized CPA φ(λ) value: 0.69 across the relevant wavelength range. 32
Figure 3.1. Synthesis of PA.[27] 37
Figure 3.2. ^{1}H NMR spectrum of PA in $CDCl_3$. 37
Figure 3.3. ^{13}C NMR spectrum of PA in $CDCl_3$. 37
Figure 3.4. Synthesis of LA. 38

Figure 3.5. (-)ESI–LC–MS selected ion monitoring (SIM) chromatogram of *m/z* 183 (corresponding to both CPA and LA) under direct photolysis. Color coding indicates irradiation time. 38
Figure 3.6. Experimental apparatus to generate and collect SOA. 39
Figure 3.7. Structures of target individual OAs and reference compounds employed in the relative kinetic method. 41
Figure 3.8. SIM chromatogram of PA (*m/z* 185) and pimelic acid (reference compound, *m/z* 159). 47
Figure 3.9. SIM chromatogram of CPA (*m/z* 183) and pimelic acid (reference compound, *m/z* 159) under 10 min of UVB irradiation. 48
Figure 3.10. SIM chromatogram of LA (*m/z* 183) and caffeine (reference compound, *m/z* 195) under 10 min of UVB irradiation. LA peak is the one most retained (longer retention time) in the chromatogram. 48
Figure 3.11. OH-oxidation and control experiments for a) PA, b) CPA and c) LA at pH 2. Signal of the target compound is shown as a function of irradiation time. The shaded area presents 1 σ from triplicates. 49
Figure 3.12. Simulated and observed CPA concentration in a) direct photolysis, b) OH-oxidation at pH 2, c) OH-oxidation at pH 4, and d) OH-oxidation at pH 10. The shaded area presents the observed data standard deviation range (1 σ). The model result in a) employs the optimized CPA Φ(λ) value: 0.69 across the relevant wavelength rage. 51
Figure 3.13. OH concentrations simulated at pH 2, 4, and 10. 52
Figure 3.14. The simulated a) [OH] and b) CPA concentration with and without the SO_4^- chemistry included in the model. 53
Figure 3.15. OH reactivities of CPA, PA, LA, and FA at pH 2, uncontrolled pH conditions and pH 10. Experiments of FA were conducted at pH 2 and 10 only... 54
Figure 3.16. a) SIM chromatogram of α-pinene SOA at uncontrolled pH conditions (with multiple *m/z* monitored) and b) OAs decay during an OH-oxidation experiment. Color coding on the left panel indicates irradiation time. 56
Figure 3.17. OH reactivities of α-pinene SOA OAs at uncontrolled pH, pH 2 and 10. 57

Figure 4.1. Structure of (a) neutral PA and (b) pinate anion (PAn). 67
Figure 4.2. Titration curve of 5.0 mM PA using a 5.0 mM NaOH titrant. The horizontal axis presents the volume of titrant added (V_{NaOH}). 67
Figure 4.3. BPC for the sample taken from the reaction at t = 0 and 5 min. 68
Figure 4.4. Fragmentation spectra of PA OH-oxidation products under uncontrolled pH conditions. 70
Figure 4.5. EIC for PA at t = 0 min, t = 5 min, and t = 15 min under acidic and basic conditions. 72
Figure 4.6. EIC for peaks of *m/z* 155 and 171 at 5 min (reaction time) detected with offline (-)ESI–LC–MS. The EIC for peaks of *m/z* 187 and 203 were obtained at 15 min reaction time. The shaded area presents 1 σ from the calculated triplicate error propagation. 72
Figure 4.7. Online PA OH-oxidation reaction monitoring and product formation evolution. 74
Figure 4.8. PILS–MS temporal oxidation of PA and formation of products of MW 156 (*m/z* 155), MW 172 (*m/z* 171), MW 188 (*m/z* 187), and MW 204 (*m/z* 203).. 74
Figure 4.9. Proposed mechanism of the *m/z* 155 product formation from PA OH-oxidation at pH 2. Similarly, at pH 8, the H-abstraction occurs at C-1 and C-2 atm of the PAn anion. 75
Figure 4.10. Proposed mechanism of the *m/z* 171 product formation from PA OH-oxidation at pH 2. 76
Figure 4.11. Proposed mechanism of the MW 188 product formation from PA OH-oxidation at pH 2, followed by reactions leading to the formation of MBTCA (MW 204). 77
Figure 4.12. Proposed formation mechanism of MBTCA under pH 8 conditions. The reaction is initiated by an electron-transfer reaction on the carboxylate A. The highlighted compound represents the PA alkyl radical formed only in the aqueous phase. 78
Figure 4.13. Proposed formation mechanism at pH 8. Electron-transfer reaction taking place on the carboxylate B. 80

Abbreviations

Table 1. Abbreviations.

Abbreviation	Explanation
2-NB	2-nitrobenzadehyde
ALW	Aerosol liquid water
AMS	Aerosol mass spectrometry
API	Atmospheric pressure ionization
aqSOA	Aqueous secondary organic aerosol
au	Atomic unit
BPC	Base peak chromatogram
BVOC	Biogenic volatile organic compound
CAF	Caffeine
CCN	Cloud condensation nuclei
CID	Collision-induced dissociation
CIMS	Chemical ionization mass spectrometry
CPA	*Cis*-pinonic acid
Cps	Counts per second
CSTRs	Continuously stirred tank reactors
DI	Deionized
EIC	Extracted ion chromatogram
ESI	Electrospray ionization
FA	Formic acid
K_H	Henry's law constant
HO_2	Hydroperoxy radical
HPLC	High performance liquid chromatography
IC	Ion chromatography
k_{OH}^{II}	Second-order rate coefficients with OH radical
LA	Limononic acid
LC	Liquid chromatography
LWC	Liquid water content
lpm	Liter per minute
m/z	Mass-to-charge ratio
MBTCA	3-Methyl-1,2,3-butanetricarboxylic acid

MS	Mass spectrometry
MW	Molecular weight
MW	Molecular weight
NMR	Nuclear magnetic resonance
NPA	Norpinic acid
OA	Organic acid
OH	OH radicals
OH	Hydroxyl radical
PA	Pinic acid
PAn	Pinate anion
PILS	Particle-into-liquid sampler
hv	Photon
p*K*a	Acid dissociation constant
PMA	Pimelic acid
ppm	Parts-per-million
PTFE	Polytetrafluoroethylene
R^2	Coefficient of determination
RH	Relative humidity
RO	Alkoxy radical
RO_2	Peroxy radical
SIM	Selected (or Single) ion monitoring
SOA	Secondary organic aerosol
ToF	Time-of-flight
t_R	Retention time
UV	Ultra-violet
VOC	Volatile organic compounds
WSOCs	Water-soluble organic compounds

Chapter 1

Introduction to Aqueous-phase Organic Chemistry in the Atmosphere

1.1 Volatile Organic Compounds in the Atmosphere

Volatile organic compounds (VOCs) are a large group of non-methane organic compounds having a vapor pressure >10 Pa at 20 °C.[1] VOCs emitted to the atmosphere arise from both anthropogenic and biogenic sources (both marine and terrestrial). The anthropogenic fraction is related to human activities, i.e., from fossil fuel combustion and various industrial processes. In terms of biogenic volatile organic compounds (BVOCs) emission, isoprene (2-methyl-1,3-butadiene, C_5H_8) and terpenoid compounds are the most important group, with estimated annual emissions of 400–600 TgC.[2] Terpenes represent another important BVOC source, among which, monoterpenes (C_{10} compounds) such as α-pinene, β-pinene, limonene, among others, account for the second highest BVOCs emission (127 TgC y^{-1}).[3]

In the presence of atmospheric oxidants, such as ozone (O_3), nitrate (NO_3), and hydroxyl radicals (OH), BVOCs are oxidized quickly, forming oxygenated compounds with a variety of functional groups and degrees of oxidation.[4,5] The oxidation products formed exhibit a lower vapor pressure, which favors their partitioning between the gas and condensed organic phases, leading to the formation of secondary organic aerosols (SOAs).[6] The gas-particle partitioning is assumed to be an equilibrium process, based solely on the saturation vapor pressures of the chemical species and their concentration in both phases.[7] In this case, the contributions of the aqueous phase and inorganic components to the formation of SOA are neglected. Many laboratory studies and field measurements have shown that models employing only the classic SOA formation mechanism significantly underpredict the extent of SOA formation.[8,9]

An alternative formation pathway of SOA, which has been the focus of many studies, involves the aqueous-phase processing of organic compounds.[8,10–13] The ability of a BVOC to form aqueous SOA (aqSOA) depends on the water solubility, chemical reactivity, and the chemical properties of the oxidation products arising from the parent

BVOC.[14] A variety of functionalized and hydrophilic oxidation products, including carbonyl, hydroperoxides, and carboxylic acids, can partition to cloudwater or aerosol liquid water (ALW) and undergo further chemical reactions. Upon water evaporation, these compounds ultimately remain in the particles and contribute to the formation of aqSOA.

1.2 Atmospheric Aqueous Phases and Partitioning of Organic Compounds

Water is the main condensed-phase component of the atmosphere and an important reaction medium for the processing of aqSOA precursors.[15–18] The condensed aqueous phases in the atmosphere can be present in a few different forms, providing dramatically different chemical environments. As water-soluble organic compounds (WSOCs) partition from the gas phase to cloud and fog droplets, they are subject to reactions unique to aqueous phases,[19,20] which will be discussed further in this chapter.

1.2.1 Aqueous Phases in the Atmosphere

Atmospheric liquid water exists in many forms, such as cloud droplets, fog, rain, and ALW; among these, cloudwater has been considered as an important reaction medium for the processing of organic compounds, leading to aqSOA. Ervens et al.[5] showed that aqSOA formation is enhanced in high-humidity environments.[5,19,21,22] Relative humidity (RH), among other factors (chemical composition, particle size distribution), is an important factor correlated to the water uptake and hygroscopic growth of aerosol particles prior to aqSOA formation.[5] In terms of hygroscopic growth conditions, RH is divided mainly into two regimes: (1) undersaturated (RH < 100%) and (2) supersaturated (RH > 100%).[7] Under RH < 100%, the water uptake can lead to an increase in the diameter of a particle up to a maximum factor of 3,[3] resulting in a liquid water content (LWC) up to 10^{-6} g m^{-3}.[14] At RH > 100%, ultrafine particles will continue to uptake water and grow until they reach 50–100 nm on average.[23,24] These aerosol particles can serve as cloud condensation nuclei (CCN), leading to the formation of cloud droplets – process commonly termed as “activation”.[3,25] As particles are activated

into a cloud or fog droplets with relatively high LWC, the WSOC present within it will be diluted accordingly. For instance, methylglyoxal, a common α-dicarbonyl oxidation product of multiple VOC precursors, has been detected in ALW at concentrations varying from 0.7 to 7 mM,[26,27] while in cloudwater samples this compound has been found at a concentration of 19.1 μM.[28] This distinct variation in methylglyoxal concentration and many other WSOCs[28] can be attributed mainly to differences in droplet sizes, LWC, salinity, and surface area to volume ratio.[5,19,29]

1.2.2 Partitioning of Organic Compounds to Aqueous Phase

An organic compound must be water-soluble to be present in atmospheric aqueous phases. As VOCs are oxidized repeatedly in the gas phase, their products become increasingly oxygenated, less volatile, and more water-soluble, which all result in more affinity for aqueous droplets.[7] The partitioning of gas-phase aqSOA precursors to ALW and cloud droplets depends highly on the bulk water-solubility of these organic compounds. The bulk solubility usually is described in terms of Henry's law constant, K_H.[30,31] Henry's law is strictly only applicable to dilute (ideal) solutions,[32] and represents the ratio of the WSOCs concentration in the aqueous and gas phase, defined as aqueous concentration (C_w) per unit gaseous partial pressure (P_{gas}) (M atm^{-1}), as shown in Eq. (1.1):

$$K_H = \frac{C_w}{P_{gas}} \qquad \text{Eq. (1.1)}$$

Due to the dilute solute concentrations (Section 1.2.1), cloud and fog droplets generally are considered ideal solutions. Partitioning of organic compounds to ALW is highly uncertain, as chemicals are concentrated, and the solution is no longer considered ideal.

Partitioning of WSOCs can also be affected by subsequent aqueous-phase reactions of a certain compound. These reactions give rise to seemingly large water solubilities, which can be described by an effective Henry's law constant (K_H*).[31] Glyoxal and other small dicarbonyls have been of particular interest to atmospheric chemists due to their ability to undergo hydration, establishing a reversible equilibrium with its geminal diol form, as shown in R1.1.[31,33] Glyoxal and other carbonyls, such as

methylglyoxal and glycolaldehyde, can undergo rapid hydration and partition to cloudwater due to their large K_H*.[25] This reaction pathway is unique to the aqueous phase where the formation of geminal diol is favorable.[33,34]

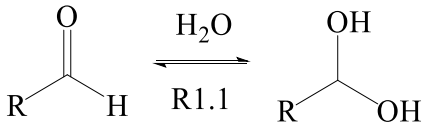

Differently from aldehydes, carboxylic acids undergo acid dissociation in cloudwater, enhancing their partitioning to the aqueous phase. The unique chemistry of carboxylic acids in aqueous phases will be discussed in Section 1.3.2.4. The cloudwater processing of aldehydes and organic acids is not considered in the classic SOA formation mechanism, which depends solely on the vapor pressure of organic compounds. Therefore, the aqueous-phase reactions of these compounds are of great atmospheric importance but often are not studied systematically.

1.3 Photochemistry in the Aqueous Phase

Reactions taking place in fog and cloudwater are extremely important because they significantly influence the lifetime of many atmospheric aerosols and yield intermediates that often play a key role in atmospheric chemistry.[7,15,35–37] The aqueous-phase processing of highly volatile species such as glyoxal, methylglyoxal, glycolaldehyde, for example, leads to the formation aqSOA.[36] Photochemistry is the most important type of chemistry in the sunlit atmosphere. Reactions initiated by photons give rise to oxidation of VOCs at faster rates than non-photochemical reactions. The importance of oxidation products has been discussed in previous sections. Photochemical reactions can be categorized into direct photolysis of photoactive compounds and processes initiated by reactive species (OH and NO_3 radicals, and ozone), usually referred to as indirect photolysis.[38]

1.3.1 Direct Photolysis

Direct photolysis refers to a process in which photochemically active molecules undergo chemical transformations induced only by light radiation. Under electromagnetic radiation of relevant wavelength, an electron can absorb energy and

shift from a molecular orbital of lower energy to an orbital of higher energy. Part of the energy absorbed by a molecule is lost due to vibrational relaxation, and the rest can induce the breaking of a chemical bond, i.e., photolysis.[38] The rate at which photolysis occurs depends on several factors that will be presented in the following sections.

1.3.1.1 Atmospheric Relevant Solar Radiation

In the atmosphere, solar radiation is the light source inducing the direct photolysis of molecules. Sunlight is composed of radiation wavelengths in the ultraviolet (100–400 nm), visible (400–700 nm), and infrared (700–1000 nm) portions of the spectrum. The UV-region is, for practical purposes, divided into three regions: UVC (100–280 nm), UVB (280–315 nm), and UVA (315–400 nm).[14]

In terms of environmentally relevant light conditions, UV-radiation with wavelengths between 100 and 200 nm (UVC) is absorbed by oxygen far out in the atmosphere.[38] This range of wavelength also is referred to as the vacuum-UV since radiation in this region is absorbed very easily and can be studied only in a vacuum. The remainder of UVC (200–280 nm) is absorbed by the ozone layer in the stratosphere.[38] Only a fraction of UVB (>290 nm) and UVA can penetrate the stratosphere and induce photochemistry of interest to this MSc. thesis. Thus, compounds that can absorb light of wavelength >290 nm undergo direct photolysis under ambient conditions.

The fundamental concepts governing any absorption can be described by Beer-Lambert's law:

$$I_x = I_0 e^{\alpha x} \qquad \text{Eq. (1.2)}$$

where I_0 is the intensity when the radiation hits the absorbing compound (i.e., when $x = 0$), I_x is the intensity at depth x, and α is a constant called the absorption coefficient.[39] The light absorption by an atom or molecule depends on the wavelength of radiation and the constant, α, which is given as the absorption per unit length. The absorption coefficient is related to the ability of a molecule to absorb a photon of a particular wavelength and polarization, i.e., its absorption cross-sectional area (σ).[40] As will be discussed in Section 1.3.1.3, σ is essential to determine the photolysis rate of organic molecules.

1.3.1.2 Common Chromophores in Atmospheric Aqueous Phases

The absorption of UV and visible light by organic molecules is restricted to certain functional groups (chromophores) containing valence electrons that can be excited readily by photons. The molecular absorption of organic compounds will vary with the structures within the molecule, thus leading to electronic transitions involving σ, π, and n electrons.[40] Those with strongly absorbing chromophores exhibit large molecular absorption cross-section values across the range of wavelengths that the chromophores absorb. Among the organic compounds present in fog and cloudwater, aldehydes and ketones are considered important chromophores. Under irradiation by atmospherically relevant light, these compounds can absorb UV radiation and undergo transitions of n or π electrons to the π^* excited state,[41] as shown in Figure 1.1.

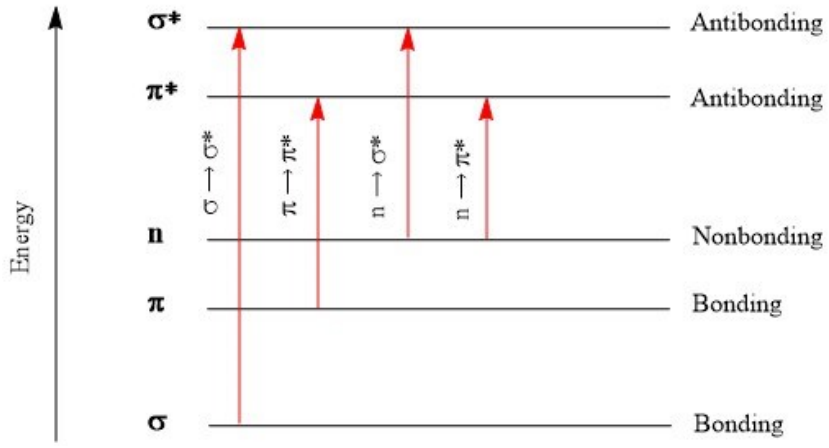

Figure 1.1. Possible electronic transitions of σ, π, and n electrons.[40]

In addition to carbonyl groups, the presence of a heteroatom, e.g., nitrogen, provides the n electrons needed for the n → π* transition upon irradiation, whereas the presence of conjugated systems favors the π → π* transitions.[40,42] Although carboxylic acids have a carbonyl group and can absorb radiation, the extent of n → π* transition is much smaller than for aldehydes and ketones, thus it is not considered a good chromophore.[3] *Cis*-pinonic acid (CPA) and pinic acid (PA) are two major carboxylic acid products of the gas-phase oxidation of α-pinene.[35,43,44] CPA has a carbonyl and carboxyl functional group, while PA has two carboxyl groups, as shown in Figure 1.2.

For CPA, the presence of a cyclobutyl ring next to the carbonyl group enhances the absorbance of UVB radiation, thus the n → π* transition, which has the highest σ value at 280 nm.[36,37] The carboxyl groups of CPA and PA are not expected to be photolyzed,[3] therefore, PA does not undergo direct photolysis upon UVB radiation, which affects its atmospheric lifetime and environmental fate, as will be seen in Chapter 3.[45]

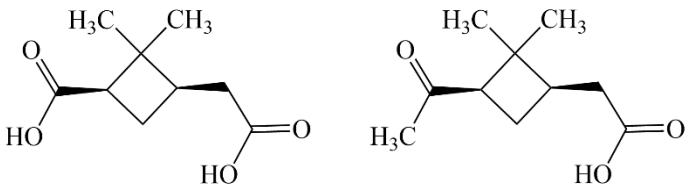

Pinic Acid (PA)
$C_9H_{14}O_4$

cis-Pinonic Acid (CPA)
$C_{10}H_{16}O_3$

Figure 1.2. Molecular structure of PA and CPA.

1.3.1.3 Photolysis Rate of a Compound

Several factors control the direct photolysis rate of organic compounds in atmospheric aqueous phases: (1) the number of photons at each wavelength reaching the molecule, i.e., the photon flux, $I(\lambda)$; (2) how efficiently the molecule absorbs photons with various wavelengths, i.e., its molecular absorption cross-section, $\sigma(\lambda)$; and (3) the chance of the excited molecule to undergo a chemical transformation, i.e., its quantum yield, $\phi(\lambda)$.[38] The first-order direct photolysis rate coefficient (k_p^I, s^{-1}) is, therefore, given by the product of all these three factors, integrated over the relevant wavelength range (Eq. (1.3))[14]:

$$k_p^I = \int_\lambda I(\lambda)\sigma(\lambda)\phi(\lambda)d\lambda \qquad \text{Eq. (1.3)}$$

The $I(\lambda)$ and $\sigma(\lambda)$ terms determine how likely a species, *i*, will reach its excited state, *i**. The actual $I(\lambda)$ available in the environment depends on the zenith angle, which is a function of time, season, latitude, etc. The $\sigma(\lambda)$ is molecule-dependent. As discussed in Section 1.3.1.2, molecules with chromophores exhibit large $\sigma(\lambda)$ in the atmospherically relevant wavelength range. The quantum yield indicates the probability that *i** undergoes chemical transformation instead of relaxation to *i*. Several photolytic mechanisms are viable for *i**, such as (1) aromatic substitution reactions, (2) dehydration and/or isomerization reactions, and (3) carbonyl photolysis, which

proceeds via two pathways: bond cleavage (Norrish Type I) and intramolecular hydrogen transfer (Norrish Type II). The closer $\phi(\lambda)$ is to 1, the more efficiently *i* is photolyzed.[38]

1.3.2 Indirect Photolysis with a Focus on OH-Oxidation

The photo-oxidation of numerous organic compounds in the atmosphere is controlled mainly by the presence of highly reactive free radicals generated through photochemistry.[23,24] Among these oxidant species, the OH radical is considered by far the most important one in the aqueous phase due to its high reactivity.

1.3.2.1 Sources of OH Radicals in Atmospheric Aqueous Phases

Several sources of OH radicals in cloud and fog droplets have been discussed extensively in the literature.[46] OH radicals are formed by photochemical processes in both gas and aqueous phases. The partition of OH radicals from the gas phase photolysis of O_3 is a process that was thought to be the dominant source of OH radicals in cloudwater. Arakaki and Faust[47] and Ervens et al.[48] have shown, on the other hand, that Fenton chemistry is the most important *in-situ* formation mechanism of OH radicals in both cloudwater and ALW. Fenton chemistry is described as iron-catalyzed reactions that convert H_2O_2 into OH radicals. In addition to Fenton chemistry, the direct photolysis of H_2O_2, NO_3^-, and NO_2^- have been investigated extensively and shown to contribute significantly to the aqueous-phase formation of OH radicals.[49–51]

1.3.2.2 Steady-State Concentrations of OH Radical

The OH radical concentration in cloudwater is dictated by the relative strengths of the sources and the sink of the OH radical. Highly variable concentrations of OH radicals have been observed, depending on the air mass origin, season, and location of the sample site.[46,52] In general, OH radicals are highly reactive and, consequently, short-lived. From Figure 1.3, the steady-state concentration of OH radicals in sunlit cloudwater (cw) ranges between 10^{-14} to 10^{-15} M, whereas ozone is present at concentrations of 10^{-9} to 10^{-11} M.[38] Although O_3 in cloudwater is present at higher concentrations, OH radicals have a larger oxidation potential than O_3 and are stronger

photo-oxidants. In addition, OH radicals can oxidize essentially any types of organic compounds and thus dominate the photochemistry within atmospheric aqueous phases.

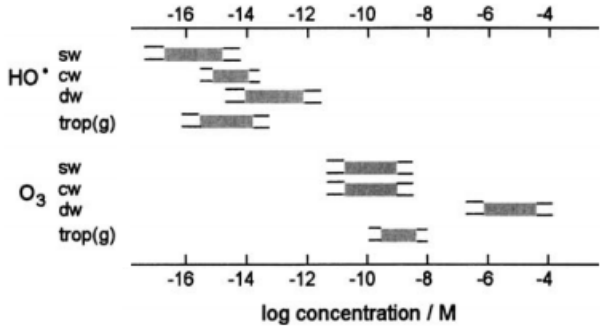

Figure 1.3. Range of steady-state concentration of OH radicals and O_3 in sunlit surface waters (sw), sunlit cloudwater (cw), drinking-water treatment (dw), and the troposphere (trop(g)). Adapted from Gschwend et al.[38]

1.3.2.3 OH Reactivity and Reaction Mechanisms

Organic compounds relevant to the atmospheric aqueous phases usually contain highly oxygenated functional groups and react rapidly with OH radicals by two main pathways: OH addition and H-abstraction. Reactions of OH radicals with aromatic and unsaturated compounds occur via OH addition (R1.2 and R1.3), while the reaction with saturated organic compounds proceeds via H-abstraction (R1.4).

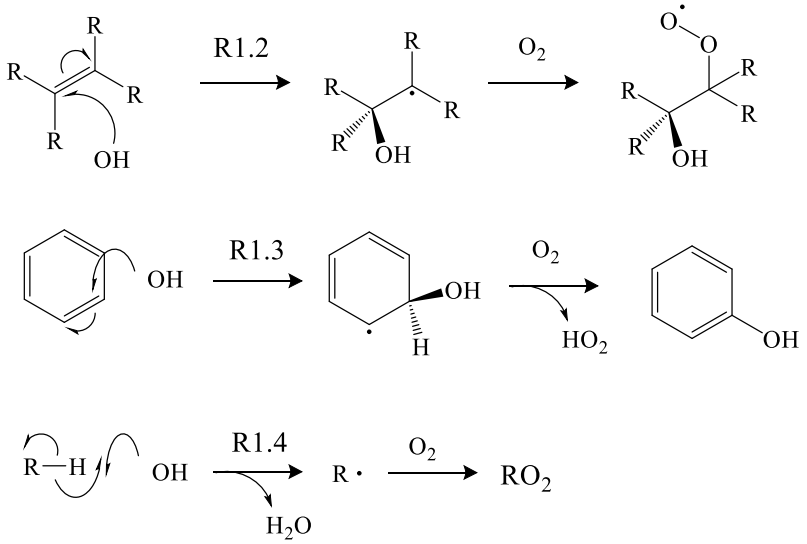

The OH radical addition to aromatic and unsaturated aliphatic compounds is diffusion-controlled, and a compilation of rate constants has been published by Buxton et al.[53] Specifically, in the case of the aqueous-phase chemistry of α-pinene SOA,

aromatic functionalities are absent, and double bonds already have been reacted away by the gas-phase chemistry. Gschwend et al.[38] have shown that OH-addition reactions proceed faster than H-abstraction at atmospherically relevant temperatures due to the formation of more stable intermediates.Therefore, H-abstraction often dominates the aqueous-phase reaction mechanisms.

1.3.2.4 Unique Radical Chemistry in the Aqueous Phase

The mechanisms in R1.2–R1.4 are universal to both gas and aqueous phases.[33] In terms of mechanisms unique to atmospheric aqueous environments, the conversion of aldehydes to carboxylic acids and electron-transfer reactions can be important. As mentioned in Section 1.2.2, the hydration of aldehydes will lead to their geminal diol forms (R1.1). Both the aldehyde and geminal diol will react with OH radicals via H-abstraction and form alkyl radicals, which also exists in hydration equilibrium (R1.5). The alkyl radicals react with oxygen leading to the formation of peroxy radicals, RO_2 (R1.6). These reactive peroxy radicals will hydrate further (R1.7), dissociate (R1.8), or react with RO_2 or hydroperoxy radical (HO_2) species to form carboxylic acids (R1.9). This carboxylic acid formation mechanism is unique to the aqueous phase because gas-phase aldehydes do not undergo geminal-diol formation.

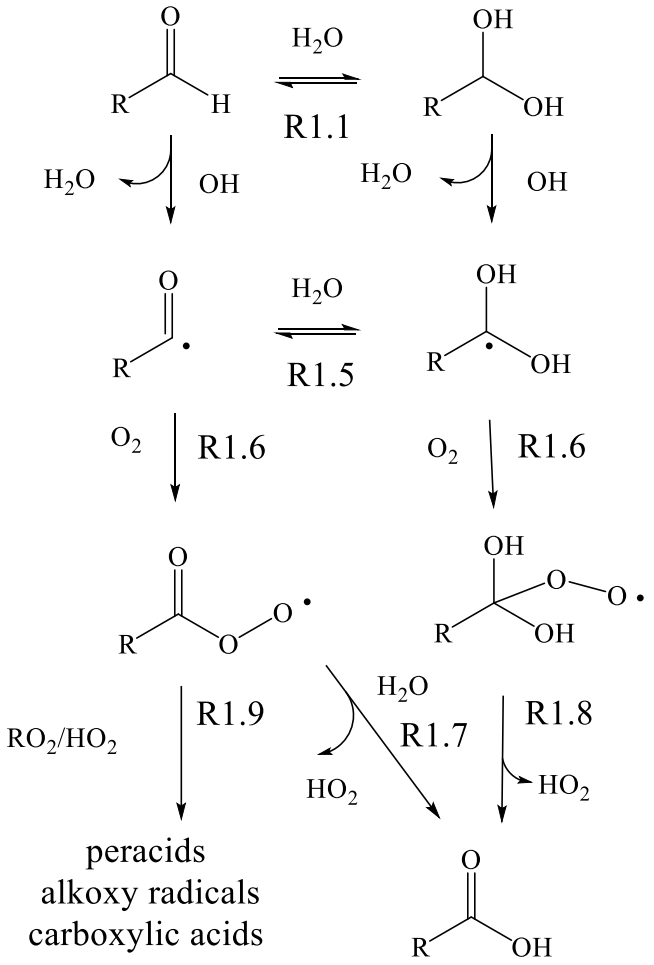

In atmospheric aqueous-phases, acid–base chemistry plays an important role in the reactivity of carboxylic acids. As the pH of cloudwater varies between 2 and 7,[54,55] organic acids can exist in both protonated and dissociated forms. Therefore, in addition to H-abstraction, electron-transfer reactions between OH radicals and the carboxylate form (R1.10) represent an additional pathway for this class of compounds.

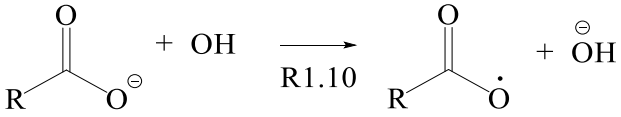

The presence of neighboring electron-withdrawing groups, such as carboxylic groups, decreases the rate of H-abstraction by the OH radicals, thus favoring the carboxylate electron-transfer reaction. Ervens et al.[20] have shown that the OH-oxidation of a series of small carboxylate species (C_1 to C_4) is faster than the non-dissociated carboxylic acids; this results in a pH dependence in the reactivity of organic acids. The carboxylic acid–carboxylate equilibrium of organic acids is highly sensitive

to the pH of cloud and fog waters. Over the past 30 years, the average pH of fog and cloudwater in Europe and the US has increased by one unit.[55] Thus, from the Ervens et al. study, this will lead to even longer lifetimes for a series of carboxylic acids present in atmospheric waters. This trend, however, has not been explored for long-chain organic acids; this led to work presented in Chapter 3.

1.4 Laboratory Approach to Study Aqueous-Phase Chemistry

Laboratory studies mainly focus on the fundamental understanding of the chemistry of key organic compounds in both gas and aqueous phases.[50] By combining the application of photoreactors and analytical techniques, one can simulate relevant atmospheric conditions for aqueous-phase reactions and obtain reliable kinetic and mechanistic information needed in cloudwater atmospheric models. Different approaches can be used to understand the chemistry of aqSOA precursors, which will be further explored in this section.

1.4.1 Photoreactors for Bulk Aqueous-Phase Experiments

The use of photoreactors is a common and practical approach for the investigation of aqueous-phase photochemistry in the laboratory. Although they can be different in design, size, and functions, the overall objective is to simulate chemical reactions relevant to the atmosphere. In particular, there are a few parameters in a photoreactor one has to consider when planning the experiment, i.e., radiation (light wavelengths), temperature, reactor volume, and material.[56]

As mentioned in Section 1.3.1.1, the UV lamps in the photoreactor serve as the initiator for photochemical reactions. The choice of UV lamps is determined by the purpose of the photo-oxidation experiment. Kahan et al.[56–58] used a xenon arc lamp to reproduce the solar photon flux reaching the earth in the wavelength region 290-700 nm^3 and investigated the photolysis rate of an array of polycyclic aromatic compounds at air-ice interfaces. Schmidt et al.[57] custom-built a photoreactor in which xenon arc lamps also were used to provide sufficient energy to induce the mineral-

mediated photochemical formation of organic sulfur compounds in aqueous aerosols. For studies focusing on the direct photolysis and OH-oxidation, lamps with shorter wavelengths typically are employed in order to use atmospherically relevant illumination profiles and to photolyze the OH radical precursor, respectively.[45,58] UVC lamps of monochromatic light at 254 nm and UVB at 310 nm, are used to induce the photolysis of H_2O_2 and generate OH radicals, as described in Section 1.3.2.1. It has been applied for the reaction kinetics and product analysis of important aqSOA precursors, such as glyoxal, isoprene, PA, CPA, among others.[18,45,59] The type of light source chosen to perform the photo-oxidation experiments will have implications on the overall OH radicals production and concentration, thus affecting the kinetics of the compounds investigated. In addition to the type of UV light, other adjustable parameters, such as temperature, will reflect mainly on the reaction kinetics. The reactor volume and vessel material will determine the minimum amount of sample required and influence the light intensity profile and reflection properties, directly affecting the extent of photolysis.[57] Therefore, photoreactors can be modified or adapted to the conditions necessary to reproduce the range of reactions in atmospheric aqueous phases.

1.4.2 Application of Offline and Online MS Techniques

Reactions in the photoreactor can be monitored using either offline or online methods. Mass spectrometry (MS) is by far the most employed analytical technique in atmospheric chemistry due to its sensitivity and the ability to reveal the molecular mass. In offline methods, samples are collected manually from the photoreactor and then analyzed, which permits the identification and quantification of compounds before and after aqueous-phase processing. Online measurement techniques allow direct and continuous reaction monitoring and chemical characterization. Thus, it is useful for monitoring the evolution of reactions with relatively fast changes in concentrations, species formations, and decomposition.

LC–MS is a method capable of structural identification of analytes found in complex mixtures.[60] Exact mass and elemental composition of analytes can be deduced by employing soft ionization techniques, such as electrospray ionization (ESI), and

high resolution mass analyzers, such as time-of-flight (ToF) MS.[61] In negative ion mode ESI, analyte molecules typically are detected in their deprotonated form ($[M–H]^-$).[61] Therefore, negative mode ionization in ESI enables chemical characterization of molecules that readily form and stabilize a negative charge, which adds an additional selectivity towards carboxylic acids.

LC–MS is used widely in studies of atmospheric aqueous-phase reactions. Witkowski et al.[12,13,62] used an offline ESI−LC−MS/MS (quadrupole tandem mass spectrometry) approach to determine the aqueous-phase kinetics and mechanism of *cis*-pinonic[12] acid and limononic acid oxidation by OH radicals.[13,61] Hamilton et al.[63] applied the LC−MS technique for the analysis of polar compounds and oligomers in SOAs. Zhao et al.[64] identified organic peroxides present in extracted SOA components of α-pinene SOA by developing a novel technique based on LC–ESI–MS. In all these aqueous-phase studies, samples were collected either from the photoreactor or collected and extracted from a filter before injection to the LC−MS system. In contrast, Turpin and co-workers applied online ESI–MS methods to monitor the aqueous-phase oxidation of relevant atmospheric organic compounds, i.e., glycolaldehyde,[65] glyoxal,[66] methylglyoxal,[27] and acetic acid,[67] by pumping samples directly from the photoreactor to the ESI–MS instrument.

Many advanced online MS techniques used by atmospheric chemists, including chemical ionization mass spectrometry (CIMS) and aerosol mass spectrometry (AMS), are specialized for samples in the forms of gas and suspended aerosol. Applying these online MS methods to aqueous samples requires the assistance of an atomizer, which breaks aqueous solutions into small droplets with compressed air. Zhao et al.[68] applied atomization and CIMS to investigate aqueous-phase oxidation of small carbonyl compounds. Atomization and AMS have been used to investigate the aqueous SOA formation from phenolic carbonyl compounds[69] and biomass burning emissions,[70] among other sources. There is still much room for method development using atomization and online MS. A novel method, based on atomization and a particle-into-liquid sampler (PILS), will be introduced in Chapter 4 of this thesis.

In summary, an array of offline and online analytical methods is available to improve our fundamental understanding of the kinetics and mechanism of organic

compounds in atmospheric aqueous phases. The use of a specific method or a combination of methods will depend mostly on the type of information needed and the instrument's limitations.

1.5 Summary and Thesis Overview

Aqueous-phase chemistry has been an emerging focus of fundamental laboratory studies in the field of atmospheric chemistry. Aqueous phases in the atmosphere are established as an important reaction media for WSOCs. Organic acids are highly abundant in SOA and can serve as further precursors for aqSOA. However, the OH-oxidation of many atmospherically relevant organic acids has not been investigated systematically. In particular, the interplay between acid–base chemistry and photochemistry in the aqueous phase remains an unexplored research area. The overall objective of my MSc. thesis is to improve our fundamental understanding in this area. In particular, three projects have been conducted to achieve this overall goal.

In Chapter 2, we used CPA as a model compound to characterize our photoreactor for the investigation of the aqueous-phase direct photolysis and OH-initiated oxidation reactions. The reactor offers the advantage of simulating the photochemistry taking place in cloud and fog droplets. The reactor light characterization is shown by acquired data related to the photochemical decay of a known chromophore in aqueous samples. Furthermore, the OH radical chemistry in the reactor was simulated further using a kinetic model to improve our assessment of the photoreactor environment.

In Chapter 3, the investigation of the pH dependence of the OH reactivity of several organic acids in the aqueous phase is presented. The OH reactivity of individual organic acids and a collective of organic acids relevant to α-pinene SOA were investigated under three different pH conditions, and its kinetics were determined. The photoreactor characterized in Chapter 2 was used here to simulate the photochemically initiated reactions and better understand how organic compounds react in cloudwater at the fundamental level.

In Chapter 4, the chemical characterization of products formed upon PA aqueous-phase OH-oxidation was investigated for the first time. This Chapter focuses on identifying PA oxidation products and proposes their possible formation mechanisms by combining data obtained from offline and online LC–MS methods. While PA's kinetics as a function of pH has been previously investigated in Chapter 3, there is a lack of information regarding its reaction mechanisms and possible differences due to acidic and basic pH conditions.

Together, the work presented in this thesis provides new insight into the aqueous-phase photochemistry of important atmospheric organic acids under different cloud and fog pH conditions. This thesis highlights the importance of major products of α-pinene oxidation, considering that some of their aqueous phase OH-reactivity has never been measured before.

Chapter 2

Characterization of the Photoreactor Using *cis*-Pinonic Acid as a Model Compound

2.1 Introduction

Laboratory studies in bulk aqueous solutions seek to mimic chemical reactions occurring in atmospheric waters (e.g., cloud water, fog, wet aerosols),[7] and it is of great importance for the fundamental understanding of the chemical behaviors of water-soluble organic compounds (WSOCs) in the atmosphere. Given that atmospheric aqueous-phase reactions contribute to the overall sink and source of aqueous secondary organic aerosols (aqSOA),[5,7,47,71] laboratory-based investigations on kinetics and mechanisms involving WSOC can provide relevant information for 3D chemical transport models that simulate concentrations of air pollutants in the atmosphere.[7,19]

Among the main oxidant species driving the cloudwater oxidation, i.e., O_3, NO_3 and OH radicals, the OH radicals are the dominant aqueous oxidant.[72] Studies on the aqueous-phase OH-oxidation of WSOC have been carried out by numerous authors.[19,66,68] Given that UV light is responsible for the majority of photochemistry in the atmosphere, experiments using photoreactors containing ultraviolet (UV) lamps often are employed to simulate the photo-initiated reactions under highly controlled irradiation. The formation of OH radicals commonly is achieved via H_2O_2 photolysis, which is one of the most important sources of aqueous OH radicals in cloudwater.[46]

The rate at which H_2O_2 is photolyzed in aqueous solution varies as a function of the intensity and wavelength (λ) of UV light.[38] Thus, the rate of OH generation can be adjusted by varying a few of the photoreactor parameters, such as the wavelength of the UV light, the number of lamps used, and the concentration of H_2O_2 added to the solution. The UV radiation is defined as electromagnetic radiation with a wavelength of 100–400 nm. In the atmosphere, UV with $\lambda < 290$ nm is filtered out by atmospheric components, such as O_3, and UV light with $\lambda > 290$ nm can reach the troposphere and drive the atmospheric photochemical processes.[38,41]

We have three types of UV lamps in our lab: UVA (polychromatic light centered at 360 nm), UVB (polychromatic light centered at 310 nm), and UVC (sharp emission at 254 nm). Among these, the use of UVB light is most suited for our application, as UVB is absorbed efficiently by H_2O_2 but is not as energetic as UVC, which may initiate unwanted photolysis of organic compounds. Each photoreactor requires careful characterization, as it is essential to evaluate the oxidative environment that is created inside the photoreactor. However, a serious challenge lies in our inability to monitor all the critical indicators for the photoreactor's performance, such as radical species forming and reacting during photo-oxidation. Thus, characterization of our photoreactor requires an in-depth study of a model compound whose photochemical behavior has been characterized previously. In addition to chemical analyses, which track the concentration change of major reactants, a modeling approach is required to simulate the concentration of radicals.

Due to its atmospheric relevance and availability from major chemical suppliers, *cis*-pinonic acid (CPA) is considered an ideal model compound for the investigation of cloudwater photochemistry. Photochemical behaviors of CPA have been reported in the literature.[12,47,72] CPA is one of the major oxidation products of α-pinene,[47,73,74] the most abundant species in the family of monoterpene.[18] Monoterpene is among the largest classes of biogenic volatile organic compounds (BVOCs) emitted to the atmosphere, besides methanol and isoprene.[18,19] The atmospheric oxidation of α-pinene by O_3, OH and NO_3 radicals results in multi-functional products with lower volatilities, which then can partition into SOA particles and water droplets.[17] Under cloudwater conditions, i.e., liquid water content (LWC) of 0.3 to 0.5 g m^{-3},[14,20] CPA is estimated to reside predominantly in the aqueous phase due to the presence of a carboxylic and a ketone functional group, resulting in an estimated Henry's law constant (K_H) of 2.0×10^7 M atm^{-1}.[75] Consequently, CPA can undergo further OH-oxidation in the cloudwater, contributing to aqSOA formation.

A database for aqueous-phase photochemistry and radical chemistry relevant to the formation of aqSOA has been established through laboratory experiments.[47,67,72] Kinetic and mechanistic information from this database can be used as input to a chemical box model, which can simulate the aqueous-phase processing of CPA and

many other important organic compounds. By prescribing the model with conditions specific to our photoreactor, including the amount and wavelength of light, we can simulate the chemical reactions occurring in our photoreactor explicitly.

This work aims to characterize the photoreactor used in our laboratory settings by investigating the direct photolysis and OH-initiated oxidation of CPA. The characterization lays the foundation for kinetic and mechanistic investigations, which are the focus of the following chapters of this thesis. Specifically, we are interested in determining the concentration of OH radicals formed during the aqueous-phase experiments, thus the rate at which CPA is oxidized. A careful characterization of the wavelength and intensity of UV light in the photoreactor is required for this purpose. By simulating CPA's direct photolysis and OH-oxidation using a kinetic model, we can assess our knowledge regarding the photochemical environment created within the photoreactor.

2.2 Materials and Methods

2.2.1 Chemicals and Materials

The following chemicals were purchased from Sigma Aldrich: CPA (98%), pimelic acid (98%), caffeine (99%), hydrogen peroxide (H_2O_2, 30% in water), sulfuric acid (50% in water), and 2-nitrobenzaldehyde (98%). Chemicals also were purchased from Fisher Chemical: sodium hydroxide (98%), acetonitrile HPLC grade, and formic acid (0.1% in water). All chemicals were used without further purification.

2.2.2 Experimental Details

2.2.2.1 Photochemical Reactor Description

A photoreactor (Rayonet, PRP200) emitting polychromatic UV-light centered at 310 nm (UVB) was used to carry out CPA's aqueous phase photo-oxidation reactions. The photoreactor was mounted in a circular setting to ensure that the lamps are equidistant from the center, and a stirring plate was placed on the bottom to ensure adequate solution mixing, as shown in Figure 2.1.

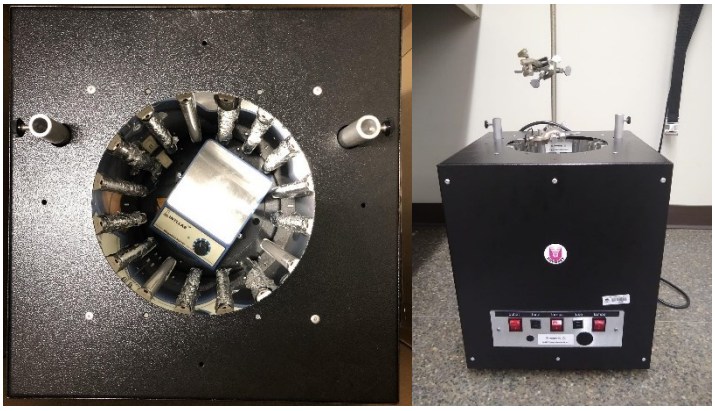

Figure 2.1. The top view (left) and front view (right) of the photoreactor used in the aqueous-phase photo-oxidation experiments.

2.2.2.2 Determination of UV Flux in the Reactor

The intensity (photo flux) and wavelength of light emitted by the UV lamps in the photoreactor dictate the rates at which photochemistry occurs within. The photon flux is determined by a combination of direct measurement and chemical actinometry. Firstly, the direct measurement was conducted with a spectroradiometer (Ocean Optics, USB2000+ER), which records the shape of the spectra emitted by the lamps. Secondly, the actual photon flux had to be determined using a photochemically sensitive compound, 2-nitrobenzaldehyde (2-NB), serving as an indicator for the light reaching the reaction mixture (i.e., a chemical actinometer). 2-NB has a well-determined absorption property;[76] thus, the amount of light emitted by the UVB lamps can be calculated, based on the photolysis rate of 2-NB, which is determined with the following method.

A 10.0 μM aqueous solution of 2-NB was prepared and irradiated with UVB. Aliquots were taken at 0, 20, 40, 60, 90, and 120 s. The concentration of 2-NB was monitored using an Agilent 1100 HPLC system equipped with a binary pump, autosampler, and a thermostat with UV-detection (set to 258 nm). The following HPLC conditions were used: 60% acetonitrile/40% H_2O (isocratic), at a flow rate of 0.30 mL/min; a Hewlett Packard G1312A pump; an Atlantis dC18 column (waters, 3 μm, 150 x 2.1 mm) column. A column heater (Agilent COLCOM G1316) was used to maintain the column at 30 °C. The photolysis rate of 2-NB corresponds to the first-order decay rate of the 2-NB signal. The photon flux in the reactor was determined by

taking the shape of the emission spectra, as mentioned above, but scaling the intensity of the emission spectra linearly until it would give a 2-NB photolysis rate that matches the observed one.

2.2.2.3 CPA Photo-Oxidation

For the experimental kinetics study of CPA, 90 mL of D.I. water, 102 μL H_2O_2 30% v/v, 10 mL of CPA 300 μM, and the reference compound were mixed. Therefore, the reactant concentrations were 10 mM H_2O_2, 30 μM CPA, and 0.3 μM of the reference compound, resulting in a solution of pH 4.85. A 150 mL quartz vessel was used to ensure an efficient UVB transmission to the solution containing the reactants. Here, H_2O_2 was photolyzed to form OH radicals and initiate CPA's aqueous-phase OH-oxidation reactions, which were carried out for 10 min. The reaction progress was monitored by sampling 1.0 mL of solution from the reactor every 2 min and analyzing it with ESI−LC−MS on the same day (see Section 2.2.2.5). On average, the temperature of the reaction mixture after the 10 min of irradiation reached 4 °C above the room temperature (22 °C). All experiments were performed in triplicate and all data are expressed as the mean ± standard deviation.

The contribution of direct photolysis to the overall CPA decay was investigated in a separate experiment. First, CPA and the reference compound were mixed in the same concentrations and irradiated for the same time as in the OH-oxidation experiments, but no H_2O_2 was added. The absence of reactions between CPA and H_2O_2 itself was confirmed with a dark control experiment. This experiment was conducted in the same way as the OH-oxidation experiment, except that the UV lamps remained off for the entire 10 min.

2.2.2.4 Deriving Kinetics Information of CPA Direct Photolysis and OH-Oxidation

The second-order rate coefficient (k^{II}_{OH}) of CPA with OH radicals was determined at room temperature and under pH 4.85 (pH of the solution containing all reactants). Using competitive kinetics, CPA's k^{II}_{OH} was determined by monitoring its loss relative

to that of a reference compound with a known OH rate coefficient. CPA's relative kinetic plot follows Eq. (2.1):

$$\ln\left(\frac{[\mathrm{CPA}]_0}{[\mathrm{CPA}]_t}\right) = \frac{k_{\mathrm{OH}}^{II}}{k_{\mathrm{R}}^{II}} \ln\left(\frac{[\mathrm{R}]_0}{[\mathrm{R}]_t}\right) \qquad \text{Eq. (2.1)}$$

where $[\mathrm{CPA}]_t$ and $[R]_t$ are the signals of CPA and the reference compound at time t, respectively, and k_{R}^{II} is the aqueous-phase OH rate constant of the reference compound used. By plotting $\ln([R]_0/[R]_t)$ versus $\ln([\mathrm{CPA}]_0/[\mathrm{CPA}]_t)$, a straight line should pass through the origin, with a slope equivalent to the ratio between k_{OH}^{II} and k_{R}^{II}. For the case of CPA, special caution was applied as CPA also undergoes direct photolysis. Its direct photolysis rate was considered when calculating k_{OH}^{II}. Pimelic acid was chosen as the reference compound, considering that its OH reactivity has been recently measured under pH 4.0,[77] $k_{\mathrm{OH}}^{II} = (3.4 \pm 0.1) \times 10^9\ \mathrm{M^{-1}\ s^{-1}}$, which is the closest to the pH of the reaction mixture (pH 4.85). In addition, pimelic acid has been used extensively as the reference compound by a series of studies performed by Witkowski and Gierczak.[12,78]

2.2.2.5 ESI−LC−MS Analysis

LC−MS experiments were carried out with an Agilent 1110 LC coupled to a quadrupole (Model G1946D) mass spectrometer using a negative electrospray ionization (ESI) source. The negative mode, (-)ESI−LC−MS, was used here due to its selectivity towards organic acids.[64] The mass spectra were acquired in the selected ion monitoring (SIM) mode, in which the *m/z* of CPA (*m/z* 183) and reference compound (pimelic acid, *m/z* 159) were targeted to achieve better sensitivity. LC separation was performed on a reverse phase Kinetex (Phenomenex) Polar C18 column (50 x 2.1 mm, 2.6 μm, 100 Å) kept at 35.0 °C and equipped with a security guard cartridge with a 2.1 mm ID C18 pre-column. Eluent A was a formic acid solution in water (pH = 2.8) and eluent B was acetonitrile, delivered at a flow rate of 0.5 mL/min; the injection volume was 15 μL. The gradient elution was programmed as follows: 0.0−0.5 min isocratic 5% B, 0.5−5.0 min linear gradient to 30% B, 5.0−6.0 min linear gradient to 95% B, 6.0−6.7 min isocratic 95% B, 6.7−7.0 min linear gradient to 5% B. Afterward, the column was re-equilibrated at 5%, and the analysis was completed in 11.5 min.

2.2.3 Kinetic Modeling of CPA Photochemistry

2.2.3.1 General Model Description

To complement our chemical analysis and to characterize the radical chemistry in the photoreactor better, a box model was developed by Shuang Wu, a PhD student in Dr. Ran Zhao's group at U of Alberta to simulate photochemistry of CPA. A model originally used for gas-phase reactions in chamber reactors and continuously stirred tank reactors (CSTRs)[79] was adapted and modified to simulate aqueous-phase photochemistry. The model was operated on the MATLAB platform. Key chemical reactions were adapted from previous literature on aqueous phase radical chemistry simulations.[66,72] The reactions and their rate coefficients used in the model are summarized in Table 2.1. Briefly, the model includes direct photolysis of CPA and H_2O_2, OH-oxidation of CPA and subsequent radical chemistry, acid-base chemistry of selected species, as well as a brief description of OH-oxidation of products arising from CPA.

Table 2.1 Reactions and Rate Coefficients Used in the CPA Photochemical Model.

Reactions	Rate Coeff.[a]	Ref.[b]	Footnote
$H_2O_2 + h\nu \rightarrow 2OH$	-		c
$HO_2 + HO_2 \rightarrow H_2O_2 + O_2$	8.3×10^5		
$OH + H_2O_2 \rightarrow HO_2 + H_2O$	2.7×10^7		
$HO_2 + H_2O_2 \rightarrow OH + O_2 + H_2O$	3.7		
$OH + HO_2 \rightarrow O_2 + H_2O$	7.1×10^9		
$H_2O \rightarrow H^+ + OH^-$	1.4×10^{-3} s^{-1}		
$H^+ + OH^- \rightarrow H_2O$	1.4×10^{11}		
$H_2O_2 \rightarrow H^+ + HO_2^-$	0.35 s^{-1}	80	
$H^+ + HO_2^- \rightarrow H_2O_2$	2.3×10^{-10}		
$OH \rightarrow H^+ + O^-$	0.18 s^{-1}		
$H^+ + O^- \rightarrow OH$	2.3×10^{-10}		

$HO_2 \rightarrow H^+ + O_2^-$	$8.0 \times 10^5\ s^{-1}$		
$H^+ + O_2^- \rightarrow HO_2$	5.0×10^{10}		
$CO_2^- + O_2 \rightarrow O_2^- + CO_2$	2.4×10^9		
$OH + O_2^- \rightarrow OH^- + O_2$	1.0×10^{10}		
$HCO_3^- + OH \rightarrow CO_3^- + H_2O$	1.0×10^7		
$CO_3^- + O_2^- \rightarrow CO_3^{2-} + O_2$	6.5×10^8		
$CO_3^- + H_2O_2 \rightarrow HCO_3^- + HO_2$	8.0×10^5		
$CO_2 \rightarrow H^+ + HCO_3^-$	$2.4 \times 10^{-2}\ s^{-1}$		
$H^+ + HCO_3^- \rightarrow CO_2$	5.6×10^4		
$HCO_3^- \rightarrow H^+ + CO_3^{2-}$	$2.3\ s^{-1}$		
$H^+ + CO_3^{2-} \rightarrow HCO_3^-$	5.0×10^{10}		
CPA + hν → CPAprod	-	11	
CPA + OH → CPAprod	Expt. values		d
CPAprod + OH → CPAprod (30%) → 2CPAprod (70%)	Expt. values		d
PMA + OH → PMAprod	2.2×10^9 (pH 2) 3.4×10^9 (pH 4)	77	
PMAprod + OH → PMAprod (30%) → 2PMAprod (70%)	2.2×10^9 (pH 2) 3.4×10^9 (pH 4)		
CAF + OH → CAFprod	6.9×10^9	12	
CAFprod + OH → CAFprod (30%) → 2CAFprod (70%)	6.9×10^9		
The following reactions are used only in the SO_4^- scenario			
$HSO_4^- \rightarrow H^+ + SO_4^{2-}$	$5.2 \times 10^8\ s^{-1}$	81	
$H^+ + SO_4^{2-} \rightarrow HSO_4^-$	5.0×10^{10}	81	
$HSO_4^- + OH \rightarrow SO_4^{2-} + H_2O$	3.5×10^5	8	

$SO_4^- + SO_4^- \rightarrow S_2O_8^{2-}$	2.6×10^{-13}	36	
$SO_4^- + H_2O_2 \rightarrow SO_4^{2-} + HO_2$	4.6×10^{-14}		
$SO_4^- + HO_2 \rightarrow SO_4^{2-} + H^+ + O_2$	5.8×10^{-12}		
$SO_4^- + O_2^- \rightarrow SO_4^{2-} + O_2$	5.8×10^{-12}		
$SO_4^- + OH^- \rightarrow SO_4^{2-} + OH$	2.3×10^{-14}		
$SO_4^- \rightarrow H^+ + OH + SO_4^{2-}$	5.0×10^2 s^{-1}	82	
$SO_4^- + S_2O_8^{2-} \rightarrow SO_4^{2-} + S_2O_8^-$	1.0×10^{-15}	83	
$SO_4^- \rightarrow OH + HSO_4^-$	1.1×10^{-18} s^{-1}		
CPA + $SO_4^- \rightarrow$ CPAprod	Expt. values		e
PMA + $SO_4^- \rightarrow$ PMAprod	2.2×10^9 (pH 2) 3.4×10^9 (pH 4)		e

Acronyms: CPA: *cis*-pinonic acid, PMA: pimelic acid, CAF: caffeine, prod: products of a species
[a] Unit of rate coefficients is M^{-1} s^{-1} unless otherwise noted.
[b] Rate coefficients are adapted from Tan et al.,[66] unless otherwise noted.
[c] Consideration for $\varphi_{OH} = 0.93$ is applied.[72]
[d] Experimentally determined values were used for pH 2, 4 (uncontrolled), and 10.
[e] Reactivity of SO_4^- is assumed to be the same as the OH reactivity.

2.2.3.2 Treatment of Direct Photolysis

The direct photolysis rate of a given species (J) was simulated by Eq.(2.2):

$$\int_{\lambda_{min}}^{\lambda_{max}} I(\lambda)\sigma(\lambda)\phi(\lambda)d\lambda \approx \sum_{\lambda} I(\lambda)\sigma(\lambda)\phi(\lambda)\Delta\lambda \qquad \text{Eq. (2.2)}$$

where $I(\lambda)$, $\sigma(\lambda)$, and $\phi(\lambda)$ are the light flux, molecular absorption cross section, and quantum yield, respectively.[38] The light flux $I(\lambda)$ in our photoreactor was obtained as described in Section 2.2.2.2. The $\sigma(\lambda)$ and $\phi(\lambda)$ data for CPA and H_2O_2 were obtained from Lignell et al.[11] and Finlayson-Pitts and Pitts,[3] respectively.

2.2.3.3 Treatment of CPA Products

A challenge in modeling the photochemistry of CPA is the treatment of the products of CPA. The direct photolysis and OH-oxidation of CPA result in numerous products and describing an explicit oxidation mechanism in the model is implausible. Given that the major purpose of the model was to simulate the decay of CPA, the products of CPA were lumped into a single category, “CPAprod”.

CPA contains a four-membered ring on its structure, and the 1st generation products of CPA (by both photolysis and OH-oxidation) are likely those arising from ring-opening and functionalization reactions. The 2nd and subsequent oxidation will, however, result in either fragmentation or functionalization reactions. The probability of fragmentation (P_{frag}) is an ongoing focus of research. Cappa and Wilson[84] parameterized using Eq. (2.3):

$$P_{frag} = c_{frag} \times N_O \quad \text{Eq. (2.3)}$$

where c_{frag} is a fitting parameter, and N_O is the number of oxygens on the molecule. The authors found that $c_{frag} = 0.18$ best reproduced α-pinene SOA formation in chamber experiments. CPA has $N_O = 3$, and its products (CPAprod) likely will contain N_O of 3, 4, or 5. Therefore, P_{frag} for CPA oxidation is estimated to be between 0.58 and 0.9. In this model, we took the value of $P_{frag} = 0.7$ as an estimated value of all the CPAprod species.

The k_{OH}^{II} values of CPAprod species can be either faster or slower than CPA itself, depending on their structures. In this model, we assumed that all the products react with OH with the same to CPA. This assumption is reasonable if the products contain similar numbers of carbon in their structures (i.e., for early-generation products). However, uncertainty cumulates towards products arising in the later generations.

2.2.3.4 Model Scenarios

Two model scenarios were explored to match the OH-oxidation and direct photolysis experiments of CPA described in Section 2.2.2.3. The initial concentrations of CPA and reactants used are shown in Table 2.2.

Table 2.2 Initial Concentrations Used in Model Scenarios.

Scenarios	CPA (μM)	H_2O_2 (mM)	Pimelic Acid (μM)	pH
CPA direct photolysis	30	0	0	4.85
CPA OH-oxidation	30	10	0.3	4.85

2.3 Results and Discussion

2.3.1 Characterization of Wavelength and Flux of UV Light

From the spectroradiometer measurements, the emission spectrum of the UVB light source is shown in Figure 2.2. The photon flux spectrum of the UVB lights in our current photoreactor has a peak of 310 nm, which is consistent within the UVB wavelength range. The light intensity of the background light in the laboratory also is recorded and is subtracted from the UVB light data.

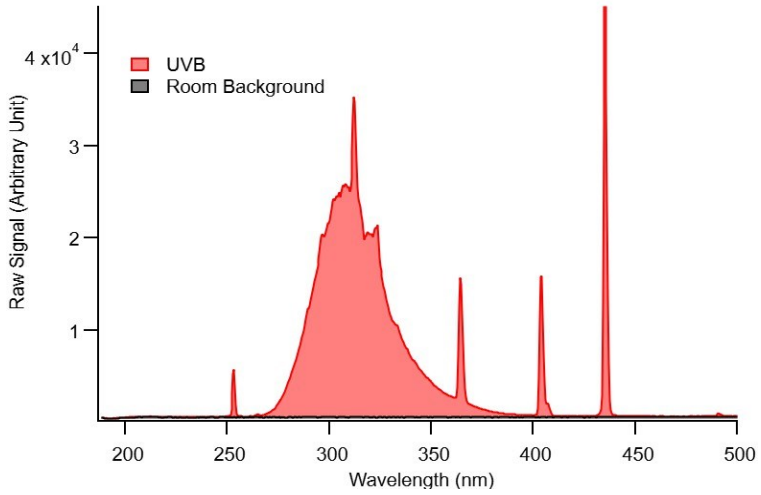

Figure 2.2. Raw spectral data recorded by the spectroradiometer for the UVB lamps (red) and background lighting in the room (black).

Similar to CPA, the direct photolysis of 2-NB, J(2-NB), can be determined theoretically using Eq. (2.2). When we use the raw spectral data from the spectroradiometer as $I(\lambda)$, in addition to 2-NB literature values of $\sigma(\lambda)$ and $\phi(\lambda)$, Eq. (2.2) yields a J(2-NB) value of 1.35×10^{-12} s^{-1}. Given that the raw spectral data were used in the calculation, this value does not match the actual J(2-NB) measured using HPLC. The actual flux can be obtained by relating this value to the measured J(2-NB), as described below.

Following the methods mentioned in Section 2.2.2.2, the actual J(2-NB) under the UVB light was measured using HPLC. From the experimental data, J(2-NB) was calculated using the first-order integrated law:

$$\ln\left(\frac{[\text{2-NB}]_t}{[\text{2-NB}]_0}\right) = -J(\text{2-NB}) \times t \qquad \text{Eq. (2.4)}$$

where $[\text{2-NB}]_t$ and $[\text{2-NB}]_0$ are the peak areas of 2-NB at irradiation times t and zero, respectively. Plotting $\ln([\text{2-NB}]_0/[\text{2-NB}]_t)$ as a function of time should result in a straight line with slope = $-J$(2-NB), as it can be seen in Figure 2.3.

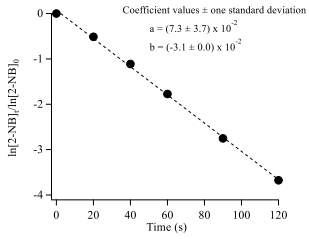

Figure 2.3. 2-NB photodecay rate constant calculation.

From Figure 2.3, J(2-NB) was determined to be 3.11×10^{-2} s^{-1}. Due to the difference between J(2-NB) when calculated using Eq. (2.2) and Eq. (2.4), an adjustment factor of 2.29×10^{10} s^{-1}, from $(3.11 \times 10^{-2} / 1.35 \times 10^{-12})$ s^{-1}, was used to convert the raw spectral data into the photon flux of the UVB light in the photoreactor. Therefore, the light flux $I(\lambda)$ in our photoreactor was adjusted resulting in the spectrum displayed in Figure 2.4.

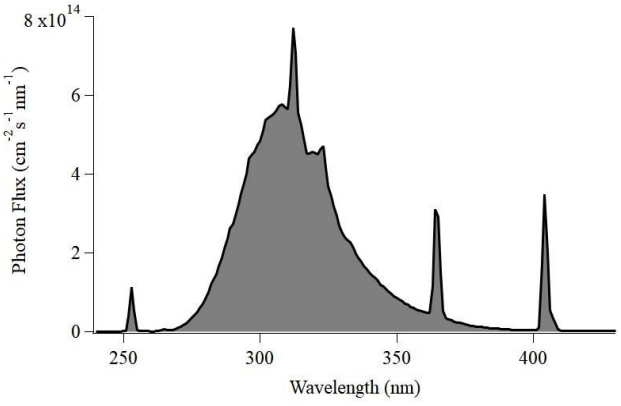

Figure 2.4. Finalized photon flux in the photoreactor.

2.3.2 OH Reactivity of CPA

Similarly to 2-NB in Section 2.3.1, CPA undergoes first-order photodegradation under UVB light, such that:

$$\ln\left(\frac{[\mathrm{CPA}]_t}{[\mathrm{CPA}]_0}\right) = -J(\mathrm{CPA}) \times t \qquad \text{Eq. (2.5)}$$

where $[\mathrm{CPA}]_t$ and $[\mathrm{CPA}]_0$ are the concentrations at irradiation times t and zero, respectively. The negative slope of $\ln([\mathrm{CPA}]_0/[\mathrm{CPA}]_t)$ versus t represents CPA's photodecay rate constant, J(CPA). Figure 2.5 shows a straight line with the slope $b = -(1.0 \pm 0.0) \times 10^{-3}$.

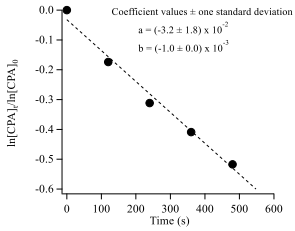

Figure 2.5. Experimental calculation of the first-order rate constant for CPA photodecay.

From Figure 2.5, the rate at which CPA is photolyzed directly is $(1.0 \pm 0.0) \times 10^{-3}$ s^{-1}. Thus, for the calculation of CPA's k_{OH}^{II}, the photolysis rate was taken into consideration. Under direct photolysis, CPA's concentration decays 50% over 10 min of UVB irradiation, as observed in Figure 2.6. The direct photolysis of CPA is 5.4 times slower than its oxidation by OH radicals, and its pseudo-first-order rate was calculated to be $(5.4 \pm 0.0) \times 10^{-3}$ s^{-1}.

For the CPA OH-oxidation, a (-)ESI−LC−MS chromatogram was obtained under selected ion acquisition mode, in which the color scheme represents the irradiation time during the experiment (Figure 2.7).

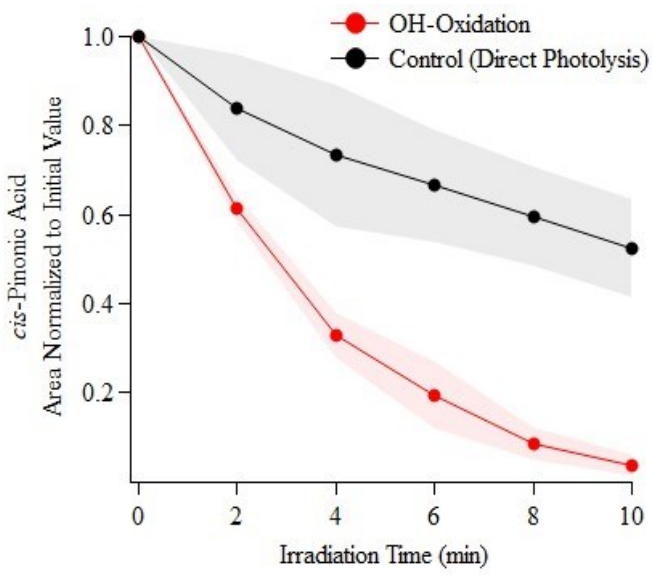

Figure 2.6. OH-oxidation and control experiment for CPA. The signal of CPA is shown as a function of irradiation time and the shaded area presents 1σ from triplicates.

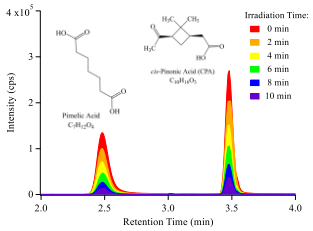

Figure 2.7. a) SIM chromatogram of CPA (*m*/*z* 183) and pimelic acid (reference compound, *m*/*z* 159) under 10 min of UVB irradiation.

Both CPA and pimelic acid show a fast decay over the 10 min of photo-oxidation, having their initial signal, which is representative of their concentrations, reduced by 90% and 99%, respectively. As explained in section 2.2.2.4, a relative kinetic data plot was obtained for CPA and pimelic acid (Figure 2.8). The linear relationship (R^2 = 0.998667) with a y-intercept close to 0 was obtained, validating the relative kinetic method used in this work. A correction was also made (blue trace in Figure 2.8) to remove the contribution of CPA direct photolysis.

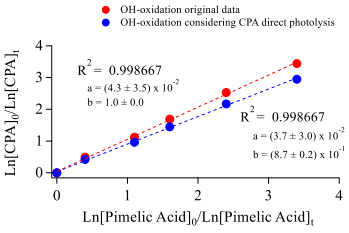

Figure 2.8. Measured OH reaction relative data for aqueous oxidation of CPA.

By following Eq. (2.1) and considering J(CPA), its k_{OH}^{II} was calculated to be $(3.0 \pm 0.3) \times 10^9$ M^{-1} s^{-1}. The measured rate constant for CPA is close to the diffusion limit of WSOC reactions with OH (10^9–10^{10} M^{-1} s^{-1}) in atmospheric aqueous phases.[5] It confirms that the oxidation of CPA by OH radicals is a potential sink of this compound in cloudwater, fogs, among other aqueous environments.

2.3.3 Model Simulation for CPA Photochemistry

For the direct photolysis of CPA, the model underestimated the decay of CPA by 25% when a quantum yield of 0.5, reported by Lignell et al.,[11] was used (Figure 2.9.a). This value was based on an estimate and was associated with a large relative uncertainty (0.5 ± 0.3). For the simulation of OH-oxidation, we have decided to make an adjustment of the quantum yield to 0.69 to achieve the best model-observation agreement in terms of the experimental photolysis rate of CPA, $(1.0 \pm 0.0) \times 10^{-3}$ s^{-1}. For the OH-oxidation experiments, the agreement between the observed and modeled pseudo-first-order decay rates of CPA was good, i.e., within 10.0% (Figure 2.9b). These results demonstrated that our model could reproduce the observed CPA decay. In other words, the light flux we determined seems to be reasonable, and our model is successful in simulating the radical chemistry occurring under UVB irradiation.

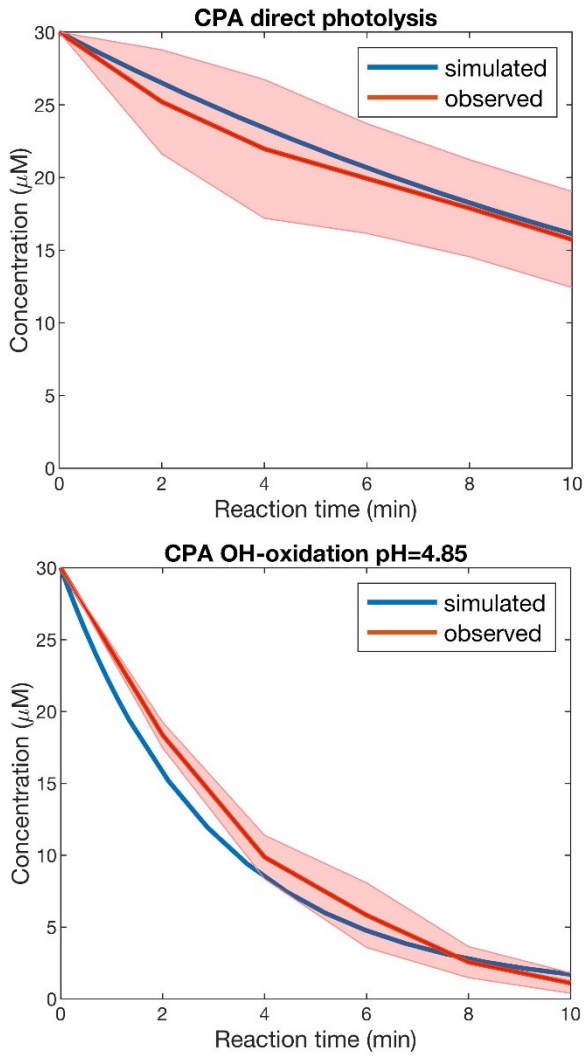

Figure 2.9. Simulated and observed CPA concentration in a) direct photolysis, b) OH-oxidation at pH 4.85. The shaded area presents observed data standard deviation range (1 σ). The model result in a) employs the optimized CPA φ(λ) value: 0.69 across the relevant wavelength range.

With the model successfully reproducing the CPA decay, it was used to investigate the concentration of OH radicals in our reaction further. In atmospheric aqueous phases, the concentration of OH radicals range between 1.4×10^{-16} and 8.0×10^{-12} M.[5,23] From our model results, the photolysis of H_2O_2 under UVB light led to an OH radical concentration of 1.8×10^{-12} M. This result confirms that our current photoreactor system can reproduce atmospherically relevant aqueous-phase reaction conditions.

2.4 Summary

A series of experimental and modeling studies were conducted, with an aim to characterize the photoreactor thoroughly. The photon flux emitted by the UVB lights in the photoreactor was characterized by using 2-NB as a chemical actinometer. This information was used in the kinetic box model to simulate CPA aqueous-phase photochemistry and determine the OH radical concentration within it. The UVB light was sufficient to generate OH radicals at relevant concentrations (1.8×10^{-12} M), and it also was efficient in inducing CPA photoreactions. A comparison of the model results with the experimental data on CPA direct photolysis and OH-oxidation indicates that our photoreactor can reproduce the oxidative environment for the aqueous oxidation of WSOCs such as CPA. The kinetic box model also serves as an essential tool to evaluate the photochemical environment when reactions of other WSOC species are studied. Overall, the results from this chapter are of great importance to better understand the aqueous-phase kinetics of other atmospheric relevant WSOCs, which are presented in the following chapters.

Chapter 3

pH Dependence of the OH Reactivity of Organic Acids in the Aqueous Phase[1a]

3.1 Introduction

Over the past decades, studies have identified atmospheric aqueous phases (e.g., cloud, fog, and aerosol liquid water) as an important reaction media for the processing of water-soluble organic compounds (WSOCs).[4,5,7] Aqueous-phase photochemistry converts WSOCs into more functionalized and oxygenated forms, leading to the formation and evolution of a secondary organic aerosol (SOA).[4–7] In addition, more volatile compounds are formed from the fragmentation of the WSOC, which decreases the potential for SOA formation.[85] Despite the role that SOA plays in air quality and the global climate,[14,86] the aqueous-phase processes taking place in cloudwater and fog related to the formation and evolution of SOA, in particular, are much less understood than the gas-phase counterparts.

Formation of SOA is driven by multiphase-chemistry involving the gas-phase oxidation of volatile organic compounds (VOCs), followed by the partitioning of the WSOCs to cloudwater or aerosol water.[7] In atmospheric aqueous phases, the hydroxyl (OH) radical is the most important oxidant, and it is generated *in-situ* in the aqueous phase or introduced from the gas phase.[23,87] In the aqueous phase, the OH-oxidation of many organic compounds occurs near the collision limit of 10^9 to 10^{10} $M^{-1}s^{-1}$, with aqueous-phase radical concentrations being in the range of 1.4×10^{-16} to 8.0×10^{-12} M.[5,23]

Aqueous-phase processing of volatile organic compounds of biogenic origin (BVOCs) is the dominant source of aqueous SOA precursors.[35,71,88] Of these BVOCs, α-pinene is a representative SOA precursor because it is one of the main monoterpenes

[a] The contents of this chapter have been copied and/or adapted from the following publication: "Amorim, J. V.; Wu, S.; Klimchuk, K.; Lau, C.; Williams, F. J.; Huang, Y.; Zhao, R. pH Dependence of the OH Reactivity of Organic Acids in the Aqueous Phase. Environ. Sci. Technol. 2020. https://doi.org/10.1021/acs.est.0c03331"

emitted by mass, with an average of 66 Tg year^{-1}.[2] Once emitted, α-pinene undergoes gas-phase oxidation, leading to the formation of many multifunctional organic compounds, with *cis*-pinonic acid (CPA) and pinic acid (PA) being two of the major products.[74,89,90] Because of the presence of carboxylic groups, CPA and PA can partition efficiently between the gas and aqueous phases, with predicted Henry's law constants of 1.02×10^7 M/atm and 1.42×10^9 M/atm, respectively.[75] Compounds with such Henry's law constants undergo partitioning exclusively to the aqueous phase when cloudwater is present in the air mass, and the photochemistry occurring in the aqueous phase will affect the atmospheric fate of these compounds clearly.[35,91]

In addition to CPA and PA, studies have confirmed that SOA is a complex mixture of compounds, including numerous organic acids (OAs), which can be detected using liquid chromatography–mass spectrometry with negative electrospray ionization ((-)ESI–LC–MS), an offline technique.[64,89,90] The acid–base chemistry may add further complexity to WSOCs of SOA. The typical pH values of fogs and clouds fall between 2 and 7,[54,55] and OAs present in α-pinene SOA can be present in their protonated or deprotonated forms, affecting reaction pathways and kinetics with OH radicals.[20,34,77] This acid–base chemistry is a unique nature of the aqueous-phase processing; however, the interplay between acid–base chemistry and photochemistry is understood poorly. In particular, Pye et al.[55] have shown that the average pH of fog and cloud waters in Europe and the US has increased by one pH unit in the past 30 years. This trend arises from reduced emissions of acid precursors to the atmosphere. The pH dependence of cloudwater chemistry must be understood to predict the impact of a constantly changing acidity in atmospheric aqueous phases as well as extracting general trends that can be extrapolated to a wider range of compounds.

Previous studies have shown that small OAs will differ in their second-order rate coefficients with OH (k^{II}_{OH}) by up to an order of magnitude.[20,77] Ervens et al.[20] proposed that deprotonated carboxylates react rapidly with the OH radicals via an electron-transfer reaction, resulting in a pH dependence in their OH reactivity. Witkowski et al.[12] and Otto et al.[92], on the other hand, did not observe this pH dependence for CPA and (+)camphoric acid. A challenge in determining the pH dependence is finding reference compounds with reliable reactivity under different pH

values. Subsequently, the overall objective of this study is to improve our understanding of how organic compounds react in cloudwater at the fundamental level. Using ESI–LC–MS, we targeted individual and collective OAs relevant to α-pinene SOA and determined their reactivities under three pH conditions. Given the infeasibility of studying each individual component of SOA, the focus of this study is placed on compounds that are representative of SOA: PA, CPA, and limononic acid (LA). We determined the k_{OH}^{II} values of these compounds experimentally, with the assistance of the kinetic box model developed in Chapter 2. Due to a lack of commercially available standards, we custom-synthesized PA and LA. To the best of our knowledge, the OH reactivity of PA has never been reported previously. We hypothesize that the OH reactivities of OAs relevant to α-pinene SOA are less pH-dependent compared to those of small OAs. The rationale is that a larger carbon chain on an organic acid presumably will reduce the relative importance of the electron-transfer reaction. To test this hypothesis, we also investigated the OH reactivity of formic acid (FA).

3.2 Experimental Methods

3.2.1 Chemicals and Materials

The following chemicals were purchased from Sigma Aldrich: (+) α-pinene (98%), CPA (98%), pimelic acid (98%), caffeine (99%), hydrogen peroxide (H_2O_2, 30% in water), ammonium sulfate (>99%), potassium hydrogen phthalate (>99.95%), and sulfuric acid (50% in water). Chemicals also were purchased from Fisher Chemical: sodium hydroxide (98%), acetonitrile HPLC grade, formic acid (0.1% in water), and methanol HPLC grade. All chemicals were used without further purification.

3.2.1.1 Synthesis of Pinic Acid

PA is a major product of α-pinene oxidation, and its synthesis was conducted with a haloform reaction similar to the one used by Steimer et al.[93] (see Figure 3.1). When treated with bromine in basic solution, polyhalogenation and cleavage of the methyl

group of CPA occurs to form PA. The structure of PA was confirmed with ^{1}H NMR and ^{13}C NMR, as presented Figures 3.2 and 3.3.

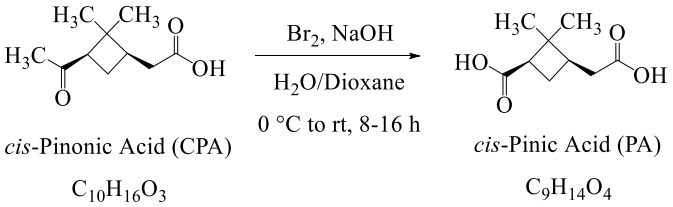

cis-Pinonic Acid (CPA)

$C_{10}H_{16}O_3$

cis-Pinic Acid (PA)

$C_9H_{14}O_4$

Figure 3.1. Synthesis of PA.[93]

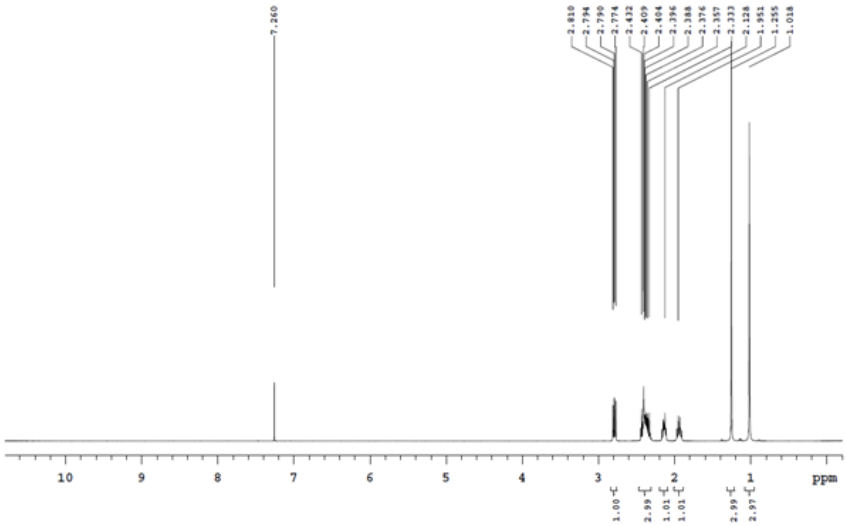

Figure 3.2. ^{1}H NMR spectrum of PA in $CDCl_3$.

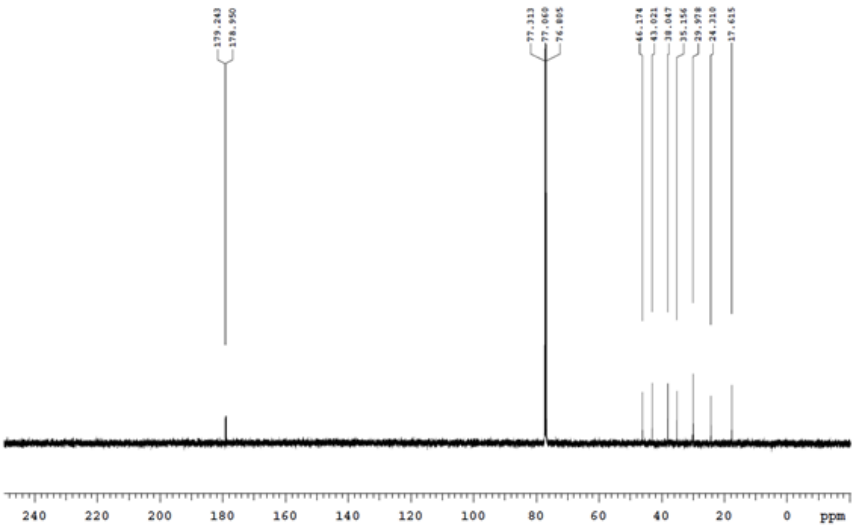

Figure 3.3. ^{13}C NMR spectrum of PA in $CDCl_3$.

3.2.1.2 Synthesis of Limononic Acid

LA is a first-generation product of limonene oxidation and a major product from CPA direct photolysis via Norrish-II type reaction (Figure 3.4).[12,13]

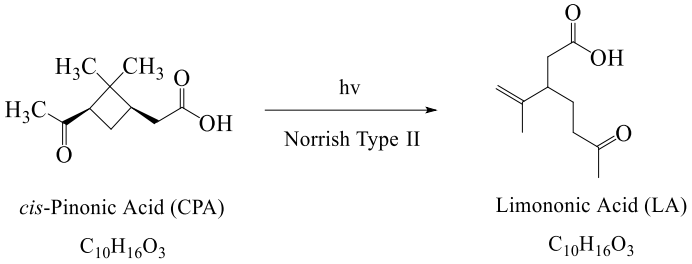

Figure 3.4. Synthesis of LA.

LA was synthesized by exposing 150 mL of a 300 µM solution of CPA in water to UVB radiation at 310 nm. Aliquots were taken every 5 min for a total time of 25 min and the reaction progress was monitored using (-)ESI–LC–MS (see Section 3.2.4.1 for details). The decay of CPA and evolution of LA are shown in Figure 3.5. We photolyzed a CPA solution for enough time to synthesize LA, i.e., until CPA was mostly gone (<10% remaining) and the LA peak shown in the chromatogram (Figure 3.5) did not increase (in terms of signal/counts). Note that the synthesized PA was purified further with preparative reverse phase HPLC, while the LA was not purified further.

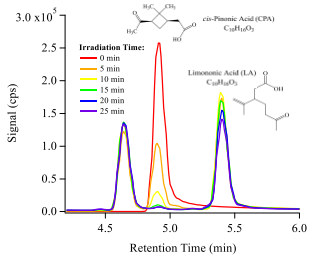

Figure 3.5. (-)ESI–LC–MS selected ion monitoring (SIM) chromatogram of *m/z* 183 (corresponding to both CPA and LA) under direct photolysis. Color coding indicates irradiation time.

3.2.2 Experimental Apparatus

3.2.2.1 SOA Generation and Collection

A flow tube reactor was used to generate α-pinene SOA (Figure 3.6). Under ambient light and in the absence of nitrogen oxides, α-pinene and O_3 react in the flow tube to generate SOA at room temperature.

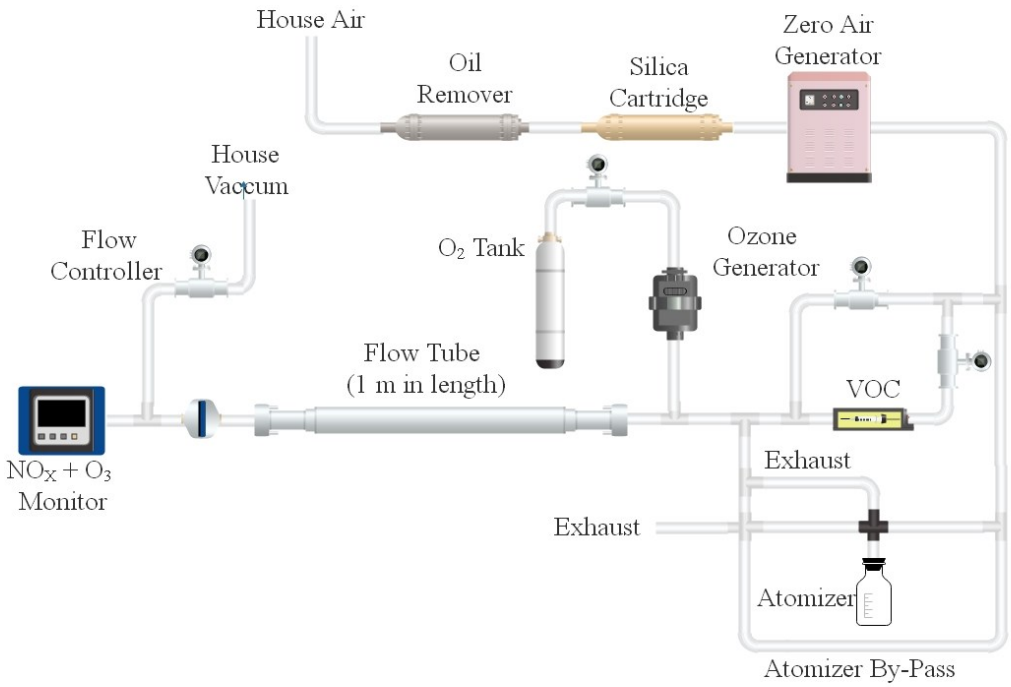

Figure 3.6. Experimental apparatus to generate and collect SOA.

No OH scavenger was added, therefore, α-pinene was oxidized primarily by O_3 but also partially by the OH radical. The flow tube reactor was operated under a steady state of gas, flowing at 2.0 lpm, leading to an average residence time of 2.0 min. The relative humidity (RH) in the flow tube reactor was less than 3%. No seed aerosol is used during SOA generation. An initial test confirmed that the presence of ammonium sulfate seed aerosol did not change the chemical composition of SOA collected using the flow tube reactor. SOA samples were collected on Millipore filters (0.7 μm pore size, hydrophilic glass fiber, 47 mm diameter) for 24 h and immediately frozen at

–16 °C. One filter sample was collected per experiment, having an average SOA mass of 1.5–2.5 mg.

Prior to performing the experiments, the frozen SOA samples were thawed and extracted in 15 mL of Milli-Q water (18.0 MΩ) by stirring with a magnetic bar for 5 min. Then, the solution was filtered using a Millipore Millex-FH Filter Syringe Filter unit (0.45 μm pore size, hydrophobic PTFE, 50 mm diameter). Aqueous SOA samples were thawed, extracted, and analyzed on the same day. The chemical composition of collected SOA was analyzed by the (-)ESI–LC–MS (method described in Section 3.2.4.1).

3.2.3 Bulk Photo-Oxidation Experiments

3.2.3.1 Aqueous Photoreactor

The experimental apparatus consisted of a 150 mL quartz vessel in which the reaction mixture was stirred constantly with a magnetic stir bar. A quartz vessel was used because efficient UV transmission is required for OH regeneration. Due to the small sample volume, a 10 mL quartz vessel was used for the SOA samples instead. For the aqueous-phase photo-oxidation, H_2O_2 30% w/w was added to act as the *in-situ* source of OH radicals, and the reactions were conducted for 10 min. A photoreactor (Rayonet, PRP200) emitting UV-light at 320 nm (UVB) was used to irradiate the reaction mixture. A series of experimental and modeling studies were conducted previously to characterize the photoreactor better (Chapter 2). Thus, we can ensure that the photoreactor used in the following experiments reproduces the appropriate oxidative environment for aqueous phase reactions.

3.2.3.2 Photo-Oxidation Experiments

The OH reactivities of individual OAs, CPA, PA, LA, FA (structures shown in Figure 3.7), as well as the WSOC of α-pinene SOA were determined as a function of pH at room temperature.

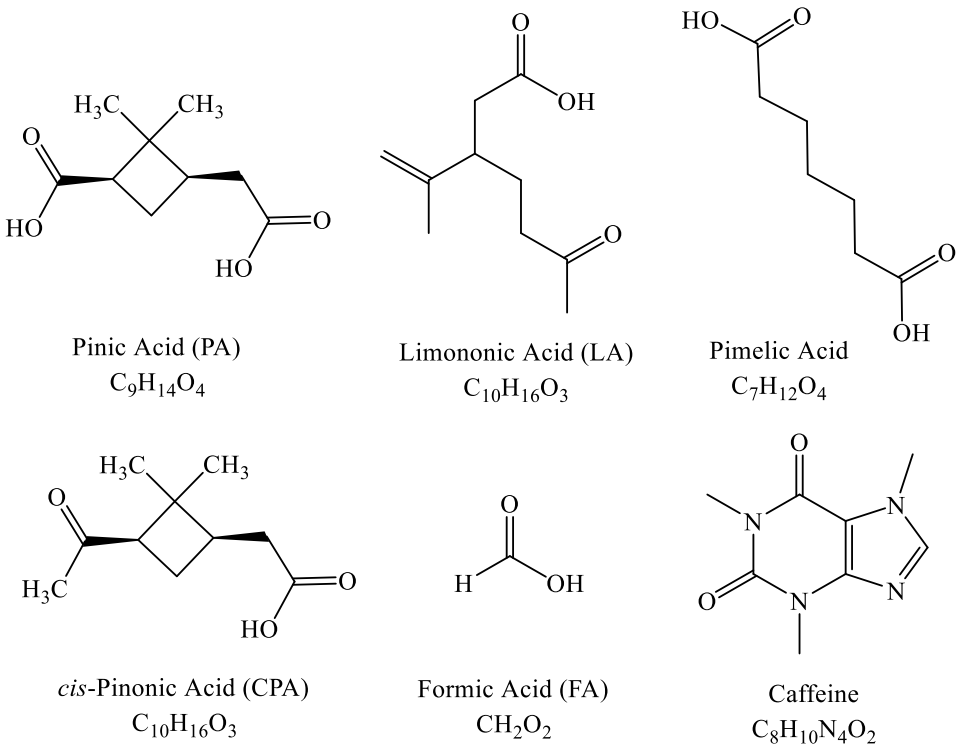

Figure 3.7. Structures of target individual OAs and reference compounds employed in the relative kinetic method.

A target compound and a reference compound were mixed at concentrations summarized in Table 3.1. The pH of the solution was adjusted by adding H_2SO_4 50% wt. (to pH 2) and NaOH 0.5 M (to pH 10). By choosing the experimental conditions at pH 2 and 10, we guarantee that the OAs are either in their protonated (AH) or dissociated forms (A^-), considering their first pK_a values of PA, CPA, and LA are 4.48, 4.83, and 4.76, respectively.[11,13,94] As a third pH condition, we used solutions with uncontrolled pH. The solution of PA, CPA, and LA resulted in pH values of 4.80, 4.85, and 4.30, as confirmed using a standard pH meter (Sartorius).

The reaction progress was monitored by sampling 600 µL of solution from the photoreactor every 2 min for a total irradiation time of 10 min. The samples were analyzed with ESI–LC–MS on the same day. As CPA kinetics was investigated under uncontrolled pH in Chapter 2, the experimental data regarding its direct photolysis and OH-oxidation rates were used in this chapter.

Table 3.1 Experimental Conditions for the Photo-Oxidation Experiments.

	CPA	PA	LA	WSOC of SOA	FA
[Organic Acid]	30 μM	30 μM	-[a]	-[a]	2.6 mM
[Pimelic Acid]$_{Ref}$	0.3 μM	0.3 μM	0.3 μM	1.0 μM	5.0 μM
[Caffeine]$_{Ref}$	0.3 μM	3.0 μM	1.5 μM	1.0 μM	3.0 μM
[H_2O_2]	10 mM	10 mM	10 mM	30.0 mM	150 mM

[a] Concentration was not determined.

We also have confirmed that H_2O_2 itself does not react with the OAs, unless light is shone to produce OH radicals. Therefore, we did not quench the excess H_2O_2 present in the reaction mixture after taking the sample out of the photoreactor. The volume and composition of reaction mixtures were identical as in the OH-oxidation experiments, but no H_2O_2 was added. Experiments were performed in triplicate for each pH condition, and all data are expressed as the mean ± standard deviation.

For the kinetics study of FA, a 2.6 mM solution of FA initially was prepared, and 50 mL were taken for each experiment. Reaction solutions were prepared at concentrations of 150 mM of H_2O_2 30% v/v, 5 μM pimelic acid for pH 2 or 3 μM caffeine for pH 10. The pH of the solution was adjusted, as described previously, and the reaction was monitored using an Ion Chromatography (IC) instrument. We had to use much higher concentrations of FA and H_2O_2 here to accommodate the concentration requirement of the IC instrument (see Section 3.2.4.2 for details).

3.2.3.3 Relative Kinetic Method and OH Rate Coefficient Determination

The relative kinetic method was employed in the determination of OH reactivities. By monitoring the loss of a target compound relative to that of a reference compound with known OH rate constant (k_R^{II}), we can infer the second-order rate coefficient of the target species (k_S^{II}) using Eq. (3.1).[35,94]

$$\ln\left(\frac{[S]_0}{[S]_t}\right) = \frac{k_S^{II}}{k_R^{II}} \ln\left(\frac{[R]_0}{[R]_t}\right) \qquad \text{Eq. (3.1)}$$

In Eq. (3.1), [*S*] represents the concentration of the target OA, i.e., PA, CPA, LA, or FA. [*R*] is the concentration of a reference compound. The k_{OH}^{II} of the target OA can be obtained by a relative kinetic plot, where $\ln([S]_0/[S]_t)$ is plotted against $\ln([R]_0/[R]_t)$. The curve should appear linear, with the slope representing the ratio between k_S^{II} and k_R^{II}. For experiments at pH 2 and uncontrolled pH, pimelic acid was chosen as the reference compound, whose k_{OH}^{II} values at pH 2 and 4 have been determined by Schaefer et al.[23] For the pH 10 experiments, caffeine was chosen as the reference compound, as its reliability has been proven by a series of studies performed by Witkowski and Gierczak.[12,78]

3.2.4 Chemical Analysis

3.2.4.1 ESI–LC–MS Analysis of PA, CPA, LA and SOA

The major analytical method employed in this study was liquid chromatography–mass spectrometer (LC–MS) (Agilent 1100 LC MSD Model G1946D), a quadrupole-based instrument with electrospray ionization (ESI). To maximize sensitivity, the acquisition was performed in selected ion monitoring (SIM) mode, in which only the *m/z* of relevant compounds (OAs and reference compounds) were monitored. The negative mode (-)ESI–LC–MS was employed primarily because of its selectivity towards OAs.[64] For caffeine, which is detectable with only the positive mode (+)ESI–LC–MS, the method was set up in the way that the polarity of the MS is changed to the positive mode only at the retention time of the caffeine peak (3.12 min, *m/z* 195).

The same column and method were employed for both individual OAs and SOA samples, as follows: ESI–LC–MS analyses were carried out using a reverse phase Kinetex (Phenomenex) Polar C18 column (50 x 2.1 mm, 2.6 µm, 100 Å) kept at 35.0 °C and equipped with a security guard cartridge with a 2.1 mm ID C18 pre-column. For the investigation of individual OAs, eluent A was a formic acid solution in water (pH = 2.8), and eluent B was acetonitrile, delivered at a flow rate of 0.5 mL/min; the injection volume was 15 µL. For the experiments involving the OAs present in a water-soluble fraction of α-Pinene SOA, methanol was used as eluent B. The ESI conditions were as follows: capillary voltage was –4.5 and +5.5 kV in the

negative and positive ionization modes. ESI in positive mode ((+)ESI) was used to detect caffeine at pH 10 conditions.

The gradient elution programs for the reactions of individual OAs were different from those in the α-pinene SOA:

Gradient Elution Program for PA, CPA and LA. 0.0−0.5 min isocratic 5% B, 0.5−5.0 min linear gradient to 30% B, 5.0−6.0 min linear gradient to 95% B, 6.0−6.7 min isocratic 95% B, 6.7−7.0 min linear gradient to 5% B. Afterward, the column was re-equilibrated at 5% and the analysis was complete in 11.5 min.

Gradient Elution Program for the a-Pinene SOA Analysis. 0.0−1.0 min isocratic 1%, 1.0−6.0 min linear gradient to 35%, 6.0−11.0 min linear gradient to 50% B, 11.0−12.5 min linear gradient to 95% B, 12.5−14.5 min isocratic 95% B, 14.5−15.0 min linear gradient to 1% B. Afterward, the column was re-equilibrated at 1%, and the analysis was complete in 19.0 min.

3.2.4.2 IC Analysis of Formic Acid

A Dionex ICS 5000+ chromatograph (Thermo Scientific) was used for the analysis of FA at pH 2 and pH 10. Separation was achieved using a Dionex IonPac® AS18 (4 x 150 mm) anion exchange column with a Dionex IonPac® AG18 guard column (4 x 30 mm). The eluent was potassium hydroxide (KOH) run at a flow rate of 1.0 mL/min. The gradient method held 12 mM KOH for 1 min, then increased to 30 mM KOH from 1–14 min, then held at 44 mM KOH from 14–15 min, then equilibrated at 12 mM KOH from 15–18 min, for a total run time of 18 min. Formate standards at concentrations of 0.25, 0.50, 0.75, 1.0, and 2.5 ppm were made from their salts for instrument calibration, and water was used as the blank (0 ppm) standard. Offline LC–MS was carried out on the same day of IC analysis to monitor the decay of reference compounds over the irradiation time.

The conductivity detector on the IC system cannot tolerate SO_4^{2-} concentrations greater than 10 ppm. This posed a challenge to our pH 2 experiment, as we had to add 600 ppm of H_2SO_4 for pH adjustment. A dilution factor of 60 was required for the sample to be compatible with the IC analysis. Hence, we had to use much higher concentrations of FA and H_2O_2 to accommodate this requirement.

3.2.5 Kinetic Modeling

A kinetic box model using CPA as a model compound was applied in Chapter 2 to characterize the photoreactor thoroughly. The same model was applied here to examine a few scenarios (Table 3.2) to assist our experiment. First, the model was extended to a wider pH range to gauge the impact of pH on radical chemistry in the system. Next, a focus was placed on the chemistry of the sulfate radical (SO_4^-), to evaluate its potential impact on the radical chemistry. This was particularly relevant to our pH 2 condition, in which H_2SO_4 was added for pH adjustment. The reactions and their rate coefficients used in the model are summarized in Chapter 2, Table 2.1.

Table 3.2 Initial Concentrations Used in Model Scenarios.

Scenarios	CPA (µM)	H_2O_2 (mM)	Ref. Compound (µM)	pH	SO_4^- Chemistry
Simulating Experimental Results					
CPA direct photolysis	30	0	0	4	No
CPA OH-oxidation	30	10	0.3	2,4,10	No
Investigating the Impact of pH					
CPA OH-oxidation	30	10	0	2,4,10	No
Investigating the Impact of SO_4^-					
CPA OH-oxidation	30	10	0.3	2	Yes

3.2.5.1 Reproducing Experimental Results

The model was operated first to reproduce experimental results of CPA direct photolysis and OH-oxidation. For CPA direct photolysis, the H_2O_2 concentration was prescribed to be 0. Given that the direct photolysis rate of CPA was not dependent on pH, we simulated only a single pH condition (pH 4). For CPA OH-oxidation experiments, the H_2O_2 initial concentration was set to match that used in the experiment, and the subsequent radical chemistry is simulated in the model. The initial pH value was set to be 2, 4, and 10, where pH 4 was used to represent the experiments conducted under uncontrolled pH. The experimentally determined k_{OH}^{II} values of CPA (Section 3.2.3.2) under each pH condition were employed in these simulations. The

reference compounds, pimelic acid (PMA) for acidic conditions and caffeine (CAF) for pH 10, also were considered in the simulations.

3.2.5.1 Impact of pH

To evaluate whether an altering pH will affect the steady-state OH concentration ($[OH]_{ss}$), and hence affect the decay rate of CPA, a case study was conducted to investigate the potential impact of pH. In this case, the reactivity of CPA was prescribed to be a fixed value (2.9×10^9 M^{-1} s^{-1}) across the entire pH range. The initial concentration was set to be pH 2, 4, and 10 for the simulations. The reference compounds and their chemistry were excluded from this case.

3.2.5.2 Potential Impact of Sulfate Radical Formation

Studies from past years have observed the formation of organo-sulfate compounds under irradiated conditions,[95,96] presumably due to the chemistry of sulfate radicals (SO_4^-) and bisulfate radicals (HSO_4). In our pH 2 experiments, H_2SO_4 was added to the solution for pH adjustment. A case study was conducted to explore whether SO_4^- can form and affect the decay of CPA at pH 2 using rate coefficients available on the literature.[36] It is assumed that the only formation mechanism of SO_4^- is from OH + bisulfate anion (HSO_4^-), with the rate coefficient provided in McNeil et al.[8] The rate coefficient of SO_4^- + CPA has not been reported. We assumed that SO_4^- reacts with CPA as rapidly as OH reacting with CPA (i.e., $k_{OH}^{II} = 2.9 \times 10^9$ M^{-1} s^{-1}). We note that this is an upper-band estimate for the impact of SO_4^-, as previous studies have shown that the reactivity of SO_4^- can be much smaller than that of OH, at times by a factor of 50 to 100.[36] Another aspect of SO_4^- that is of great interest is its ability to regenerate OH radical through reactions with H_2O and OH^-. The rate coefficient of this reaction has been reported by Hermann et al.[82]

3.3 Results and Discussion

3.3.1 OH Reactivities of PA, CPA, and LA

Figure 3.8 shows a (-)ESI–LC–MS selected ion chromatogram for a typical PA OH-oxidation experiment at pH 2. The color scheme represents the irradiation time during the photo-oxidation experiment. Figure 3.8 clearly demonstrates that both PA and pimelic acid exhibit rapid decay with photo-oxidation. Experiments for CPA and LA yielded similar results, and their selected ion chromatograms are shown in Figures 3.6 and 3.7. The inset in Figures 3.8–3.10 presents a relative kinetic plot, as explained in Section 3.2.3.3. For PA, CPA, and LA plots, the curve is linear (R^2 = 0.999983, 0.998667, and 0.99415, respectively), indicating the validity of the relative kinetic method. Among these three OAs, only CPA underwent observable direct photolysis, as shown in Figure 3.11.

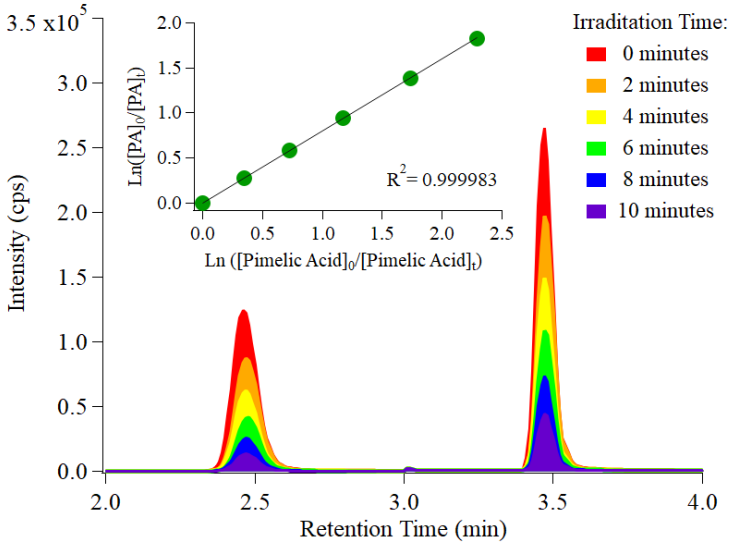

Figure 3.8. SIM chromatogram of PA (*m/z* 185) and pimelic acid (reference compound, *m/z* 159).

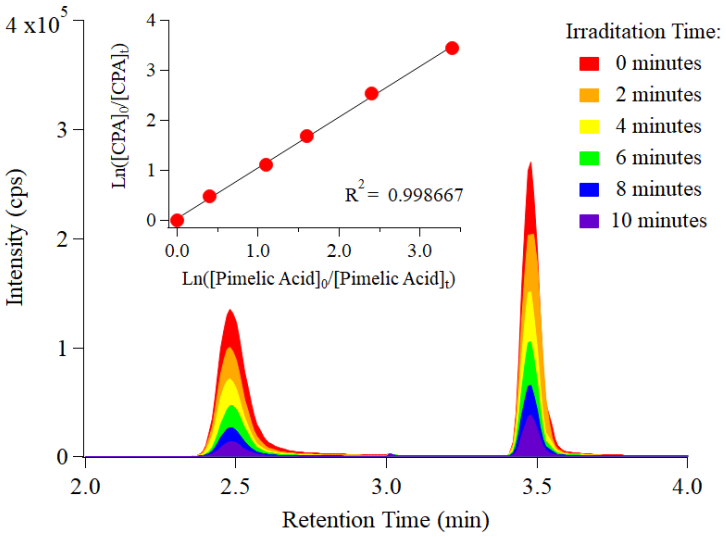

Figure 3.9. SIM chromatogram of CPA (*m/z* 183) and pimelic acid (reference compound, *m/z* 159) under 10 min of UVB irradiation.

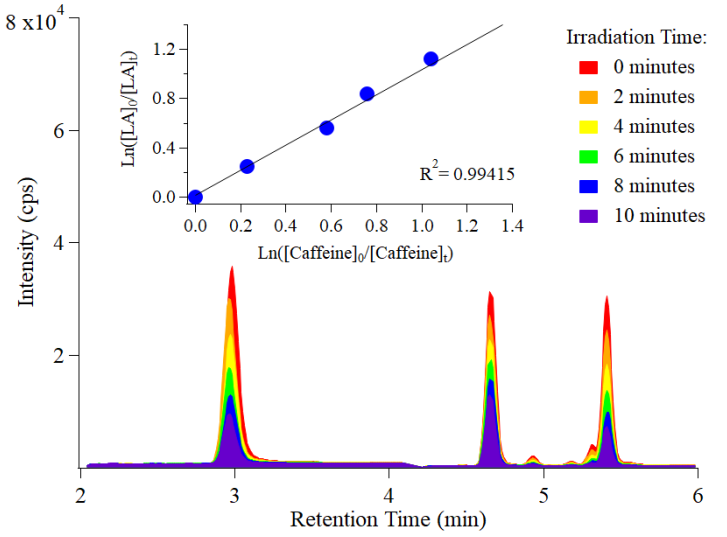

Figure 3.10. SIM chromatogram of LA (*m/z* 183) and caffeine (reference compound, *m/z* 195) under 10 min of UVB irradiation. LA peak is the one most retained (longer retention time) in the chromatogram.

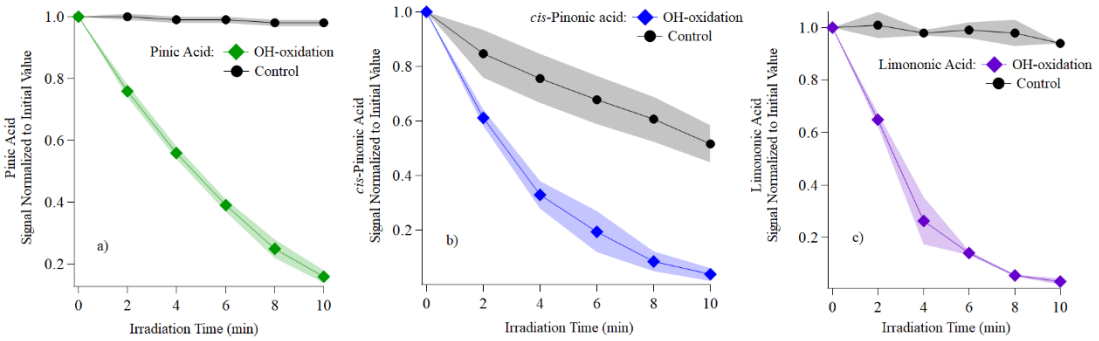

Figure 3.11. OH-oxidation and control experiments for a) PA, b) CPA and c) LA at pH 2. Signal of the target compound is shown as a function of irradiation time. The shaded area presents 1 σ from triplicates.

Figure 3.11 shows a comparison of the behavior of PA, CPA, and LA under direct photolysis and OH-oxidation at pH 2 only, but similar results were obtained under uncontrolled pH and pH 10. Thus, the contribution of CPA direct photolysis was considered when determining the pseudo-first-order decay rate of CPA observed during OH-oxidation. Using Eq. (3.1), the k_{OH}^{II} for these three individual OAs are calculated and summarized in Table 3.3, along with literature values where applicable. While CPA kinetics has been studied extensively,[12,35,97] the photochemical behaviour of PA in the aqueous phase is still unknown. Regarding LA, Witkowski et al.[13,62] have investigated its aqueous phase oxidation by OH radicals under acidic (pH 2) and basic (pH 10) conditions. The determined k_{OH}^{II} values of PA, CPA, and LA are near to but are not achieving the diffusion limitation of aqueous phase reactions with OH radicals. The diffusion-limited k_{OH}^{II} for CPA at 298 K is estimated to be approximately 9×10^9 M^{-1} s^{-1}, based on an equation used by He et al.[39] LA has a relatively larger k_{OH}^{II} than CPA and PA because LA has an unsaturated bond in its structure (Figure 3.7), which makes this OA more reactive toward OH radicals via the OH-addition mechanism.[13] Table 3.3 shows that the measured k_{OH}^{II} at pH 2, uncontrolled pH and pH 10 for these three individual OAs increases slightly with the pH. This pH dependence is likely attributed to the electron-transfer reaction unique to carboxylate.

Table 3.3 Calculated Bimolecular Rate Coefficient for OAs Reactions with OH Radicals (k^{II}_{OH} in $\times 10^9$ M^{-1} s^{-1}).

pH	Reference Compound	OAs	k^{II}_{OH} This study	k^{II}_{OH} Literature [12,77]
2	Pimelic Acid	PA	(1.7 ± 0.0)	N/A
		CPA	(2.1 ± 0.1)	(3.6 ±0 .3)
		LA	(5.1 ± 0.1)	(13.0 ± 0.3)
Uncontrolled	Pimelic Acid	PA	(2.9 ± 0.0)	N/A
		CPA	(3.0 ± 0.0)	N/A
		LA	(7.1 ± 0.1)	N/A
10	Caffeine	PA	(2.9 ± 0.0)	N/A
		CPA	(3.7 ± 0.0)	(3. 0 ± 0.3)
		LA	(7.9 ± 0.1)	(5.7 ±0 .6)

In contrast to our findings, Aljawhary et al.[35] and Witkowski et al.[12] did not observe a pH dependence on the k^{II}_{OH} value of CPA. This is likely because the rate coefficient of the OAs determined by the relative kinetic method depends strictly on the reference compound k^{II}_{OH} values. We are aware that Witkowski et al.[12,13,98] conducted a series of studies on monoterpene related compounds and have been using a different reference value for pimelic acid's rate constant under acidic conditions ($k^{II}_{OH} = 3.5 \times 10^{-9}$ M^{-1} s^{-1}). When we used this reference k^{II}_{OH} value, we also obtained very similar CPA k^{II}_{OH} values across the three pH conditions (i.e., in agreement with Witkowski et al.[25]).

Our LA results are consistent with the results by Witkowski et. al.[13] in terms of pH dependence. However, the absolute values differ up to a factor of 4 (at pH 2). We note that the LA synthesized in our work is not purified further. The LA experiments were conducted when its precursor, CPA, is consumed completely by photolysis. Therefore, further formation of LA due to CPA photolysis should make a minor

contribution (<1%, based on our estimation) to the decay kinetics of LA. However, we recommend that our results be confirmed with pure LA standards in future studies.

3.3.2 Model Simulation for CPA Photochemistry

Given that the direct photolysis rate of CPA was not dependent on pH, we simulated only a single pH condition (pH 4). From Chapter 2 observations, a CPA quantum yield of 0.69 is the appropriate value to be used in order to match the simulated direct photolysis rate of CPA to the observation (1.04×10^{-3} s^{-1}) at pH 4. For OH-oxidation experiments, the agreement between observation and simulation was generally good. In particular, the agreement of pseudo-first order rate coefficients of CPA were within 1.6% and 6.1% for pH 2 and 4, respectively. For pH 10, the simulation overestimated the rate of CPA decay by 23%. A model-observation comparison is performed and is shown in Figure 3.12.

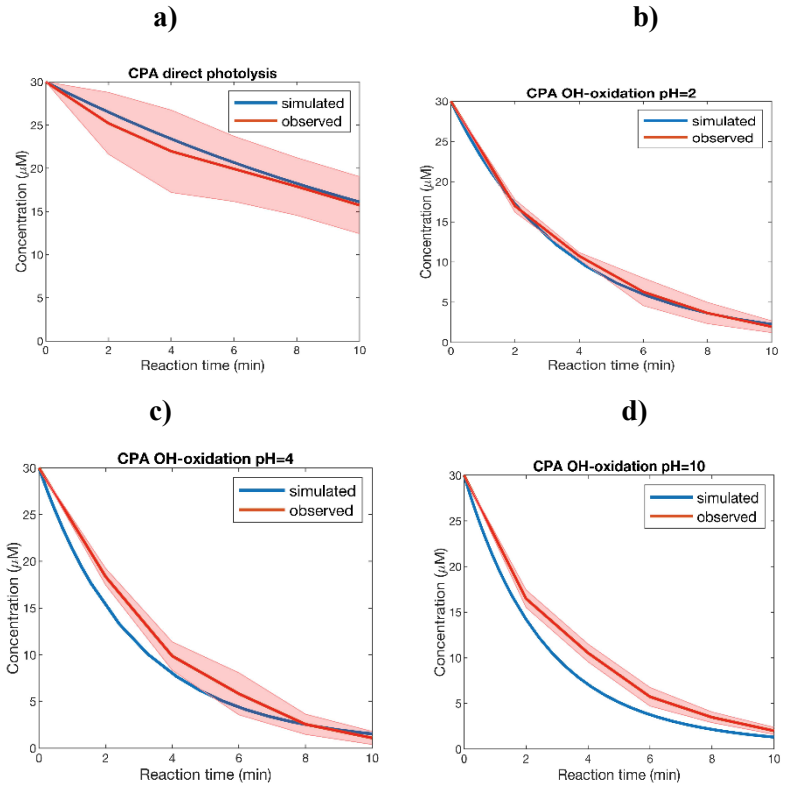

Figure 3.12. Simulated and observed CPA concentration in **a)** direct photolysis, **b)** OH-oxidation at pH 2, **c)** OH-oxidation at pH 4, and **d)** OH-oxidation at pH 10. The shaded area presents the observed data standard deviation range (1 σ). The model result in **a)** employs the optimized CPA Φ(λ) value: 0.69 across the relevant wavelength rage.

3.3.2.1 Impact of pH conditions

The impact of pH on the concentration of OH radicals ([OH]) was investigated and is shown in Figure 3.13. [OH] was indifferent between the pH 2 and 4 conditions. At pH 10, the [OH] was lower by approximately 10% at the beginning of the experiment. This is due to the dissociation of HO_2 into O_2^-, leading to a significant sink of OH by $OH + O_2^- \rightarrow OH^- + O_2$. At pH 10, this reaction consumes 25 and 2.5×10^3 times more OH than at pH 4 and 2, respectively. Despite this reaction, our simulation confirms that acid-base chemistry leads only to a minor difference in [OH] across the pH range investigated in this work.

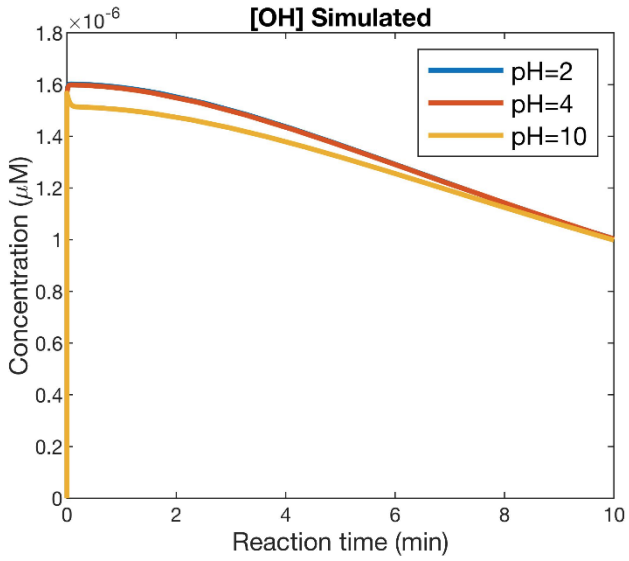

Figure 3.13. OH concentrations simulated at pH 2, 4, and 10.

3.3.2.2 Impact of SO_4^-

The potential impact of the SO_4^- chemistry is presented in Figure 3.14. Previous studies have demonstrated that SO_4^- can form during irradiation, reacting with organic compounds[8,23] and affecting the OH radical cycle in the chemical system. However, the SO_4^- chemistry made negligible differences in both the [OH] and CPA decay rate. Overall, the model results provide more insights into photochemistry occurring in our photoreactor, which adds more confidence to our conclusion in Section 3.3.1.

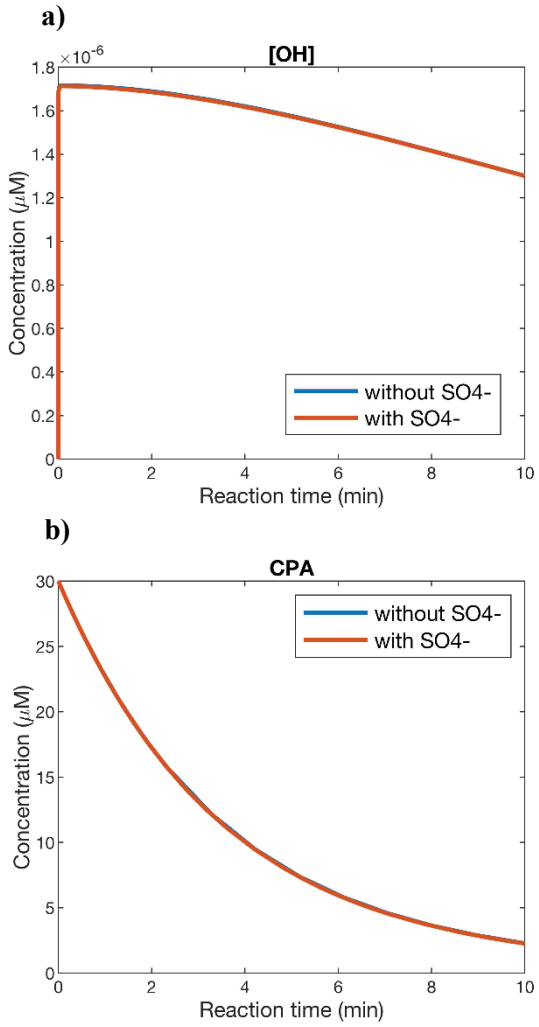

Figure 3.14. The simulated **a)** [OH] and **b)** CPA concentration with and without the SO_4^- chemistry included in the model.

3.3.3 Comparison between Larger and Smaller OAs

The pH dependence in k_{OH}^{II} for PA, CPA, and LA is much less pronounced than in the cases of small OAs. As mentioned in Section 3.1, a study conducted by Ervens et al.[20] showed that for small OAs, the OH reactivity under basic conditions could be larger by up to an order of magnitude. To verify this trend for small OAs, we used IC to monitor the photo-oxidation of FA using the same photoreactor. We found that k_{OH}^{II} of FA (at pH 2) was 0.8×10^8 M^{-1} s^{-1}, while that under basic conditions (pH 10, for formate) was 2.9×10^9 M^{-1} s^{-1}. The values determined in this work are in reasonable agreement with Ervens et al.,[20] 1.0×10^8 M^{-1} s^{-1} at pH 2 and 2.4×10^9 M^{-1} s^{-1} at pH 10. Such pH dependence in OH reactivity is observed not only for FA but for a suite of small OAs,

typically up to C3: glyoxylic acid, pyruvic acid, lactic acid, and malonic acid, as reviewed by Zhao et al.[99] Although our results for PA, CPA, and LA show an increase in their k_{OH}^{II} with increasing pH, their overall k_{OH}^{II} values are within a factor of 2 compared to a factor of 38 for FA. To make a clear comparison between OAs studied in this work, their k_{OH}^{II} values are summarized in Figure 3.15. Note that the y-axis is presented in the log scale to accommodate the drastically different k_{OH}^{II} of FA at pH 2 and 10. It is clear that the pH dependence in k_{OH}^{II} values of PA, CPA, and LA is drastically smaller than that of FA.

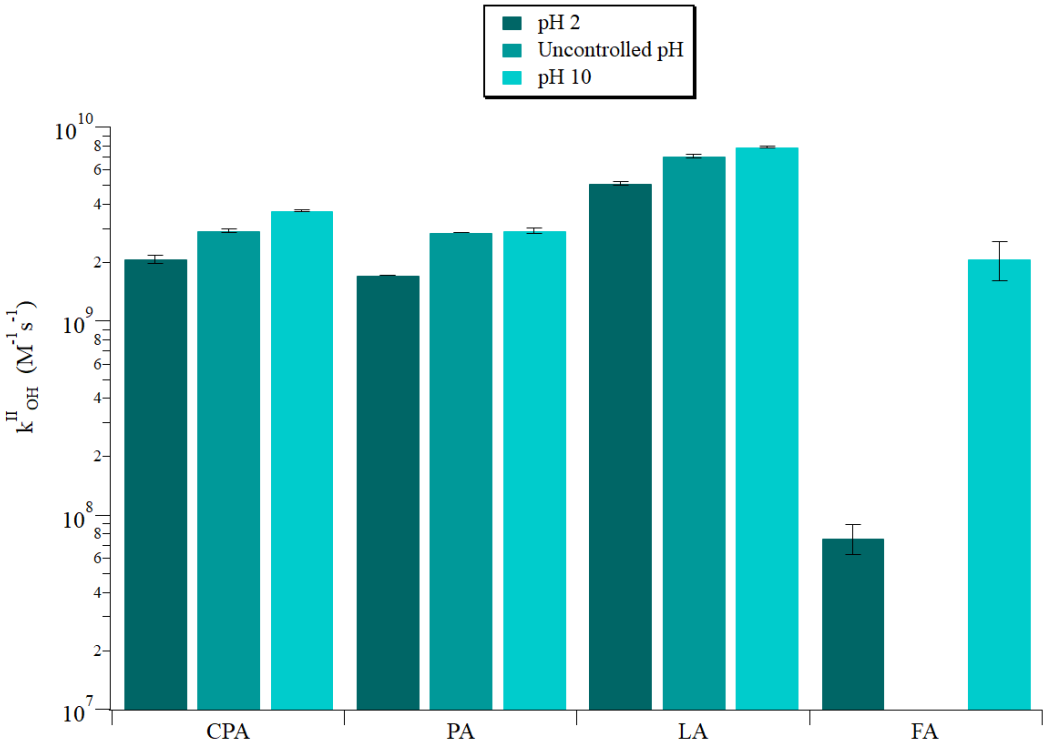

Figure 3.15. OH reactivities of CPA, PA, LA, and FA at pH 2, uncontrolled pH conditions and pH 10. Experiments of FA were conducted at pH 2 and 10 only.

These results support our hypothesis that C_9 to C_{10} OAs relevant to α-pinene photo-oxidation do not exhibit a significant pH dependence in their OH reactivities. Similar results were found recently by Schaefer et al.[77] when investigating the kinetics of the aqueous phase oxidation of pimelic acid and succinic acid under different temperature and pH conditions, in addition to several mono- and dicarboxylic acids.

The smaller pH dependence in the k_{OH}^{II} values of PA (C_9), CPA (C_{10}), and LA (C_9) with increasing atmospheric pH is likely due to the large alkyl group (>C_5). The alkyl group provides multiple sites with which an OH radical can react, diminishing the relative importance of the carboxylate and electron-transfer reaction. On the other hand, the larger increase of rate constant with increasing pH of FA and other small OAs could be explained by the electron-transfer reaction of carboxylate as well as a greater carboxylate group effect on the molecule. This effect causes a reduction of the C-H bond dissociation energy, resulting in a faster reaction with OH radicals under basic conditions.

3.3.4 OH Reactivities of Other OAs in α-Pinene SOA

PA, CPA, and LA are three representatives among a countless number of OAs present in α-pinene SOA,[11,35,99] and the observations made for these three OAs also may be applicable to others. To test this hypothesis, we have extended our study to other long-chain OAs detected in the WSOC of α-pinene SOA and investigated their k_{OH}^{II} values at uncontrolled pH, pH 2 and 10. An example of a SOA base peak intensity chromatogram measured with our (-)ESI–LC–MS method is available in Section 3.2.4.1. The chromatogram is in good agreement with previous works on the water-soluble fraction of α-pinene SOA.[100–104] We focused on six major OA peaks, including those with *m/z* 171, 183, 185, 199, 215, and 357. These species have been detected by previous studies[64,89,90,102] and were proposed as norpinic or terpenylic acid, CPA, PA, an isomer of OH-CPA, a potential peroxide and pinyl-diaterpenylic ester, respectively. We note that PA and CPA are included in this list again to investigate whether they behave in a similar manner when treated individually or as part of SOA WSOC.

The photo-oxidation of α-pinene SOA in aqueous phases is highly complex. Here, the assumptions are that direct photolysis and OH-oxidation are the only loss pathways for WSOCs and that the photochemical formation of each compound is negligible during the experiment. The decay of these OAs over time is presented in Figure 3.16, along with their chemical structures. In order to extract the k_{OH}^{II} of each

OAs, the importance of direct photolysis was taken into account at uncontrolled pH, pH 2 and 10 based on the control experiment (no H_2O_2 added).

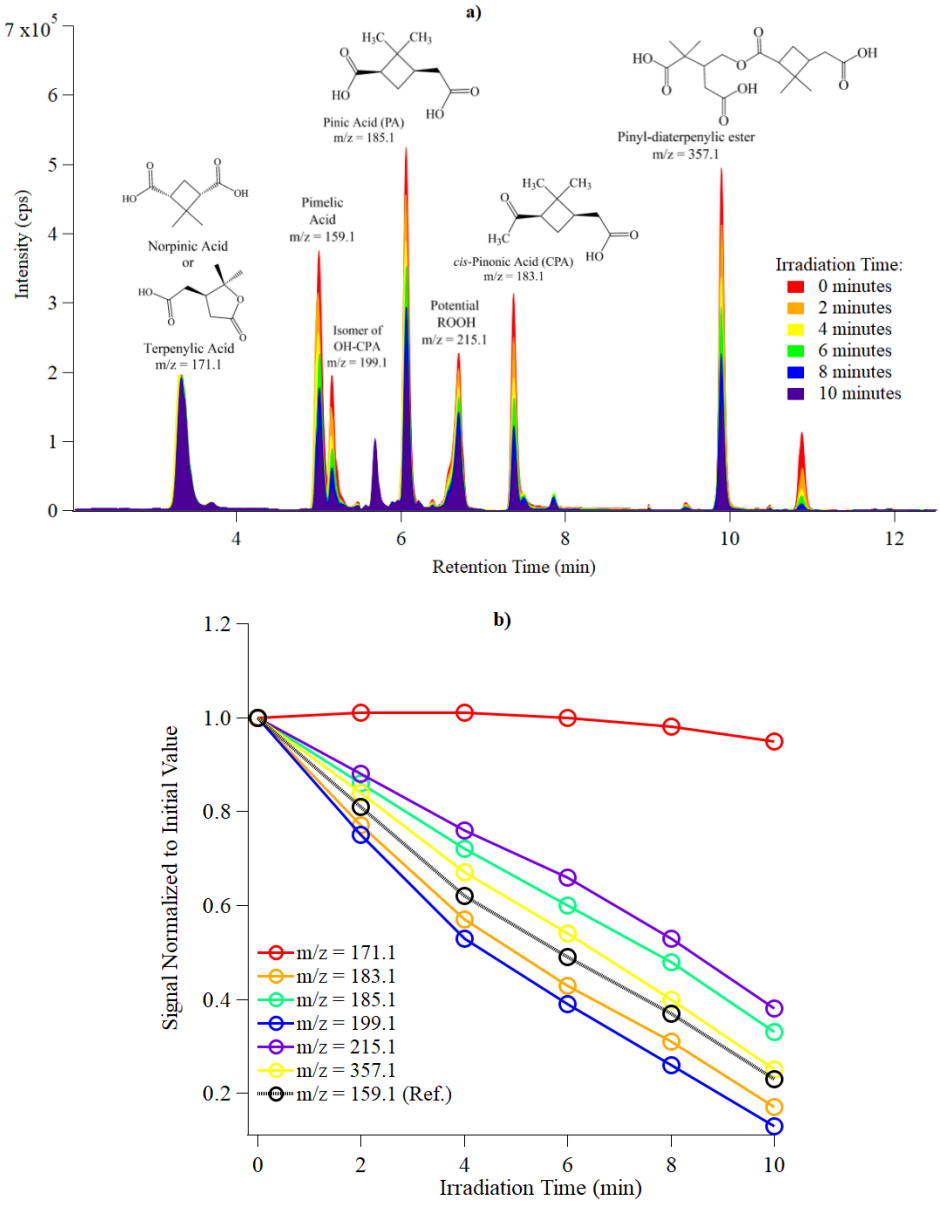

Figure 3.16. a) SIM chromatogram of α-pinene SOA at uncontrolled pH conditions (with multiple *m/z* monitored) and **b)** OAs decay during an OH-oxidation experiment. Color coding on the left panel indicates irradiation time.

Among the OAs, only the species with *m/z* 215 and *m/z* 183 underwent direct photolysis; therefore, their first-order loss rates (min^{-1}) were considered when calculating k_{OH}^{II}. The peak of *m/z* 183 is attributed to CPA, whose direct photolysis has

been discussed in Section 3.3.1 already. Studies have shown that organic peroxides can be photolyzed readily in aqueous-phases,[103,104] and the OA of *m/z* 215 has been proposed previously to be an unknown peroxide.[64] Figure 3.17 shows the comparison of the calculated k_{OH}^{II} values for the OAs extracted from α-pinene SOA under varied pH conditions. A table containing the calculated k_{OH}^{II} for each OAs is presented below (Table 3.4). The k_{OH}^{II} values of PA and CPA obtained in the SOA WSOC showed good agreement with values obtained from their individual solutions (Table 3.3).

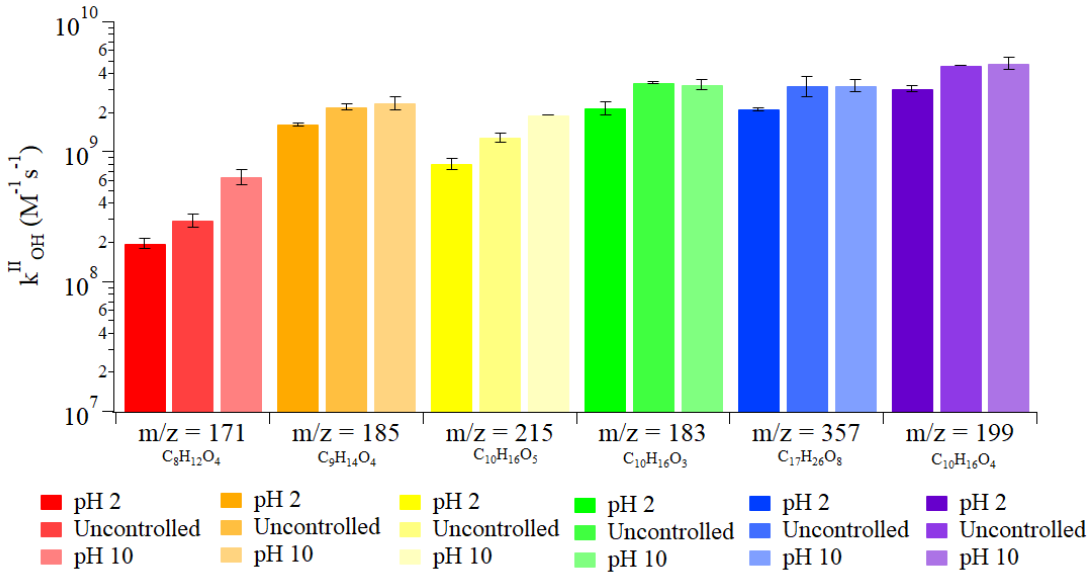

Figure 3.17. OH reactivities of α-pinene SOA OAs at uncontrolled pH, pH 2 and 10.

Table 3.4 Bimolecular Rate Coefficient for α-Pinene SOA WSOC's Reactions with OH Radicals (k_{OH}^{II} in M^{-1} s^{-1}).

	m/z	pH 2	Uncontrolled pH	pH 10
Norpinic or Terpenylic Acid	171	$(2.0 \pm 0.2) \times 10^8$	$(2.9 \pm 0.4) \times 10^8$	$(6.4 \pm 0.9) \times 10^8$
PA	185	$(1.6 \pm 0.0) \times 10^9$	$(2.2 \pm 0.1) \times 10^9$	$(2.4 \pm 0.3) \times 10^9$
Potential Peroxide	215	$(8.2 \pm 0.1) \times 10^8$	$(1.3 \pm 0.1) \times 10^9$	$(1.9 \pm 0.0) \times 10^9$
CPA	183	$(2.2 \pm 0.3) \times 10^9$	$(3.4 \pm 0.1) \times 10^9$	$(3.3 \pm 0.3) \times 10^9$
Pinyl-diaterpenylic Ester	357	$(2.1 \pm 0.1) \times 10^9$	$(3.2 \pm 0.6) \times 10^9$	$(3.2 \pm 0.4) \times 10^9$
Isomer of OH-CPA	199	$(3.1 \pm 0.0) \times 10^9$	$(4.7 \pm 0.0) \times 10^9$	$(4.8 \pm 0.1) \times 10^9$

This result confirms that our relative kinetic method is valid in both individual aqueous solutions and complex mixtures, such as WSOC. These results again confirm that the OH reactivity of PA and CPA in atmospheric aqueous phases are less affected by the medium pH. The data summarized in Table 3.4 shows that the k_{OH}^{II} values of the investigated OAs all increase slightly with increasing pH, which is expected considering the contribution of the carboxylate electron-transfer reaction. In particular, the dimeric compound with *m/z* 357 (C_{17}) exhibited a rate constant similar to the value published by Zhao et al.[58] The fact that the k_{OH}^{II} value of this dimer is similar to those of monomers implies that the reaction may be diffusion-limited. The kinetics of dimers important to α-pinene SOA has been studied previously by Zhao et al.,[58] though the relationship between the k_{OH}^{II} of dimers and aqueous-phase pH has not been investigated. Dimers of similar molecular structures, e.g., pinonyl-pinyl ester and pinyl-diaterbyl ester, likely will show a similar pH dependence.

The peak at *m/z* 171 did not follow the trend of other OAs. In Figure 3.17, we notice that the decay of this compound was an order of magnitude slower than those of others. Judging from its proposed structure, there is no reason for this compound to be particularly resilient to OH-oxidation. Thus, the compound at *m/z* 171 seems to be reacting with OH radicals and being formed simultaneously. Currently, we have treated it in the same way as other compounds, assuming it is undergoing a pseudo-first-order decay. More careful analysis should be done for the identification of its sources and sinks in the future. The compound at *m/z* 215 reacted faster at pH 10 than at the other pH conditions by 40%. The reason for such a trend is unclear. This compound has been proposed previously to be an unknown organic peroxide. [58] Whether organic peroxides (e.g., peracids) behave differently at different pH warrants future investigations.

The k_{OH}^{II} values of the six OAs in the WSOC are summarized in Table 3.4. Overall, despite the complexity of WSOC and its photochemistry, our results show that the OAs follow a relatively uniform pH dependence in their OH reactivities. The ratio of OH reactivity between carboxylate (pH 10) and carboxylic acid in the current set of OAs is 1.7 ± 0.3. In future, the list of compounds can be extended to investigate whether this ratio can cover a wider spectrum of OAs in SOA.

3.4 Environmental Implications

Cloudwater and fogs are important reaction media for many organic compounds in the atmosphere.[4,7,46] The investigation of the kinetics of relevant species is necessary to improve our fundamental understanding of the pH dependence of the aqueous-phase photochemistry. To examine the impact of our result on the atmospheric lifetimes of OAs, we did a case study on PA. PA does not undergo direct photolysis, and OH-oxidation is its only sink in the aqueous phase. At pH 2, uncontrolled pH, and pH 10, the k_{OH}^{II} values of PA are 1.7×10^9, 2.9×10^9, and 2.9×10^9 M^{-1} s^{-1}, respectively. Assuming a typical $[OH]_{ss}$ of 2.2×10^{-14} M,[23] the lifetime of PA (τ_{aq}) in atmospheric aqueous phases under different pH conditions can be calculated using Eq. (3.2):

$$\tau_{aq,\,OH} = 1/(k_{OH}^{II} \times [OH]_{ss}) \qquad \text{Eq. (3.2)}$$

The $\tau_{aq,\,OH}$ for PA was calculated to be 7.3 h at pH 2, 4.4 h under uncontrolled pH, and 4.3 h at pH 10. Assuming that cloud water is present 15% of the time,[105] these values can be translated into atmospheric lifetimes of 51 h, 31 h, and 30 h, respectively. CPA and LA follow a similar trend, driven by the difference of their k_{OH}^{II} values. Their OH-oxidation lifetimes under basic conditions can be shorter by a factor of up to 1.7, compared to those under acidic conditions. Our investigation for other species in α-pinene SOA indicates that many other OAs may follow a similar pH dependence. According to Pye et al.[55], the reduction of emissions of acid precursors in the past 30 years led to an increase in the pH of fogs and cloud waters in many regions around the globe. The results obtained here show that this change in pH likely will affect the lifetime of OAs. However, the impact on a-pinene relevant OAs is not nearly as much as in the case of small OAs, such as FA. A similar lifetime analysis performed on FA yields an atmospheric lifetime of 1163 h (48 days) under acidic conditions and 30 h at basic conditions, which is a factor of 38 difference. Thus, the cloud and fog processing of small OAs, e.g., formic acid, glyoxylic acid, pyruvic acid, will occur much more rapidly with an increasing cloudwater pH. Many of these small OAs have been shown to be aqSOA components.[67,106–108] Thus, the aqSOA formation rate and loading may be affected by changes in the pH of fog and cloud waters.

Given that SOA contains tens of hundreds of compounds, with the majority currently unidentified, it is important to extract trends that can be extrapolated to a wider range of species. A few studies have made progress in this direction. Arakaki et al.[108] investigated the relationship between the k_{OH}^{II} and the numbers of carbon in molecules. While the k_{OH}^{II} of small OAs can vary over 3 orders of magnitude, the same is not true for larger molecules since k_{OH}^{II} values reach a diffusion-controlled rate constant. Zhao et al.[58] looked into a lumped reactivity of specific dimers present in α-pinene SOA components. Their findings indicate that many of the dimers had similar reactivities. Our conclusion adds to their studies by showing that many of the OAs relevant to α-pinene SOA, such as CPA, PA, and LA, indeed show similar k_{OH}^{II} values, despite their structural differences. This similarity implies that these OAs can be lumped into a single compound in 3D chemical transport models to reduce model complexity. We further show that there may be generalizable trends to the pH dependence of OH reactivity. The pH dependence of α-pinene relevant OAs was observed but was significantly smaller than that of smaller OAs. In addition, the ratio of k_{OH}^{II} for their carboxylate and carboxylic forms fall into a reasonably narrow range of 1.7 ± 0.3 for the compounds we investigated here. It would be interesting to observe whether a larger suite of OAs follows a similar ratio, which can be used to improve and extend structure-activity relationships (SARs) for the empirical estimation of a wider spectrum of OH reactivities.

Chapter 4

Photo-Oxidation of *cis*-Pinic Acid in the Aqueous Phase: A Mechanistic Investigation

4.1 Introduction

Atmospheric aqueous phases, i.e., cloud, fog, and aerosol liquid water, are an important reaction medium for the processing of many of the water-soluble organic acids (OA) and further formation of secondary organic aerosols (SOA).[4,5,7] The gas-phase oxidation of biogenic volatile organic compounds (BVOC), such as α-pinene, are known sources of OAs and other multifunctional compounds found in cloud and fog waters. One of the largest BVOCs emitted annually is α-pinene ; thus, numerous studies have focused on its gas-phase kinetics and mechanism reactions leading to SOA formation.[90,99,109–111]

It has been recognized that the aqueous-phase processing of semi volatile oxidation products of α-pinene can contribute to SOA formation,[5,35,69,71] but these processes are characterized poorly and limited to a few model compounds. Among the multifunctional α-pinene SOA products, *cis*-pinonic acid (CPA) is the most targeted among the OAs, mainly due to its commercial availability. Aljawhary et al.[35] used a surrogate to investigate the reaction mechanisms and kinetics of 3-methyl-1,2,3-butanetricarboxylic acid (MBTCA, MW 204), a low volatile α-pinene oxidation product and a tracer compound for terpene SOA. Although several compounds have been assigned as tracers for α-pinene SOA, there is a need for an in-depth investigation of oxidation products partitioning to the cloudwater or aerosol water.

Pinic acid (PA) is a major first-generation oxidation product of α-pinene, in addition to CPA and pinonaldehyde.[110,112,113] PA was identified first by Holloway et al.[111] in 1955 as the product of liquid-phase ozonolysis of α-pinene. Forty years later, Christoffersen et al.[114] initiated a series of smog chamber studies that identified PA as one of the main oxidation products of α-pinene ozonolysis and as an important α-pinene SOA precursor. A detailed gas-phase formation mechanism of PA has been proposed by Jenkin et al.[115] The formation of PA in the gas phase and its

particle-phase OH-oxidation has been investigated by many studies,[109,112,114,116,117] but there is a lack of information on PA kinetics and thermodynamics in atmospheric aqueous phases. In terms of known physicochemical properties of PA, Bilde et al.[118] applied tandem differential mobility analysis to measure the evaporation rate and vapor pressure of PA and other semi volatile oxidation products of α-pinene. Kołodziejczyk et al.[119] used a differential scanning microcalorimetry technique to measure PA's thermal properties and a solid–liquid phase equilibria method for the determination of PA solubility in water. An interesting finding from Kołodziejczyk et al.[119] is that PA is the most water soluble among other keys α-pinene SOA oxidation products (PA > *cis*-norpinic acid > CPA > *cis*-norpinonic acid). Using a chemical equilibrium partitioning space, Wania et al.[91] have demonstrated that PA and many α-pinene oxidation products will be present almost exclusively in the aqueous phase when cloudwater is present in an air mass. These results reinforce our interest in this key α-pinene tracer and its chemistry taking place in cloud and fog waters.

The aqueous-phase OH-oxidation mechanism shares many similarities with that in the gas phase; however, mechanisms unique to the aqueous phase may lead to reaction pathways that are absent in the gas phase. Acid–base chemistry and rapid formation of carboxylic acids from aldehydes are representative examples.[45] Under this premise, Amorim et al.[45] recently investigated for the first time the pH dependence of the OH-reactivity of PA. Although the results revealed that the kinetics of PA aqueous-phase oxidation is not affected significantly by the medium pH, there is no information available related to possible mechanistic differences under acidic and basic conditions. Investigating the product distribution of PA photooxidation can serve as a case study that is relevant to many other atmospherically relevant OAs.

A lack of laboratory confirmation of PA's reaction mechanism in the aqueous phase represents a major missing piece in aqueous aerosol and cloudwater radical chemistry models. As previously introduced in Chapter 1, offline analysis has been applied extensively for high-resolution MS data for elemental assignment, while online MS is a good analytical technique that is applied to measure the temporal evolution of multi-generational oxidation occurring in a reaction system. Electrospray ionization

(ESI) is a soft ionization source, and it has been used widely in the analysis of organic compounds. The gas-phase oxidation of α-pinene has been investigated by Winterhalter et al.[90] by ESI–LC–MS. Witkowski et al.[13,78,114] used ESI–LC–MS for the kinetics study of CPA, limonene, and limononic acid in the aqueous phase. Xu et al.[120] investigated the production of nitrooxy organosulfates in the aqueous phase with ESI–LC–MS.

The combination of offline and online MS methods provides means to: (1) identify chemical species, (2) obtain kinetic and thermodynamic information, and (3) derive reaction mechanisms. All this information is helpful to understand the fundamental chemistry taking place in cloud and fog waters and serves as input data for atmospheric models. The objective of this work was to use both offline LC–MS and online MS to understand the fundamental chemistry of PA OH-oxidation in aqueous phase better; this has never been studied previously. The impact of solution pH on the reaction mechanism and product formations remains a poorly explored research area.

4.2 Experimental Methods

4.2.1 Chemicals and Materials

The following chemicals were purchased from Sigma Aldrich: hydrogen peroxide (H_2O_2, 30% in water), sulfuric acid (50% in water), and potassium hydrogen phthalate (>99.95%). Chemicals also were purchased from Fisher Chemical: sodium hydroxide (98%), acetonitrile HPLC grade, and formic acid 99.0+%. All chemicals were used without further purification. PA was custom synthesized via haloform reaction,[93] and further purified. The ^{1}H NMR and ^{13}C NMR of PA synthesis are available in Chapter 3.

4.2.2 PA Aqueous-Phase OH-Oxidation

The aqueous-phase photo-oxidation of PA was performed using a photoreactor emitting UV-light centered at 310 nm (UVB). As shown in Chapter 2, the photoreactor (Rayonet, PRP200) employed here was able to reproduce the appropriate oxidative environment for aqueous-phase reactions. The reaction progress was monitored via

offline and online methods, and the experimental conditions used are summarized in Table 4.1.

Table 4.1 Experimental Parameters Used for Offline LC–MS and Online MS.

	Offline LC–MS	**Online MS**
Quartz vessel	15 mL	150 mL
Volume of PA solution	10 mL	100 mL
PA concentration	600 μM	1.6 mM
H_2O_2 concentration	7 mM	20 mM
Solution pH	2 and 8	Uncontrolled
Reaction time	60 min	55 min
Sample collection time	0, 5, 15, 30, and 60 min	Continuous
Volume of sample collected	300 μL	-

For the offline reaction monitoring, the effect of pH on the reaction mechanism of PA was evaluated, and the pH of the solution was adjusted by adding H_2SO_4 50% wt. (to pH 2) and NaOH 0.5 M (to pH 8). The contribution of direct photolysis to the overall PA decay was investigated in Chapter 3. A dark control experiment showed no reactions between PA and H_2O_2 itself. This experiment was conducted in the same way as the OH-oxidation experiment, except that the UVB lamps remained off for the entire 60 min. A H_2O_2 control experiment also was conducted, confirming that PA does not undergo direct photolysis in the absence of H_2O_2, and this result is consistent with that reported in Chapter 3.

For the online analysis, the reaction progress was monitored by constantly atomizing the solution directly from the photoreactor, followed by collection into a particle-into-liquid sampler (PILS) and direct analysis on a triple-quadrupole ESI–MS (details in Section 4.2.3.2). The pH of the solutions was kept uncontrolled, i.e., with no addition of acid or base. The presence of water-soluble inorganic ions, such as Na^+ and SO_4^{2-} can affect the particle size and growth, thereby affecting the detection by PILS.

In addition, these salts can cause the suppression of the analyte signal in ESI; thus, no base or acid was added for the online analysis.

4.2.3 Offline and Online MS Analysis

4.2.3.1 Offline LC–MS Analysis of PA

The separation and identification of the elemental composition of PA oxidation products were performed offline with an Agilent 6220 accurate-mass time-of-flight (ToF) LC–MS system (Agilent, CA, USA). The chromatographic separation was performed on a Kinetex C18 reverse phase (50 mm × 2.1 mm I.D., 3.0 µm particle size). The C18 column was equipped with a security guard cartridge with a 2.1 mm ID C18 pre-column and kept at 50 °C. Mobile phase A consisted of 0.1% FA solution in water (pH = 2.8), and mobile phase B was 0.1% FA in acetonitrile (ACN), delivered at a flow rate of 0.5 mL/min; the injection volume was 2.0 µL. The following mobile phase gradient was applied: 0.0−0.5 min isocratic 1% B, 0.5−5.5 min linear gradient to 95% B, 5.5−6.5 min isocratic 95% B, 6.5−7.0 min linear gradient to 1% B. The column was re-equilibrated at 1% B, and the analysis was complete in 12.0 min. The MS acquisition was performed in scan mode (*m/z* of 0−500) and the detection of compounds was performed using negative ion ESI ((-)ESI) due to its selectivity towards OAs.[64] The following ESI conditions were applied: capillary voltage, 3000 V; fragmentor, 125 V; drying gas temperature, 325 °C; drying gas flow, 9 L/min, and nebulizer pressure, 20 psi.

4.2.3.2 Online PILS–MS Analysis of PA

In order to monitor the evolution of PA OH-oxidation and product formation continually, an atomizer was used to draw the sample solution up from the reaction vessel by using a fast airflow that creates a negative pressure. Therefore, a small proportion of sample solution is sprayed out as an aerosol, while the rest of the solution returns to the original container. The sprayed aerosol is introduced to a PILS (Brechtel Manufacturing, Inc., Model 4001), which collects and extracts the atomized aerosol particles in real-time. The operation mechanism of PILS has been discussed extensively in the literature.[121–124] Briefly, the sample aerosol is mixed with saturated water vapor

to grow the particles into larger droplets. Then, the droplets are impacted onto a vertical impactor surface, and the water-soluble species collected on the impact are washed off with an aqueous solution. This aqueous solution is sent to a triple-quadrupole MS (Varian, 320-MS) by a peristaltic pump at a flow rate of 18 μL/min via flow injection.

For the online PILS–ESI–MS experiments, the MS was operated in the continuous single-ion monitoring (SIM) acquisition mode to track the evolution of selected species. A list of targeted species was generated by consulting the literature[10,12] and our own offline measurements. To assist product identification, the MS was operated occasionally in the flow injection mode, with the experimental solution injected with a syringe pump. During this time, the MS was operated under the MS/MS mode (MS^2). A list of parameters for the ESI–MS is summarized in Table 4.2.

Table 4.2 Online PILS–MS Instrument's Parameters for the Analysis of PA OH-Oxidation.

Injection flow rate	~18 μL/min	ESI- Capillary voltage	–40 V
Nebulizer gas (air) pressure	20 psi	ESI- Detector Voltage	1270 V
Drying gas (N_2) pressure	20 psi	ESI+ Shield voltage	+600 V
Drying gas temperature	200℃	ESI+ Capillary voltage	100 V
API housing temperature	50℃	ESI+ Detector voltage	1270 V
Manifold temperature	40℃	ESI- Needle voltage	–3700 V
CID gas	Ar	ESI- Shield voltage	–600 V
CID gas pressure	1.50 mTorr	ESI+ Needle voltage	+4000 V

4.2.4 Determination of the Acid Dissociation Constant (pK_a) of PA

The experimental determination of PA's pK_a was conducted via titration with NaOH The pK_a value can be determined fairly accurately from the titration curve using the "half-volume" method.[125] Therefore, 25 mL of 5.0 mM PA solution was titrated manually with a 5.0 mM NaOH. The NaOH solution was standardized previously by titration with potassium hydrogen phthalate. The pH of the PA solution was measured constantly with a calibrated pH meter (Sartorius).

4.3 Results and Discussion

4.3.1 Determination of PA pK_a

PA contains two ionizable carboxyl functional groups (see Figure 4.1) sharing a chemically similar environment; thus, under acidic conditions, the dissociation of both acidic protons will happen independently. Because of this, there is no pH at which the dissociation, $PA \rightarrow PA^{-} + H^{+}$, can be defined as "complete", while at the same time, the second dissociation, i.e., $PA^{-} \rightarrow PA^{2-} + H^{+}$, occurred at a negligible extent. Therefore, the expected rise in the pH from the dissociation of PA's first acidic proton will be prevented by the consumption of base by the second dissociation step, which at this point, will be well underway. Consequently, the titration curve of PA (Figure 4.2) appears as if there were only one dissociation step.

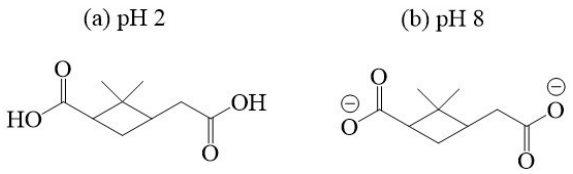

Figure 4.1. Structure of (a) neutral PA and (b) pinate anion (PAn).

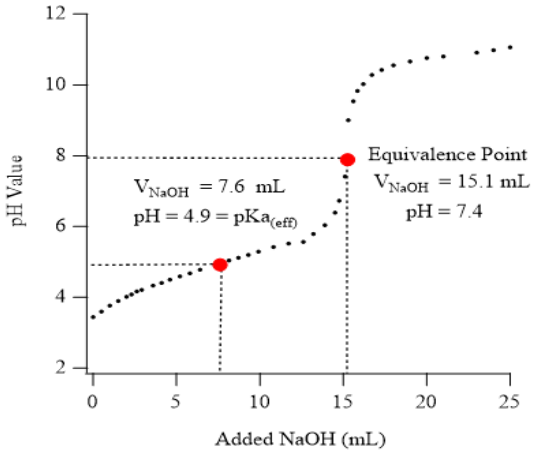

Figure 4.2. Titration curve of 5.0 mM PA using a 5.0 mM NaOH titrant. The horizontal axis presents the volume of titrant added (V_{NaOH}).

Although it is not possible to determine PA's first and second pKa values experimentally via acid–base titration, one can use the "half-volume" method to

determine its "effective" pK_a (p$K_{a(eff)}$). The p$K_{a(eff)}$ is useful to estimate the fraction of neutral PA and pinate anion (PAn) in a solution.

By applying the method described in Section 4.2.4, the PA's p$K_{a(eff)}$ was measured to be 4.9. To the best of our knowledge, the pK_a value of PA has never been determined experimentally previously. A computationally determined value of 4.48 was used in the literature.[97] Based on our observation, subsequent experiments in this work were conducted under pH values of 2 and 8. The PA's p$K_{a(eff)}$ indicates that the neutral form of PA (Figure 4.1(a)) dominates at pH 2 (99.9%), while at pH 8, the majority of PA will be dissociated fully and be present as PAn (Figure 4.1(b)). The pH values for the OH-oxidation of PA were chosen to cover the entire pH range of ambient cloudwater and fogs, which fall between 2 and 7.[54,55] Therefore, in atmospheric aqueous phases, PA can exist in both its neutral form and as a PAn anion, which makes it important to study PA oxidation mechanisms under both acidic and basic conditions.

4.3.2 Offline ESI–LC–MS for Elemental Analysis

The products arising from the aqueous-phase PA OH-oxidation were detected and identified using (-)ESI–LC–MS. Figure 4.3 shows a base peak chromatogram (BPC) for a typical PA OH-oxidation experiment at pH 8.

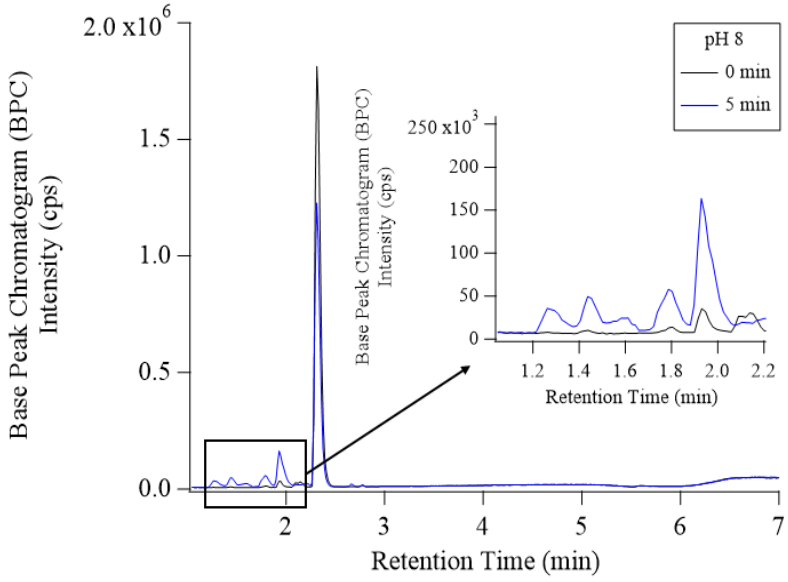

Figure 4.3. BPC for the sample taken from the reaction at t = 0 and 5 min.

Many peaks were detected at retention times shorter than that of PA (t_R = 2.3 min), which indicates the formation of products of higher polarity, i.e., more oxygenated compounds. The inset in Figure 4.3 shows a closer look at the BPC of the products formed. Although we observe co-eluting peaks, a variety of products were detected and identified. Table 4.3 shows the major products detected, with their elemental compositions and potential identities. The *m/z* values are corresponding to their deprotonated forms ($[M–H]^-$). Although many products were identified, we will be presenting MS data for the MW 156, 172, 188, and 204 compounds, as they have been identified previously as known α-pinene SOA tracers and/or intermediates.

Table 4.3 List of Major PA OH-oxidation Peaks Detected by (-)ESI–LC–MS Under pH 2 and pH 8.

MW (g/mol)	$[M–H]^-$	Elemental Composition	Note [a]	Ref. [b]
156	155	$C_8H_{12}O_3$		
172	171	$C_8H_{12}O_4$	Terpenylic acid or norpinic acid	Yasmeen et al., 2012
188	187	$C_9H_{16}O_4$	Hydroxynorpinic acid	Yasmeen et al., 2011
200	199	$C_9H_{12}O_5$		
204	203	$C_8H_{12}O_6$	MBTCA and/or isomers	Szmigielski et al., 2005
216	215	$C_9H_{12}O_6$		
218	217	$C_9H_{14}O_6$		

[a] Compound's name hasn't been identified previously as an oxidation product of α-pinene;
[b] Not available in the literature;

4.3.3 MS/MS for Further Structural Confirmation

The structural information of PA OH-oxidation products was confirmed using the fragmentation patterns obtained from the triple-quadrupole MS instrument. The

oxidation products formed typically produced ions corresponding to losses summarized in Table 4.4.[126]

Table 4.4 Commonly Observed Loss of Small Fragments in (-)ESI spectra of PA OH-oxidation Products.

m/z	Fragment	Note
18	H_2O	Presence of OH or carbonyl group
34	H_2O_2	Presence of a peroxide (loss of H_2O_2)
44	CO_2	Presence of mono-acid
62	$CO_2 + H_2O$	Presence of OH + mono-acid
88	$CO_2 + CO_2$	Presence of a di-acid
132	$CO_2 + CO_2 + CO_2$	Presence of a tri-acid

The MS fragmentation spectra for the PA oxidation products with MW 156, 172, 188, 204 are presented in Figure 4.4.

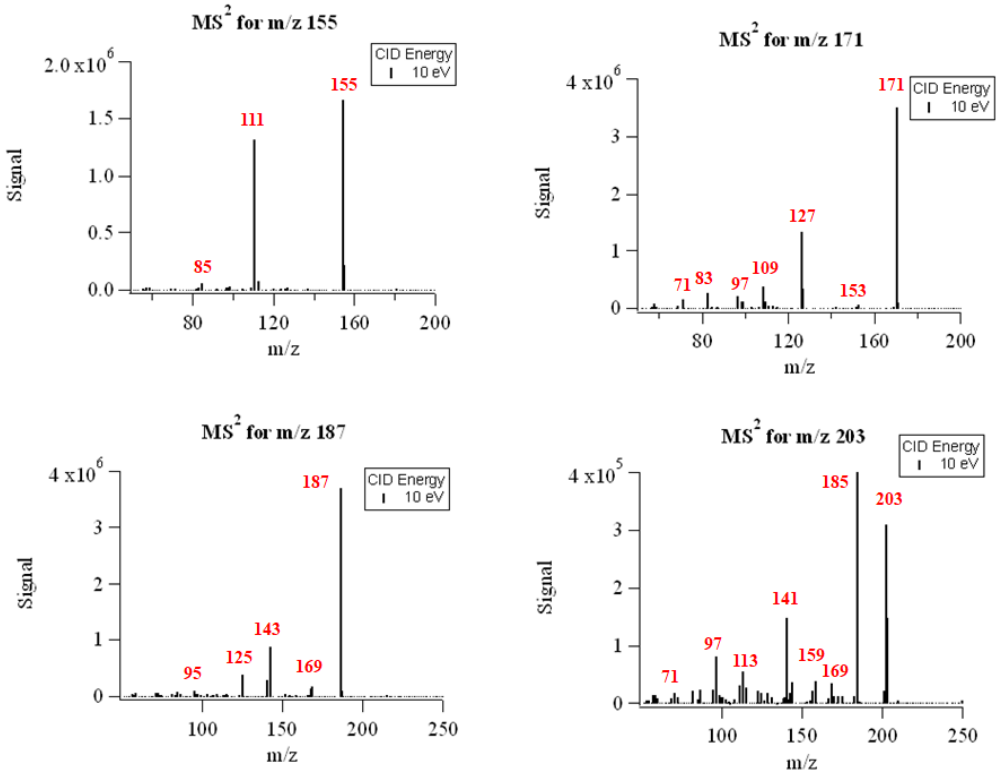

Figure 4.4. Fragmentation spectra of PA OH-oxidation products under uncontrolled pH conditions.

The product detected as *m/z* 155 produced an intense fragmentation ion at *m/z* 111 due to CO_2 elimination, which indicates the presence of a carboxylic group. The compound detected as *m/z* 171 ion produced fragment ions of *m/z* 153 (–18 au) and *m/z* 83 (–88 au), indicating the loss of H_2O, and the presence of up to two carboxylic acids, respectively. The ion detected at *m/z* 171 was identified as one of the major PA oxidation products. Previous studies have shown that both gas-phase ozonolysis and aqueous-phase OH-oxidation of α-pinene SOA lead to the formation of compounds of *m/z* 171.[45,73] These compounds have been assigned previously to terpenylic acid and/or norpinic acid (NPA). Although there are no standards available to confirm the identity of the peaks observed as *m/z* 171, we propose it to be mainly NPA (3-carboxy-2,2-dimethyl), based on a few fragmentation observations. First, the fragmentation pattern of *m/z* 171 agrees with previous literature on NPA and related compounds,[127] showing a double loss of 44 au, which indicated the presence of two carboxylic groups. While NPA has two carboxylic groups in its chemical structure, terpenylic acid has a carboxyl and a carbonyl group. Secondly, terpenylic acid undergoes hydrolysis and forms diaterpenylic acid of *m/z* 231. Both compounds serve as monomeric precursors to the dimer of MW 344 (*m/z* 343), present in α-pinene ozonolysis SOA. Neither one of these compounds was detected during PA aqueous-phase OH-oxidation, thus, the compound of *m/z* 171 was proposed as NPA. The formation mechanism for NPA, as well as for the oxidation products of *m/z* 155, *m/z* 187, and *m/z* 203, are proposed in Section 4.3.6.

The *m/z* 187 fragmentation spectrum produced ions of *m/z* 169 (–18 au) and *m/z* 143 (–44 au), indicating the presence of a carboxylic acid, and *m/z* 125 (–62 au). By changing the fragmentor voltage to 20 eV, a fragment ion of *m/z* 99 (–88 au) was observed, representing the loss of two carboxylic acid functional groups. The fragmentation of the product detected as *m/z* 203 was similar to the fragmentation spectrum of 3-methyl-1,2,3-butanetricarboxylic acid (MBTCA, MW = 204) and its isomers.[117,128] For *m/z* 203 MS product ion formation, the ions include *m/z* 185 (–18 au), *m/z* 173 (–44 au), *m/z* 141 (–62 au), and *m/z* 97 (–18 au and –88 au combined). Although small, the presence of a product ion of *m/z* 71 represents

a combined loss of three CO_2, which implies the presence of a tricarboxylic acid in its structure.

4.3.4 Differences Observed at pH 2 and pH 8

The extracted ion chromatograms (EICs) of PA and the four selected oxidation products (Table 4.3) are shown in Figures 4.5 and 4.6, respectively.

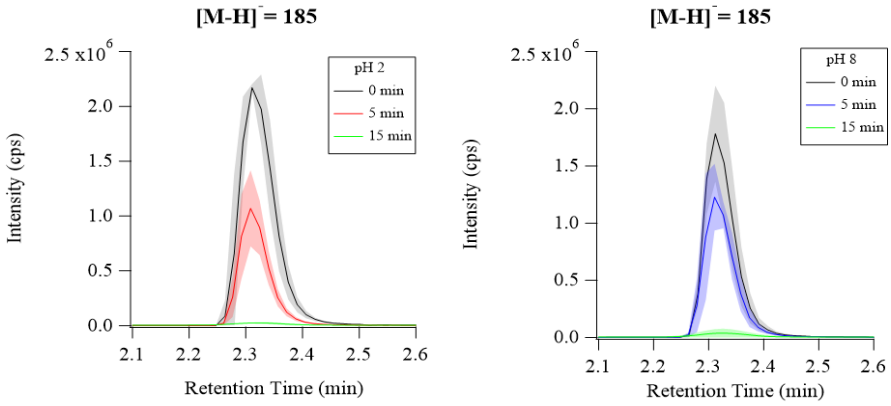

Figure 4.5. EIC for PA at t = 0 min, t = 5 min, and t = 15 min under acidic and basic conditions.

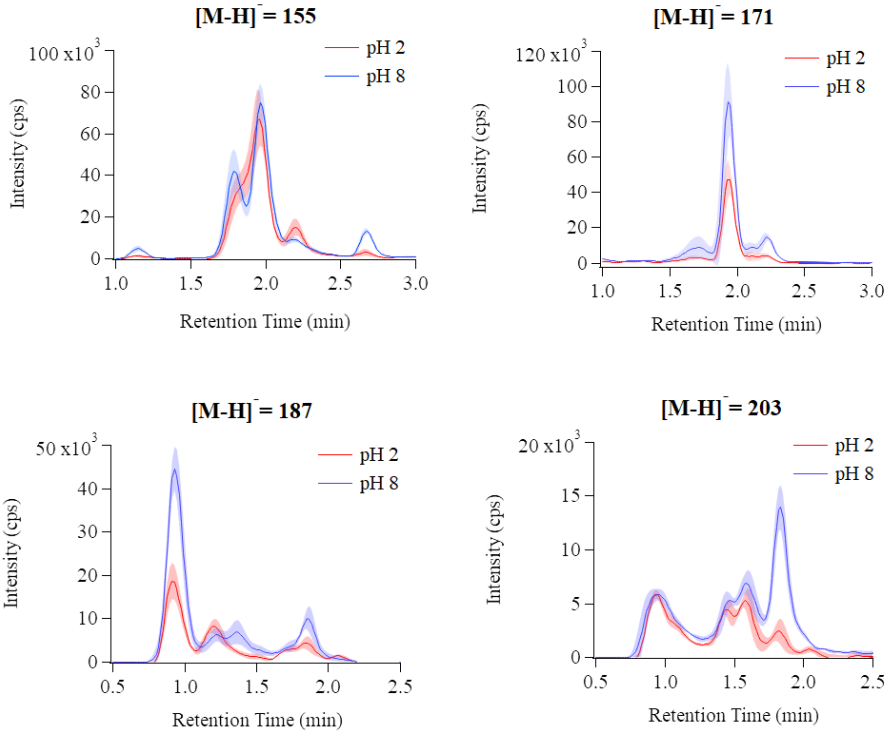

Figure 4.6. EIC for peaks of *m/z* 155 and 171 at 5 min (reaction time) detected with offline (-)ESI–LC–MS. The EIC for peaks of *m/z* 187 and 203 were obtained at 15 min reaction time. The shaded area presents 1 σ from the calculated triplicate error propagation.

For the compounds of *m/z* 155 and *m/z* 171, their EICs at t = 5 min was subtracted from those at t = 0 min to focus on the amount of product formed. The chromatogram of the *m/z* 187 and *m/z* 203 compounds were obtained by subtracting their EIC at t = 15 min and t = 0 min. The shaded area in the chromatograms represents the error propagation of the triplicates performed.

As shown in Table 4.3, many products are formed from the aqueous OH-oxidation of PA, and the characterization of each compound is rather complex. From Figure 4.6, we can see that even for the case of the major product of *m/z* 171 (t_R = 1.93 min), isomer compounds also are formed (t_R = 1.71 min and t_R = 2.22 min). Although one can determine its elemental composition, the LC–MS method applied is not applicable for the identification of structural isomers. Comparing the *m/z* 203 isomers at t_R = 0.93 min, t_R = 1.47 min, and t_R = 1.59 min to the isomer at t_R = 1.59 min, a dramatic difference in intensity can be observed under pH 2 and pH 8. Similar observations in intensity difference under acidic and basic conditions can be made for the compounds of *m/z* 155 and *m/z* 187. Therefore, it is evident that the pH of the aqueous phase will affect PA's reaction mechanism. Currently, the literature available focuses on the pH-dependence of a few small α-keto acids,[34,106] and to the best of our knowledge, the effect of pH on the aqueous-phase reaction mechanisms of other atmospherically relevant OAs has not been investigated.

4.3.5 Online PILS–MS Results

The evolution of PA OH-oxidation followed by the formation of its oxidation products can be observed in Figure 4.7. The online PILS–MS method applied here was able to detect all the products previously identified using offline (-)ESI–LC–MS (Table 4.3). The initial signal for the PA solution shows that some products were already there prior to the start of the experiment, which likely is attributed to the long storage time of PA solution. Control experiments (Section 4.2.2) showed that PA does not react with H_2O_2 under dark conditions, therefore, the products observed are not due to rapid oxidation as H_2O_2 is added to PA solution but, rather, due to slow reactions occurring during its storage.

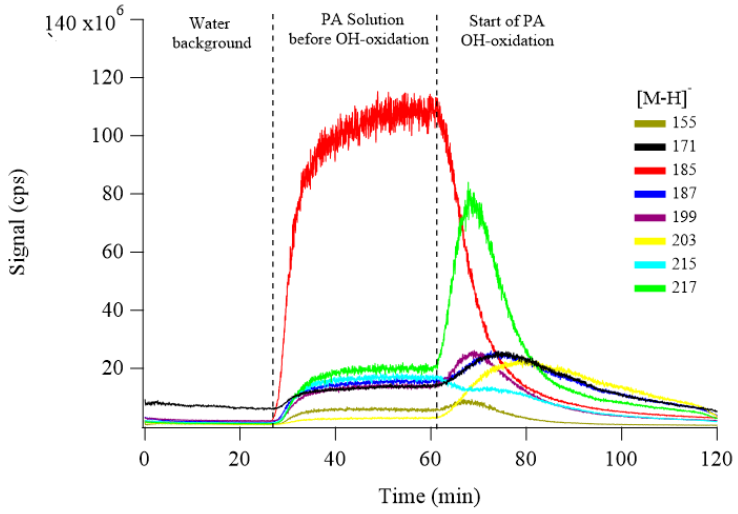

Figure 4.7. Online PA OH-oxidation reaction monitoring and product formation evolution.

Figure 4.8 shows the evolution of PA OH-oxidation and formation of the four targeted compounds over time. By observing the formation and decay profile of each compound, we propose that the MW 156 compound is the intermediate product for the formation of the MW 172 and MW 188 products. In addition, it can be noted that the intensity of the compound of MW 204 increases as the MW 188 signal reaches its maximum. Thus, the MW 188 compound likely leads to the formation of the product of MW 204. These observations were useful when proposing the formation mechanisms of the four targeted compounds in Section 4.3.6.

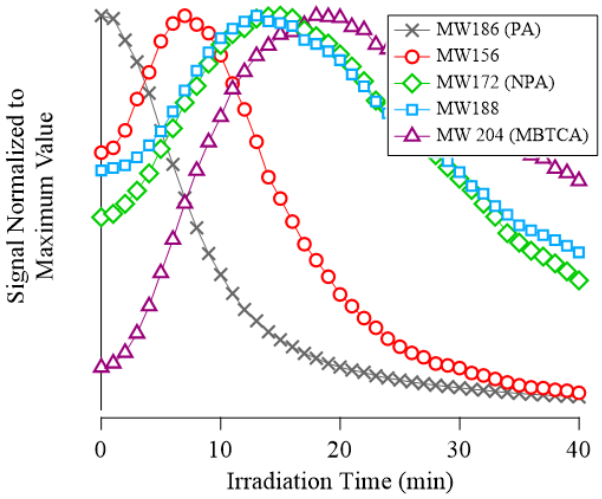

Figure 4.8. PILS–MS temporal oxidation of PA and formation of products of MW 156 (*m/z* 155), MW 172 (*m/z* 171), MW 188 (*m/z* 187), and MW 204 (*m/z* 203).

4.3.6 Proposed Formation Mechanisms

The proposed mechanisms were based on the offline MS data obtained in the (-)ESI mode, in addition to the results obtained by the online PILS–MS method. Thus, by combining the information of Sections 4.3.2 to 4.3.5 and the widely known aqueous-phase radical chemistry, we propose the possible mechanisms leading to the formation of the compounds with MW 156, MW 172, MW 188, and MW 204. These products are of particular interest to atmospheric chemistry, as mentioned previously, because NPA (MW 172) and MBTCA (MW 204) are major compounds and tracers for monoterpene oxidation. Figure 4.9 shows the formation mechanisms of MW 156 under pH 2, at which PA exits in its protonated form. The mechanism shown in Figure 4.9 is pH-independent, as it does not involve the carboxylic groups.

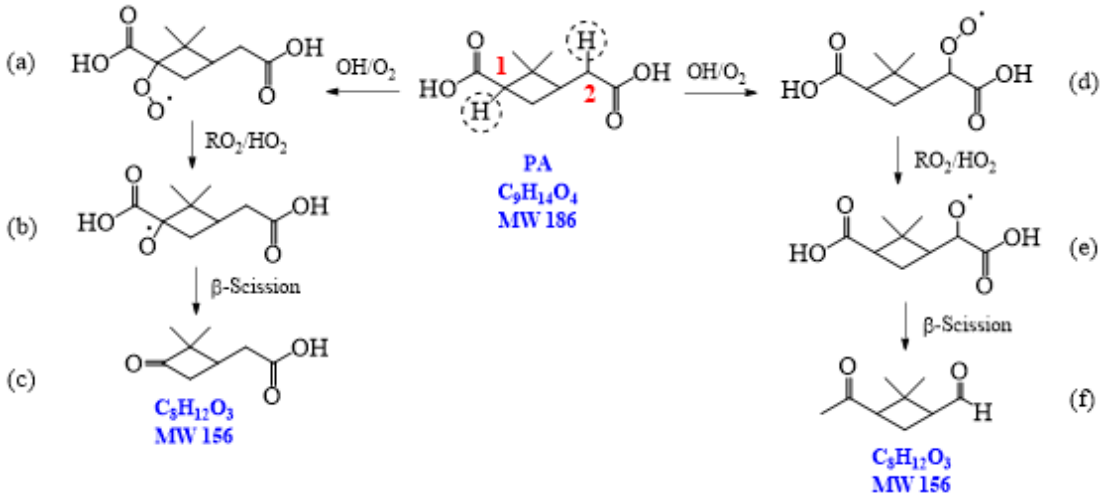

Figure 4.9. Proposed mechanism of the *m/z* 155 product formation from PA OH-oxidation at pH 2. Similarly, at pH 8, the H-abstraction occurs at C-1 and C-2 atm of the PAn anion.

As the initial step of OH-oxidation, H-abstraction by OH radicals can occur at multiple locations on a PA molecule. Figure 4.9 illustrates the cases in which the initiation step occurs at the C-1 or C-2 positions, followed by O_2 addition and formation of peroxy radicals (RO_2), labeled as (a) and (d). Reactions of NO are not expected to be significant in atmospheric aqueous phases due to the low solubility of NO.[129] The peroxy radicals (a) and (d) mainly react with another RO_2 in solution or with a hydroperoxy radical (HO_2), forming the corresponding alkoxy radical (RO),[130] labeled as (b) and (e). The ROs further undergoes β-scission to form a variety of possible

products, including an aldehyde (c) and a ketone (f) of *m/z* 155. From Table 4.3, the accurate mass indicated the elemental composition of $C_8H_{12}O_3$, in agreement with (c) and (f). We considered that the ion at *m/z* 155 is an important intermediate product leading to the formation of products at *m/z* 171, and *m/z* 203.

As introduced in Chapter 1 (Section 1.3.2.4), in an aqueous solution, aldehydes can hydrate forming their geminal diols. Thus, for the aldehylic product of *m/z* 155 (f), the OH radicals can abstract a hydrogen atom from both aldehylic and geminal diol forms (j). The respective alkyl radicals formed are also in hydration equilibrium ((g) and (k)). This geminal–diol pathway (Figure 4.10) is unique to the atmospheric aqueous phase and it does not occur via gas-phase oxidation.

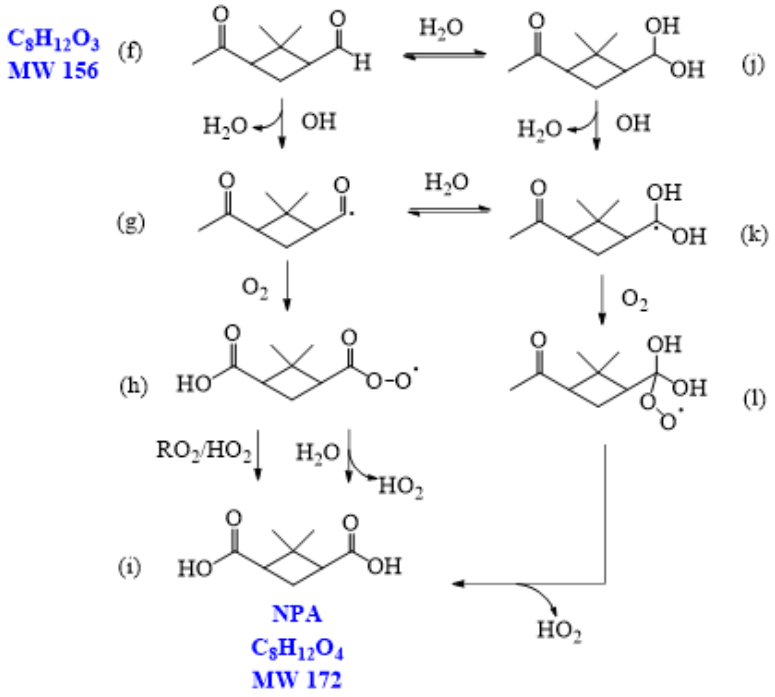

Figure 4.10. Proposed mechanism of the *m/z* 171 product formation from PA OH-oxidation at pH 2.

The addition of dissolved O_2 to (g) and (k) forms two types of peroxy radicals, as shown in Figure 4.10(h) and (l). The peroxy radical (l) dissociates rapidly to form NPA (i). The structure of (i) is consistent with its elemental composition determined in Section 4.3.2 and the MS^2 fragmentation pattern discussed in Section 4.3.3 (i.e., it possesses up to two carboxylic groups). In parallel, the acylperoxy radical formed via H-abstraction of the aldehydic form (h) can either hydrate or react with other species

in solution (RO_2 or HO_2) to form NPA ((i)). The observation that NPA is a major product of PA explains a previous observation (Chapter 3) that could not be explained at the time. The OA with *m/z* 171 exhibited a completely different decay profile during photooxidation of α-pinene SOA, indicating that it was forming from other species. The results obtained here can, therefore, confirm that the OA at *m/z* 171 was likely NPA and was formed from PA present in the SOA extract.

In the case of the ketone product of *m/z* 155 (c), the OH radical can abstract an H-atom from different sites of the molecule. The mechanism shown in Figure 4.11 focuses on the H-abstraction from C-3, followed by the addition of dissolved O_2 to form the corresponding peroxy radical (m). The reaction with another RO_2 produces an alkoxy radical (n) that proceeds via β-scission to break the 4-membered cyclic structure. The resulting peroxy radical (o) can react with RO_2 or HO_2 or also be hydrated to form the corresponding carboxylic acid with MW 188 (p). The elemental composition and fragmentation pattern of (p) was confirmed by the results presented in Sections 4.3.3 and 4.3.5. From Section 4.3.5, the MW 188 compound has been proposed as the intermediate for MBTCA (q) formation. The mechanism proposed in Figure 4.11 follows Enami and Sakamato's work on MBTCA formation from CPA oxidation,[10] in which the authors also identified the MW 188 compound as a byproduct of MBTCA.

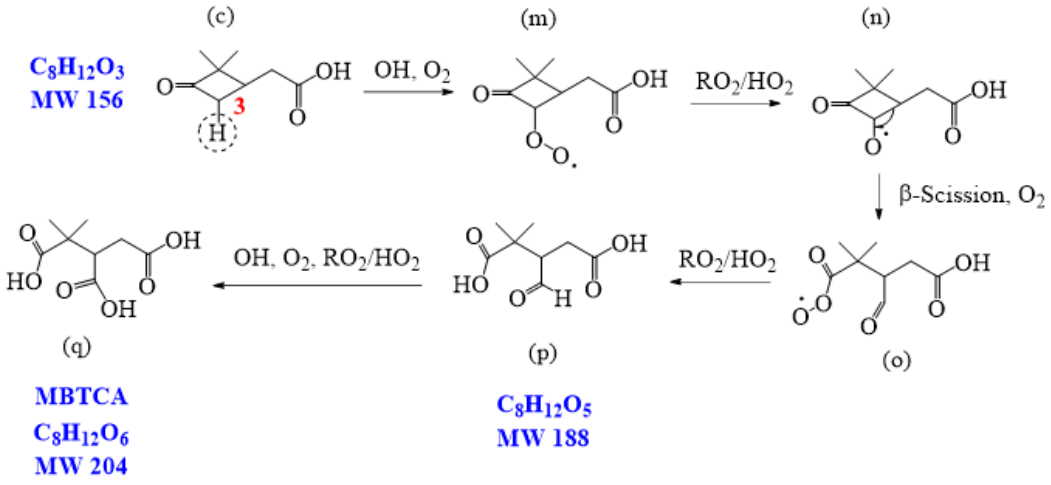

Figure 4.11. Proposed mechanism of the MW 188 product formation from PA OH-oxidation at pH 2, followed by reactions leading to the formation of MBTCA (MW 204).

The aldehyde functional group of MW 188 (p) also can undergo hydration equilibrium. Similar to the mechanism proposed in Figure 4.10, OH radicals can abstract the aldehydic or the geminal diol hydrogen of (p) leading to the formation of MBTCA via both H-abstraction pathways. This reaction pathway agrees with the mechanism proposed by Witkowski et al.[12] and Enami and Sakamato[10] for MBTCA formation from the aqueous phase oxidation of CPA.

The mechanisms presented thus far are pH-independent, as the carboxylic groups are not involved. At pH 8, in addition to the H-abstraction reactions occurring over the PA structure, a unique electron-transfer reaction occurs in the aqueous phase that already has been discussed in depth in Chapter 1 and 3. At pH 8, PAn undergoes electron-transfer reaction with OH radicals at two different sites of the molecule, labeled as A and B in Figure 4.12.

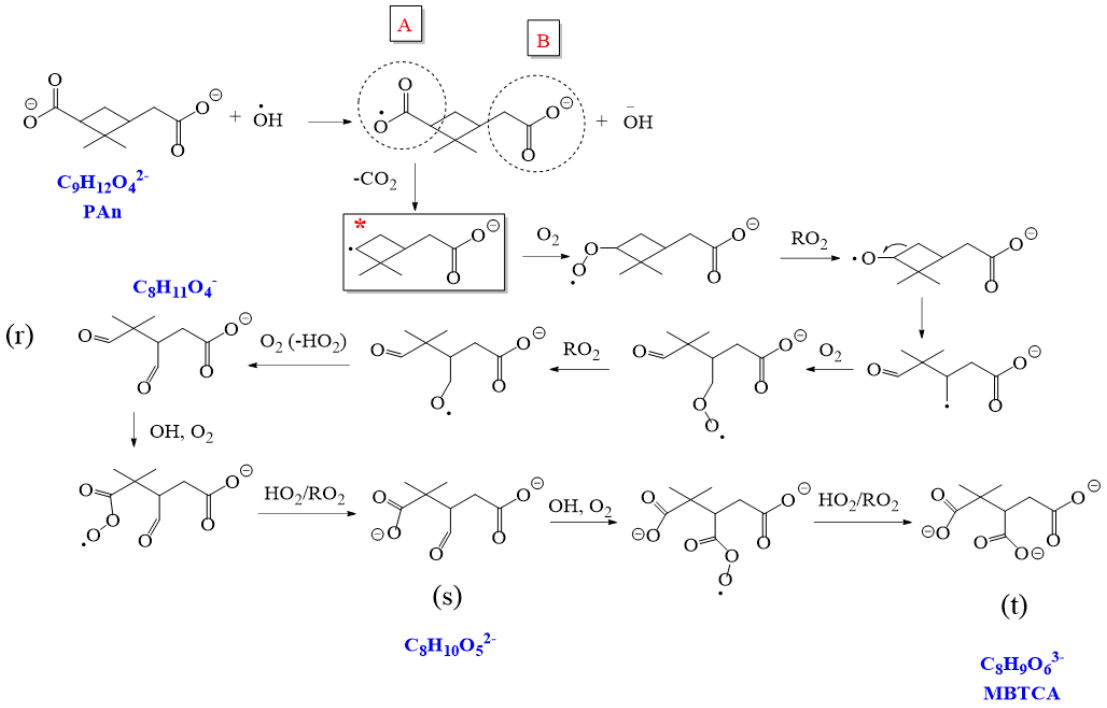

Figure 4.12. Proposed formation mechanism of MBTCA under pH 8 conditions. The reaction is initiated by an electron-transfer reaction on the carboxylate A. The highlighted compound represents the PA alkyl radical formed only in the aqueous phase.

The electron-transfer reaction taking place at site A is followed by a decarboxylation step, which is the key step in this part of the mechanism. A series of radical reactions, previously discussed in this section, takes place, resulting in the

formation of the deprotonated form of the intermediate compounds of MW 172 (r) and MW 188 (s). Further steps involving H-abstraction by OH radicals, addition of dissolved O_2, and reactions with RO_2 or HO_2 radicals lead to the formation of the tricarboxylate assigned to MBTCA (t). The initial decarboxylation of PA and formation of the corresponding alkyl radical (denoted with * in Figure 4.12) only occur in the aqueous phase due to the favored electron-transfer reaction.

The mechanism shown in Figure 4.12 was proposed on the basis of the mechanism for the gas-phase formation of MBTCA from CPA oxidation.[128] Szmigielski et al.[128] proposed that PA is only an intermediate product of CPA oxidation reactions, leading to MBTCA, and not a primary precursor of this compound. In the gas phase, the decarboxylation of PA at site A does not occur as proposed in Figure 4.12. The molecular structure of CPA differs from PA at site A, in which CPA poses a ketone functional group, while PA has a carboxylic acid. The aqueous-phase formation of MBTCA from PA is, however, possible due to the electron-transfer reaction under basic pH conditions. These results agree with the higher yields of MW 188 and MW 204 compounds under pH 8 (Figure 4.6). Therefore, we propose a new mechanism pathway for MBTCA formation that is unique in the aqueous phase and gains importance as the solution becomes less acidic.

The proposed electron-transfer reaction mechanism taking place at site B is shown in Figure 4.13. PA undergoes decarboxylation, followed by a series of radical chemistry reactions similarly to site A. The reaction at site B leads to the formation of the deprotonated MW 156 intermediate compound (u) and NPA (v). Additional hydration equilibrium reactions also can take place on the aldehydic intermediate product formed (u), leading to the formation of NPA. The mechanisms presented in Figure 4.13 are supported by the observation that the yield of NPA was higher under pH 8 (Figure 4.6).

With these in-depth mechanistic analyses, we have arrived at the following conclusion. Although reactions occurring at pH 8 lead to similar compounds, as in the case of pH 2, the electron–transfer reaction serves as additional formation pathways and thus accelerates the formation of several key oxidation products, including NPA and MBTCA (Figures 4.12 and 4.13).

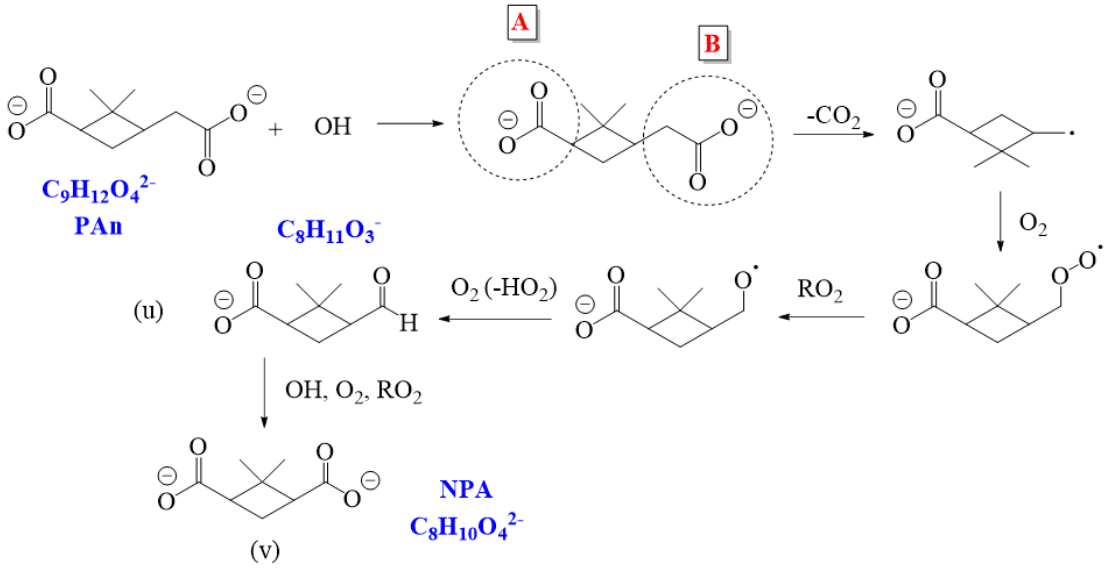

Figure 4.13. Proposed formation mechanism at pH 8. Electron-transfer reaction taking place on the carboxylate B.

4.4 Summary and Atmospheric Implications

In this chapter, we have, for the first time, investigated PA aqueous-phase mechanisms in detail. The p$K_{a(eff)}$ of PA was determined to be 4.9, thus, it can exist in its protonated form or as pinate anion, considering that the pH of cloudwater and fogs can vary between 2 and 7.[54,55] A large number of oxidation products were detected using offline (-)ESI–LC–MS; among them, the compounds of MW 156, MW 172, MW 188, and MW 204 were targeted. Online PILS–MS measurements were used to monitor the oxidation of PA and product formation continually, obtaining the fragment spectrum for structural analysis. Therefore, by combining (-)ESI–LC–MS and PILS–MS, we proposed the possible reaction mechanisms for the targeted compounds.

From our observations, the compounds of MW 156 and MW 188 serve as intermediate products for the products assigned to NPA (MW 172), and MBTCA (MW 204). NPA is one of the major monoterpene OH-oxidation products, and MBTCA is an important tracer of α-pinene SOA. The detection of MBTCA was surprising and disagreed with the current understanding that MBTCA arises only from CPA.[117,128] We propose that it is the unique electron-transfer reaction occurring only in the aqueous phase that leads to the formation of MBTCA from PA.

Many oxidation products of PA exhibited drastic differences in yields and isomer distributions at pH 2 and pH 8. Such an impact of pH on the photochemical products of OAs has never been reported in the literature. Combining observations from Chapter 3 and 4, a complex interplay between acid–base chemistry and photochemistry has become clear. As shown in Chapter 3, the electron-transfer reaction does not change the overall OH reactivity of PA significantly . However, this chapter demonstrates that the underlying reaction mechanisms have been altered, changing the yield of reaction products. Although our study has focused on a single compound, PA, we believe that it serves as a vivid demonstration for how pH can affect the reaction mechanisms of many other atmospherically relevant OAs under cloudwater-relevant conditions. Our results suggest the importance of further understanding the impact of pH on aqueous-phase photochemistry, particularly acids and bases that are sensitive to the highly variable pH of atmospheric aqueous phases.

Chapter 5

Conclusions and Future Directions

5.1 Photoreactor Characterization using *cis*-Pinonic Acid as a Model Compound

In Chapter 2 we characterized the photoreactor used in our laboratory settings for the aqueous-phase experiments performed in Chapters 3 and 4. Given that photoreactors commonly are employed to simulate the photo-initiated reactions taking place in the atmospheric aqueous phases, the wavelength and intensity of the UVB lamps used were determined. By combining chemical actinometry and direct measurements performed using a spectroradiometer, the emission spectrum of the UVB light in our photoreactor was measured to be centered at 310 nm. This indicates that the UVB light was a suitable lamp option, as it can efficiently photolyze H_2O_2 into OH radicals, the dominant aqueous-phase oxidant driving cloudwater processing of organic compounds, while minimizing other unwanted photolysis reactions. By using a model compound with known photochemistry such as *cis*-pinonic acid (CPA), we evaluated the capability of our photoreactor to reproduce the oxidative environments in cloud and fog waters. The photoreactor was, therefore, used to simulate CPA aqueous-phase photochemistry with OH radicals experimentally.

Liquid chromatography–mass spectrometry (LC–MS) was applied to derive CPA kinetic information under uncontrolled pH conditions. In addition, a kinetic box model was built to simulate the photochemistry of CPA in our current photoreactor, and characterize the radical chemistry taking place upon UVB radiation. Overall, CPA photo-oxidation was reproduced successfully, with CPA's observed and modeled pseudo-first-order decay rates agreeing within 10%. From the model results, the concentration of OH radicals being generated from H_2O_2 photolysis was determined to be 1.8×10^{-12} M, which is within the atmospherically relevant range detected in cloud and fog waters (1.4×10^{-16} – 8.0×10^{-12} M).[23] Therefore, our photoreactor can be used to simulate the atmospheric conditions needed for aqueous-phase oxidation of important water-soluble organic compounds, such as CPA.

5.2 pH Dependence of the OH Reactivity of Organic Acids in the Aqueous Phase

A novel investigation on the pH dependence of the aqueous-phase photochemistry of atmospherically relevant organic acids (OAs) is presented in Chapter 3. Although acid–base chemistry is a unique property of aqueous phases, the effect of pH on the reactivity of water-soluble organic compounds (WSOCs) with oxidants such as OH radicals is understood poorly. In this chapter, we used LC–MS and applied a relative rate technique to determine the second-order rate coefficient (k_{OH}^{II}) of pinic acid (PA), CPA, and limononic acid (LA) as a function of pH. Ion chromatography was used for the analysis of formic acid (FA), instead. The k_{OH}^{II} of these individual OAs, and of several WSOCs of α-pinene secondary organic aerosols (SOAs) was determined. Assuming that the OA was lost due to reaction with OH radicals only, their k_{OH}^{II} was obtained by monitoring the loss of the OAs and of a reference compound with known k_{OH}^{II}. The impact of pH on radical chemistry in the system was evaluated using the model developed in Chapter 2 and expanding it to a wider pH range of 2 and 10. From the model simulations, the concentration of OH radicals across the pH range investigated varied only to a small extent. The potential impact of sulfate radicals also was investigated for our pH 2 condition, as the solutions were acidified with H_2SO_4, though negligible differences were observed, therefore, not affecting the overall OAs k_{OH}^{II}.

In contrast to FA, the smallest OA, the measured k_{OH}^{II} for all other OAs increased only by a small fraction with the pH. The greater pH dependence observed for FA is attributed to an electron-transfer reaction unique to its carboxylate form. In addition to H-abstraction by OH radicals, electron-transfer reactions also take place, contributing to a faster reaction with OH radicals under basic conditions. In contrast, the larger OAs did not exhibit a significant pH dependence on their OH-reactivity under basic conditions. From these observations, we proposed that the importance of the carboxylate and electron-transfer reactions is not as pronounced for the total OH reactivity of large OAs and the WSOCs of α-pinene SOA. These results led to the generalized trend regarding the lifetime of small and large OAs. As FA showed to be

highly sensitive to cloud and fog water pH, its aqueous phase processing, as well as other small OAs, will occur more rapidly with increasing pH, affecting the SOA formation rate in these aqueous phases and its loading.

The current study applied a relative rate technique to determine the k_{OH}^{II} of several OAs and used pimelic acid and caffeine as reference compounds for acid and basic conditions, respectively. The choice of the two reference compounds was based on previous kinetic studies on CPA, though an array of compounds were available. The choice of reference compounds is contingent to the quality and reliability of kinetic data obtained by the relative kinetic method. Future directions would be to incorporate different reference compounds in order to confirm if the results obtained in this chapter were not affected directly by the reference compound used. The research field should develop more standardized and universal reference compounds to make intercomparison of kinetic data feasible.

Regarding the kinetic box model used, while the simulation of CPA OH-oxidation at uncontrolled pH and pH 2 agreed with the experimental observations, the same was not true under basic conditions. At pH 10, a 23% discrepancy between the modeled and experimental results was observed. This outcome can be overcome by better characterization of the radical chemistry under basic conditions. As mentioned in Section 3.2.1.2, LA was synthesized from CPA oxidation and used for the OH-oxidation experiments without further purification. Consequently, the k_{OH}^{II} of LA at uncontrolled pH conditions, pH 2, and pH 10 did not agree with the literature values available. Thus, further steps would be a purification of the LA solution, followed by OH-oxidation experiments to confirm LA's k_{OH}^{II}. Finally, a systematic analysis of the OH-reactivity of organic acids with varied chain length is necessary for a fundamental understanding of the cut-point at which the carboxylate electron reaction becomes the dominant contributor to the overall molecular OH reactivity.

5.3 Photo-Oxidation of *cis*-Pinic Acid in the Aqueous Phase: A Mechanistic Investigation

In Chapter 4, we investigated for the first time the aqueous-phase oxidation mechanisms of PA as a function of pH. PA's effective pKa was determined

experimentally, and a value of 4.9 was obtained. Considering that the pH of cloud and fog waters varies between 2 and 7, PA can exist in the protonated form (PA) or as pinate anions (PAn). Due to PA's importance as a major oxidation product of α-pinene SOA and the lack of information in the literature, a detailed aqueous-phase mechanistic analysis was needed, in addition to the kinetics information obtained in Chapter 3. Offline LC–MS was applied to identify and provide the elemental composition of PA oxidation products, while online MS was used to track the temporal evolution of PA oxidation and product formation in the reaction system. For the online analysis, a particle-into-liquid sampler (PILS) was employed to collect the solution from the photoreactor system, and the direct measurement was conducted using an electrospray ionization (ESI)–MS.

A large number of peaks were detected as oxidation products of PA, and the formation of norpinic acid (NPA) and 3-methyl-1,2,3-butanetricarboxylic acid (MBTCA) were proposed under acidic and basic conditions. Although NPA and MBTCA are two known α-pinene oxidation products, their formation in both gas and aqueous phases usually are not assigned to PA oxidation, but to α-pinene and CPA oxidation, respectively.[117,119,128] Thus, these results highlight PA as a novel source of important atmospheric tracers, especially MBTCA,

From the kinetic studies, PA did not show any significant pH dependence in its reactivity with OH radicals; however, a different outcome was observed when looking into the mechanisms leading to the formation of NPA and MBTCA in Chapter 4. Because of the additional electron-transfer reaction (briefly discussed in Section 5.2) taking place at pH 8, many oxidation products and their isomers showed drastic differences in their yield. Thus, although the pH exhibits a relatively small impact on the overall OH reactivity of PA, it clearly affects PA reaction mechanisms. This PA behavior serves as an indicator of how the pH of atmospheric aqueous phases can affect other relevant OAs undergoing cloudwater processing. Further investigations on the elemental composition and behavior of the detected PA oxidation products are still in process.

One important aspect to note is that the reversed-phase LC-MS used in this aqueous-phase study is not suited for the separation, detection, and identification of

small organic acids that always elute near the void volume. As their interactions with C18 columns are minimum, these organic compounds are not retained effectively by reversed-phase LC. Hydrophilic interaction liquid chromatography (HILIC) is an alternative approach for the separation of polar compounds in complex systems.[131] Although not presented in the thesis, we have already obtained preliminary results showing that the use of a HILIC column has led to more detected oxidation products. Future studies should be conducted for the optimization of HILIC-MS, in particular, to investigate the impact of solution pH on HILIC separation.

References

(1) Olsen, E.; Nielsen, F. Predicting Vapour Pressures of Organic Compounds from Their Chemical Structure for Classification According to the VOC Directive and Risk Assessment in General. *Mol. J. Synth. Chem. Nat. Prod. Chem.* **2001**, *6* (4), 370–389.

(2) Guenther, A. B.; Jiang, X.; Heald, C. L.; Sakulyanontvittaya, T.; Duhl, T.; Emmons, L. K.; Wang, X. The Model of Emissions of Gases and Aerosols from Nature Version 2.1 (MEGAN2.1): An Extended and Updated Framework for Modeling Biogenic Emissions. *Geosci. Model Dev.* **2012**, *5* (6), 1471–1492.

(3) Finlayson-Pitts, B. J.; Pitts Jr, J. N. *Chemistry of the Upper and Lower Atmosphere: Theory, Experiments, and Applications*; Academic Press, 2000.

(4) Blando, J. D.; Turpin, B. J. Secondary Organic Aerosol Formation in Cloud and Fog Droplets: A Literature Evaluation of Plausibility. *Atmos. Environ.* **2000**, *34* (10), 1623–1632.

(5) Ervens, B.; Turpin, B. J.; Weber, R. J. Secondary Organic Aerosol Formation in Cloud Droplets and Aqueous Particles (AqSOA): A Review of Laboratory, Field and Model Studies. *Atmos. Chem. Phys.* **2011**, *11* (21), 11069–11102.

(6) Hallquist, M.; Wenger, J. C.; Baltensperger, U.; Rudich, Y.; Simpson, D.; Claeys, M.; Dommen, J.; Donahue, N. M.; George, C.; Goldstein, A. H.; Hamilton, J. F.; Herrmann, H.; Hoffmann, T.; Iinuma, Y.; Jang, M.; Jenkin, M. E.; Jimenez, J. L.; Kiendler-Scharr, A.; Maenhaut, W.; McFiggans, G.; Mentel, T. F.; Monod, A.; Prevot, A. S. H.; Seinfeld, J. H.; Surratt, J. D.; Szmigielski, R.; Wildt, J. The Formation, Properties and Impact of Secondary Organic Aerosol: Current and Emerging Issues. *Atmos. Chem. Phys.* **2009**, *9 (14)*, 5515–5236.

(7) McNeill, V. F. Aqueous Organic Chemistry in the Atmosphere: Sources and Chemical Processing of Organic Aerosols. *Environ. Sci. Technol.* **2015**, *49* (3), 1237–1244.

(8) McNeill, V. F.; Woo, J. L.; Kim, D. D.; Schwier, A. N.; Wannell, N. J.; Sumner, A. J.; Barakat, J. M. Aqueous-Phase Secondary Organic Aerosol and Organosulfate Formation in Atmospheric Aerosols: A Modeling Study. *Environ. Sci. Technol.* **2012**, *46* (15), 8075–8081.

(9) Pankow. An Absorption Model of the Gas/Aerosol Partitioning Involved in the Formation of Secondary Organic Aerosol. *Atmos. Environ.* **1994**, *28* (2), 189–193.

(10) Enami, S.; Sakamoto, Y. OH-Radical Oxidation of Surface-Active Cis-Pinonic Acid at the Air–Water Interface. *J. Phys. Chem. A* **2016**, *120* (20), 3578–3587.

(11) Lignell, H.; Epstein, S. A.; Marvin, M. R.; Shemesh, D.; Gerber, B.; Nizkorodov, S. Experimental and Theoretical Study of Aqueous Cis-Pinonic Acid Photolysis. *J. Phys. Chem. A* **2013**, *117* (48), 12930–12945.

(12) Witkowski, B.; Gierczak, T. Cis-Pinonic Acid Oxidation by Hydroxyl Radicals in the Aqueous Phase under Acidic and Basic Conditions: Kinetics and Mechanism. *Environ. Sci. Technol.* **2017**, *51* (17), 9765–9773.

(13) Witkowski, B.; Jurdana, S.; Gierczak, T. Limononic Acid Oxidation by Hydroxyl Radicals and Ozone in the Aqueous Phase. *Environ. Sci. Technol.* **2018**, *52* (6), 3402–3411.

(14) Seinfeld, J. H.; Pandis, S. N. *Atmospheric Chemistry and Physics: From Air Pollution to Climate Change*; John Wiley & Sons, Incorporated: New York, United States, 2016.

(15) Sullivan, A. P.; Hodas, N.; Turpin, B. J.; Skog, K.; Keutsch, F. N.; Gilardoni, S.; Paglione, M.; Rinaldi, M.; Decesari, S.; Facchini, M. C.; Poulain, L.; Herrmann, H.; Wiedensohler, A.; Nemitz, E.; Twigg, M. M.; Collett Jr., J. L. Evidence for Ambient Dark Aqueous SOA Formation in the Po Valley, Italy. *Atmos. Chem. Phys.* **2016**, *16* (13), 8095–8108.

(16) Xu, W.; Han, T.; Du, W.; Wang, Q.; Chen, C.; Zhao, J.; Zhang, Y.; Li, J.; Fu, P.; Wang, Z.; Worsnop, D. R.; Sun, Y. Effects of Aqueous-Phase and Photochemical Processing on Secondary Organic Aerosol Formation and Evolution in Beijing, China. *Environ. Sci. Technol.* **2017**, *51* (2), 762–770.

(17) Woo, J. L.; Kim, D. D.; Schwier, A. N.; Li, R.; McNeill, V. F. Aqueous Aerosol SOA Formation: Impact on Aerosol Physical Properties. *Faraday Discuss.* **2013**, *165*, 357.

(18) Marais, E. A.; Jacob, D. J.; Jimenez, J. L.; Campuzano-Jost, P.; Day, D. A.; Hu, W.; Krechmer, J.; Zhu, L.; Kim, P. S.; Miller, C. C.; Fisher, J. A.; Travis, K.; Yu, K.; Hanisco, T. F.; Wolfe, G. M.; Arkinson, H. L.; Pye, H. O. T.; Froyd, K. D.; Liao, J.; McNeill, V. F. Aqueous-Phase Mechanism for Secondary Organic Aerosol Formation from Isoprene: Application to the Southeast United States and Co-Benefit of SO2 Emission Controls. *Atmos. Chem. Phys.* **2016**, *16* (3), 1603–1618.

(19) Ervens, B.; Volkamer, R. Glyoxal Processing by Aerosol Multiphase Chemistry: Towards a Kinetic Modeling Framework of Secondary Organic Aerosol Formation in Aqueous Particles. *Atmos. Chem. Phys.* **2010**, *10* (17), 8219–8244.

(20) Ervens, B.; Gligorovski, S.; Herrmann, H. Temperature-Dependent Rate Constants for Hydroxyl Radical Reactions with Organic Compounds in Aqueous Solutions. *Phys. Chem. Chem. Phys.* **2003**, *5* (9), 1811–1824.

(21) Herckes, P.; Valsaraj, K. T.; Collett Jr, J. L. A Review of Observations of Organic Matter in Fogs and Clouds: Origin, Processing and Fate. *Atmos. Res.* **2013**, *132*, 434–449.

(22) Ervens, B.; Sorooshian, A.; Aldhaif, A. M.; Shingler, T.; Crosbie, E.; Ziemba, L.; Campuzano-Jost, P.; Jimenez, J. L.; Wisthaler, A. Is There an Aerosol Signature of Chemical Cloud Processing? *Atmos. Chem. Phys.* **2018**, *18* (21), 16099–16119.

(23) Herrmann, H.; Schaefer, T.; Tilgner, A.; Styler, S. A.; Weller, C.; Teich, M.; Otto, T. Tropospheric Aqueous-Phase Chemistry: Kinetics, Mechanisms, and Its Coupling to a Changing Gas Phase. *Chem. Rev.* **2015**, *115* (10), 4259–4334.

(24) Gaillard de Sémainville, Ph.; Hoffmann, D.; George, Ch.; Herrmann, H. Study of Nitrate Radical (NO_3) Reactions with Carbonyls and Acids in Aqueous Solution as a Function of Temperature. *Phys. Chem. Chem. Phys.* **2007**, *9* (8), 958–968.

(25) Volkamer, R.; Ziemann, P. J.; Molina, M. J. Secondary Organic Aerosol Formation from Acetylene (C_2H_2): Seed Effect on SOA Yields Due to Organic Photochemistry in the Aerosol Aqueous Phase. *Atmos. Chem. Phys.* **2009**, *9* (6), 1907–1928.

(26) Sareen, N.; Schwier, A. N.; Shapiro, E. L.; Mitroo, D.; McNeill, V. F. Secondary Organic Material Formed by Methylglyoxal in Aqueous Aerosol Mimics. *Atmos. Chem. Phys.* **2010**, *10* (3), 997–1016.

(27) Tan, Y.; Carlton, A. G.; Seitzinger, S. P.; Turpin, B. J. SOA from Methylglyoxal in Clouds and Wet Aerosols: Measurement and Prediction of Key Products. *Atmos. Environ.* **2010**, *44* (39), 5218–5226.

(28) Li, T.; Wang, Z.; Wang, Y.; Wu, C.; Liang, Y.; Xia, M.; Yu, C.; Yun, H.; Wang, W.; Wang, Y.; Guo, J.; Herrmann, H.; Wang, T. Chemical Characteristics of Cloud Water and the Impacts on Aerosol Properties at a Subtropical Mountain Site in Hong Kong SAR. *Atmos. Chem. Phys.* **2020**, *20* (1), 391–407.

(29) Lim, Y. B.; Tan, Y.; Perri, M. J.; Seitzinger, S. P.; Turpin, B. J. Aqueous Chemistry and Its Role in Secondary Organic Aerosol (SOA) Formation. *Atmos. Chem. Phys.* **2010**, *10* (21), 10521–10539.

(30) Betterton, E. A.; Hoffmann, M. R. Henry's Law Constants of Some Environmentally Important Aldehydes. *Environ. Sci. Technol.* **1988**, *22* (12), 1415–1418.

(31) Ip, H. S. S.; Huang, X. H. H.; Yu, J. Z. Effective Henry's Law Constants of Glyoxal, Glyoxylic Acid, and Glycolic Acid. *Geophys. Res. Lett.* **2009**, *36* (1).

(32) Kroll, J. H.; Ng, N. L.; Murphy, S. M.; Varutbangkul, V.; Flagan, R. C.; Seinfeld, J. H. Chamber Studies of Secondary Organic Aerosol Growth by Reactive Uptake of Simple Carbonyl Compounds. *J. Geophys. Res. Atmos.* **2005**, *110* (D23).

(33) Zhao, R.; Lee, A. K. Y.; Wang, C.; Wania, F.; Wong, J. P. S.; Zhou, S.; Abbatt, J. P. D. The Role of Water in Organic Aerosol Multiphase Chemistry: Focus on Partitioning and Reactivity. In *Advances in Atmospheric Chemistry*; Advances in Atmospheric Chemistry; World Scientific, 2016; Vol. Volume 1, pp 95–184.

(34) Rapf, R. J.; Dooley, M. R.; Kappes, K.; Perkins, R. J.; Vaida, V. pH Dependence of the Aqueous Photochemistry of α-Keto Acids. *J. Phys. Chem. A* **2017**, *121* (44), 8368–8379.

(35) Aljawhary, D.; Zhao, R.; Lee, A. K. Y.; Wang, C.; Abbatt, J. P. D. Kinetics, Mechanism, and Secondary Organic Aerosol Yield of Aqueous Phase Photo-Oxidation of α-Pinene Oxidation Products. *J. Phys. Chem. A* **2016**, *120* (9), 1395–1407.

(36) Herrmann, H.; Ervens, B.; Jacobi, H.-W.; Wolke, R.; Nowacki, P.; Zellner, R. CAPRAM2.3: A Chemical Aqueous Phase Radical Mechanism for Tropospheric Chemistry. *J. Atmos. Chem.* **2000**, *36* (3), 231–284.

(37) Sareen, N.; Carlton, A. G.; Surratt, J. D.; Gold, A.; Lee, B.; Lopez-Hilfiker, F. D.; Mohr, C.; Thornton, J. A.; Zhang, Z.; Lim, Y. B.; Turpin, B. J. Identifying Precursors and Aqueous Organic Aerosol Formation Pathways during the SOAS Campaign. *Atmos. Chem. Phys.* **2016**, *16* (22), 14409–14420.

(38) Gschwend, P. M.; Imboden, D. M.; Schwarzenbach, R. P. *Environmental Organic Chemistry*; John Wiley & Sons, Incorporated: New York, UNITED STATES, 2016.

(39) Bateman, A. P.; Nizkorodov, S. A.; Laskin, J.; Laskin, A. Photolytic Processing of Secondary Organic Aerosols Dissolved in Cloud Droplets. *Phys. Chem. Chem. Phys.* **2011**, *13* (26), 12199–12212.

(40) Steinberg, C. E. W.; Paul, A. Photolysis. In *Encyclopedia of Ecology*; Jørgensen, S. E., Fath, B. D., Eds.; Academic Press: Oxford, 2008; pp 2724–2732.

(41) Akash, M. S. H.; Rehman, K. Ultraviolet-Visible (UV-VIS) Spectroscopy. In *Essentials of Pharmaceutical Analysis*; Akash, M. S. H., Rehman, K., Eds.; Springer: Singapore, 2020; pp 29–56.

(42) Epstein, S. A.; Tapavicza, E.; Furche, F.; Nizkorodov, S. A. Direct Photolysis of Carbonyl Compounds Dissolved in Cloud and Fog-Droplets. *Atmos. Chem. Phys.* **2013**, *13* (18), 9461–9477.

(43) Zhang, X.; McVay, R. C.; Huang, D. D.; Dalleska, N. F.; Aumont, B.; Flagan, R. C.; Seinfeld, J. H. Formation and Evolution of Molecular Products in α-Pinene Secondary Organic Aerosol. *Proc. Natl. Acad. Sci.* **2015**, *112* (46), 14168–14173.

(44) Ma, Y.; Willcox, T. R.; Russell, A. T.; Marston, G. Pinic and Pinonic Acid Formation in the Reaction of Ozone with α-Pinene. *Chem Commun* **2007**, No. 13, 1328–1330.

(45) Amorim, J. V.; Wu, S.; Klimchuk, K.; Lau, C.; Williams, F. J.; Huang, Y.; Zhao, R. pH Dependence of the OH Reactivity of Organic Acids in the Aqueous Phase. *Environ. Sci. Technol.* **2020**, *54* (19), 12484–12492.

(46) Bianco, A.; Passananti, M.; Brigante, M.; Mailhot, G. Photochemistry of the Cloud Aqueous Phase: A Review. *Molecules* **2020**, *25* (2), 423

(47) Arakaki, T.; Faust, B. C. Sources, Sinks, and Mechanisms of Hydroxyl Radical (•OH) Photoproduction and Consumption in Authentic Acidic Continental Cloud Waters from Whiteface Mountain, New York: The Role of the Fe(r) (r = II, III) Photochemical Cycle. *J. Geophys. Res. Atmos.* **1998**, *103* (D3), 3487–3504.

(48) Ervens, B.; Sorooshian, A.; Lim, Y. B.; Turpin, B. J. Key Parameters Controlling OH-Initiated Formation of Secondary Organic Aerosol in the Aqueous Phase (AqSOA). *J. Geophys. Res. Atmos.* **2014**, *119* (7), 3997–4016.

(49) Faust, B. C.; Allen, J. M. Aqueous-Phase Photochemical Formation of Hydroxyl Radical in Authentic Cloudwaters and Fogwaters. *Environ. Sci. Technol.* **1993**, *27* (6), 1221–1224.

(50) Goldstein, S.; Aschengrau, D.; Diamant, Y.; Rabani, J. Photolysis of Aqueous H_2O_2: Quantum Yield and Applications for Polychromatic UV Actinometry in Photoreactors. *Environ. Sci. Technol.* **2007**, *41* (21), 7486–7490.

(51) Zellner, R.; Exner, M.; Herrmann, H. Absolute OH Quantum Yields in the Laser Photolysis of Nitrate, Nitrite and Dissolved H2O2 at 308 and 351 Nm in the Temperature Range 278–353 K. *J. Atmos. Chem.* **1990**, *10* (4), 411–425.

(52) Vaughan, S.; Ingham, T.; Whalley, L. K.; Stone, D.; Evans, M. J.; Read, K. A.; Lee, J. D.; Moller, S. J.; Carpenter, L. J.; Lewis, A. C.; Fleming, Z. L.; Heard, D. E. Seasonal Observations of OH and HO_2 in the Remote Tropical Marine Boundary Layer. *Atmos. Chem. Phys.* **2012**, *12* (4), 2149–2172.

(53) Buxton, G. V.; Greenstock, C. L.; Helman, W. P.; Ross, A. B. Critical Review of Rate Constants for Reactions of Hydrated Electrons, Hydrogen Atoms and Hydroxyl Radicals (· OH/· O- in Aqueous Solution. *J. Phys. Chem. Ref. Data* **1988**, *17* (2), 513–886.

(54) Collett, J. L.; Bator, A.; Rao, X.; Demoz, B. B. Acidity Variations across the Cloud Drop Size Spectrum and Their Influence on Rates of Atmospheric Sulfate Production. *Geophys. Res. Lett.* **1994**, *21* (22), 2393–2396.

(55) Pye, H. O. T.; Nenes, A.; Alexander, B.; Ault, A. P.; Barth, M. C.; Clegg, S. L.; Collett Jr., J. L.; Fahey, K. M.; Hennigan, C. J.; Herrmann, H.; Kanakidou, M.; Kelly, J. T.; Ku, I.-T.; McNeill, V. F.; Riemer, N.; Schaefer, T.; Shi, G.; Tilgner, A.; Walker, J. T.; Wang, T.; Weber, R.; Xing, J.; Zaveri, R. A.; Zuend, A. The Acidity of Atmospheric Particles and Clouds. *Atmos. Chem. Phys.* **2020**, *20* (8), 4809–4888.

(56) Cassano, A. E.; Martin, C. A.; Brandi, R. J.; Alfano, O. M. Photoreactor Analysis and Design: Fundamentals and Applications. *Ind. Eng. Chem. Res.* **1995**, *34* (7), 2155–2201.

(57) Schmidt, M.; Jansen van Beek, S. M.; Abou-Ghanem, M.; Oliynyk, A. O.; Locock, A. J.; Styler, S. A. Production of Atmospheric Organosulfates via Mineral-Mediated Photochemistry. *ACS Earth Space Chem.* **2019**, *3* (3), 424–431.

(58) Zhao, R.; Aljawhary, D.; Lee, A. K. Y.; Abbatt, J. P. D. Rapid Aqueous-Phase Photooxidation of Dimers in the α-Pinene Secondary Organic Aerosol. *Environ. Sci. Technol. Lett.* **2017**, *4* (6), 205–210.

(59) Carlton, A. G.; Turpin, B. J.; Altieri, K. E.; Seitzinger, S.; Reff, A.; Lim, H.-J.; Ervens, B. Atmospheric Oxalic Acid and SOA Production from Glyoxal: Results of Aqueous Photooxidation Experiments. *Atmos. Environ.* **2007**, *41* (35), 7588–7602.

(60) Bonfiglio, R.; King, R. C.; Olah, T. V.; Merkle, K. The Effects of Sample Preparation Methods on the Variability of the Electrospray Ionization Response for Model Drug Compounds. *Rapid Commun. Mass Spectrom.* **1999**, *13* (12), 1175–1185.

(61) Kind, T.; Fiehn, O. Advances in Structure Elucidation of Small Molecules Using Mass Spectrometry. *Bioanal. Rev.* **2010**, *2* (1–4), 23–60.

(62) Witkowski, B.; Gierczak, T. Characterization of the Limonene Oxidation Products with Liquid Chromatography Coupled to the Tandem Mass Spectrometry. *Atmos. Environ.* **2017**, *154*, 297–307.

(63) Hamilton, J. F.; Lewis, A. C.; Carey, T. J.; Wenger, J. C. Characterization of Polar Compounds and Oligomers in Secondary Organic Aerosol Using Liquid Chromatography Coupled to Mass Spectrometry. *Anal. Chem.* **2008**, *80* (2), 474–480.

(64) Zhao, R.; Kenseth, C. M.; Huang, Y.; Dalleska, N. F.; Seinfeld, J. H. Iodometry-Assisted Liquid Chromatography Electrospray Ionization Mass Spectrometry for Analysis of Organic Peroxides: An

Application to Atmospheric Secondary Organic Aerosol. *Environ. Sci. Technol.* **2018**, *52* (4), 2108–2117.

(65) Perri, M. J.; Seitzinger, S.; Turpin, B. J. Secondary Organic Aerosol Production from Aqueous Photooxidation of Glycolaldehyde: Laboratory Experiments. *Atmos. Environ.* **2009**, *43* (8), 1487–1497.

(66) Tan, Y.; Perri, M. J.; Seitzinger, S. P.; Turpin, B. J. Effects of Precursor Concentration and Acidic Sulfate in Aqueous Glyoxal−OH Radical Oxidation and Implications for Secondary Organic Aerosol. *Environ. Sci. Technol.* **2009**, *43* (21), 8105–8112.

(67) Tan, Y.; Lim, Y. B.; Altieri, K. E.; Seitzinger, S. P.; Turpin, B. J. Mechanisms Leading to Oligomers and SOA through Aqueous Photooxidation: Insights from OH Radical Oxidation of Acetic Acid and Methylglyoxal. *Atmos. Chem. Phys.* **2012**, *12* (2), 801–813.

(68) Zhao, R.; Mungall, E. L.; Lee, A. K.; Aljawhary, D.; Abbatt, J. P. Aqueous-Phase Photooxidation of Levoglucosan–a Mechanistic Study Using Aerosol Time-of-Flight Chemical Ionization Mass Spectrometry (Aerosol ToF-CIMS). *Atmos. Chem. Phys.* **2014**, *14* (18), 9695–9706.

(69) Huang, D. D.; Zhang, Q.; Cheung, H. H. Y.; Yu, L.; Zhou, S.; Anastasio, C.; Smith, J. D.; Chan, C. K. Formation and Evolution of AqSOA from Aqueous-Phase Reactions of Phenolic Carbonyls: Comparison between Ammonium Sulfate and Ammonium Nitrate Solutions. *Environ. Sci. Technol.* **2018**, *52* (16), 9215–9224.

(70) Bertram, T. H.; Thornton, J. A.; Riedel, T. P.; Middlebrook, A. M.; Bahreini, R.; Bates, T. S.; Quinn, P. K.; Coffman, D. J. Direct Observations of N_2O_5 Reactivity on Ambient Aerosol Particles. *Geophys. Res. Lett.* **2009**, *36*.

(71) Cortés, D. A.; Elrod, M. J. Kinetics of the Aqueous Phase Reactions of Atmospherically Relevant Monoterpene Epoxides. *J. Phys. Chem. A* **2017**, *121* (48), 9297–9305.

(72) Herrmann, H.; Hoffmann, D.; Schaefer, T.; Bräuer, P.; Tilgner, A. Tropospheric Aqueous-Phase Free-Radical Chemistry: Radical Sources, Spectra, Reaction Kinetics and Prediction Tools. *Chem. Phys, Chem,* **2010**, *11* (18), 3796–3822.

(73) Yasmeen, F.; Vermeylen, R.; Maurin, N.; Perraudin, E.; Doussin, J.-F.; Claeys, M. Characterisation of Tracers for Aging of α-Pinene Secondary Organic Aerosol Using Liquid Chromatography/Negative Ion Electrospray Ionisation Mass Spectrometry. *Environ. Chem.* **2012**, *9* (3), 236.

(74) Mutzel, A.; Rodigast, M.; Iinuma, Y.; Böge, O.; Herrmann, H. Monoterpene SOA – Contribution of First-Generation Oxidation Products to Formation and Chemical Composition. *Atmos. Environ.* **2016**, *130*, 136–144.

(75) Wang, C.; Yuan, T.; Wood, S. A.; Goss, K.-U.; Li, J.; Ying, Q.; Wania, F. Uncertain Henry's Law Constants Compromise Equilibrium Partitioning Calculations of Atmospheric Oxidation Products. *Atmos. Chem. Phys.* **2017**, *17* (12), 7529–7540.

(76) Galbavy, E. S.; Ram, K.; Anastasio, C. 2-Nitrobenzaldehyde as a Chemical Actinometer for Solution and Ice Photochemistry. *J. Photochem. Photobiol. Chem.* **2010**, *209* (2), 186–192.

(77) Schaefer, T.; Herrmann, H. Competition Kinetics of OH Radical Reactions with Oxygenated Organic Compounds in Aqueous Solution: Rate Constants and Internal Optical Absorption Effects. *Phys. Chem. Chem. Phys.* **2018**, *20* (16), 10939–10948.

(78) Witkowski, B.; Al-sharafi, M.; Gierczak, T. Kinetics of Limonene Secondary Organic Aerosol Oxidation in the Aqueous Phase. *Environ. Sci. Technol.* **2018**, *52* (20), 11583–11590.

(79) Zhang, X.; Ortega, J.; Huang, Y.; Shertz, S.; Tyndall, G. S.; Orlando, J. J. A Steady-State Continuous Flow Chamber for the Study of Daytime and Nighttime Chemistry under Atmospherically Relevant NO Levels. *Atmos. Meas. Tech.* **2018**, *11* (5), 2537–2551.

(80) Zhang, Y.; Xiao, Y.; Zhang, J.; Chang, V. W. C.; Lim, T.-T. Degradation of Cyclophosphamide and 5-Fluorouracil in Water Using UV and UV/H_2O_2: Kinetics Investigation, Pathways and Energetic Analysis. *J. Environ. Chem. Eng.* **2017**, *5* (1), 1133–1139.

(81) Lim, H. J.; Carlton, A. G.; Turpin, B. J. Isoprene Forms Secondary Organic Aerosol through Cloud Processing: Model Simulations. *Environ. Sci. Technol.* **2005**, *39* (12), 4441–4446.

(82) Herrmann, H. On the Photolysis of Simple Anions and Neutral Molecules as Sources of O−/OH, SOx^- and Cl in Aqueous Solution. *Phys. Chem. Chem. Phys.* **2007**, *9* (30), 3935–3964.

(83) Herrmann, H.; Reese, A.; Zellner, R. Time-Resolved UV/VIS Diode Array Absorption Spectroscopy of SO_x^- (X=3, 4, 5) Radical Anions in Aqueous Solution. *J. Mol. Struct.* **1995**, *348*, 183–186.

(84) Cappa, C. D.; Wilson, K. R. Multi-Generation Gas-Phase Oxidation, Equilibrium Partitioning, and the Formation and Evolution of Secondary Organic Aerosol. *Atmos. Chem. Phys.* **2012**, *12* (20), 9505–9528.

(85) Mouchel-Vallon, C.; Deguillaume, L.; Monod, A.; Perroux, H.; Rose, C.; Ghigo, G.; Long, Y.; Leriche, M.; Aumont, B.; Patryl, L.; Armand, P.; Chaumerliac, N. CLEPS 1.0: A New Protocol for Cloud Aqueous Phase Oxidation of VOC Mechanisms. *Geosci. Model Dev.* **2017**, *10* (3), 1339–1362.

(86) Hodzic, A.; Kasibhatla, P. S.; Jo, D. S.; Cappa, C. D.; Jimenez, J. L.; Madronich, S.; Park, R. J. Rethinking the Global Secondary Organic Aerosol (SOA) Budget: Stronger Production, Faster Removal, Shorter Lifetime. *Atmos. Chem. Phys.* **2016**, *16* (12), 7917–7941.

(87) Arakaki, T.; Kuroki, Y.; Okada, K.; Nakama, Y.; Ikota, H.; Kinjo, M.; Higuchi, T.; Uehara, M.; Tanahara, A. Chemical Composition and Photochemical Formation of Hydroxyl Radicals in Aqueous Extracts of Aerosol Particles Collected in Okinawa, Japan. *Atmos. Environ.* **2006**, *40* (25), 4764–4774.

(88) Zhang, X.; Chen, Z.; Wang, H.; He, S.; Huang, D. An Important Pathway for Ozonolysis of α-Pinene and β-Pinene in Aqueous Phase and Its Atmospheric Implications. *Atmos. Environ.* **2009**, *43* (29), 4465–4471.

(89) Yasmeen, F.; Szmigielski, R.; Vermeylen, R.; Gómez-González, Y.; Surratt, J. D.; Chan, A. W. H.; Seinfeld, J. H.; Maenhaut, W.; Claeys, M. Mass Spectrometric Characterization of Isomeric Terpenoic Acids from the Oxidation of α-Pinene, β-Pinene, d-Limonene, and Δ3-Carene in Fine Forest Aerosol. *J. Mass Spectrom.* **2011**, *46* (4), 425–442.

(90) Winterhalter, R.; Dingenen, R. V.; Larsen, B. R.; Jensen, N. R.; Hjorth, J. LC-MS Analysis of Aerosol Particles from the Oxidation of α-Pinene by Ozone and OH-Radicals. *Atmos. Chem. Phys. Discuss.* **2003**, *3* (1), 1–39.

(91) Wania, F.; Lei, Y. D.; Wang, C.; Abbatt, J. P. D.; Goss, K.-U. Using the Chemical Equilibrium Partitioning Space to Explore Factors Influencing the Phase Distribution of Compounds Involved in Secondary Organic Aerosol Formation. *Atmos. Chem. Phys.* **2015**, *15* (6), 3395–3412.

(92) Otto, T.; Schaefer, T.; Herrmann, H. Aqueous-Phase Oxidation of Terpene-Derived Acids by Atmospherically Relevant Radicals. *J. Phys. Chem. A* **2018**, *122* (47), 9233–9241.

(93) Steimer, S. S.; Delvaux, A.; Campbell, S. J.; Gallimore, P. J.; Grice, P.; Howe, D. J.; Pitton, D.; Claeys, M.; Hoffmann, T.; Kalberer, M. Synthesis and Characterisation of Peroxypinic Acids as Proxies for Highly Oxygenated Molecules (HOMs) in Secondary Organic Aerosol. *Atmos. Chem. Phys.* **2018**, *18* (15), 10973–10983.

(94) Atkinson, R.; Carter, W. P. L.; Winer, A. M.; Pitts, J. N. An Experimental Protocol for the Determination of OH Radical Rate Constants with Organics Using Methyl Nitrite Photolysis as an OH Radical Source. *J. Air Pollut. Control Assoc.* **1981**, *31* (10), 1090–1092.

(95) Altieri, K. E.; Seitzinger, S. P.; Carlton, A. G.; Turpin, B. J.; Klein, G. C.; Marshall, A. G. Oligomers Formed through In-Cloud Methylglyoxal Reactions: Chemical Composition, Properties, and Mechanisms Investigated by Ultra-High Resolution FT-ICR Mass Spectrometry. *Atmos. Environ.* **2008**, *42* (7), 1476–1490.

(96) Nozière, B.; Ekström, S.; Alsberg, T.; Holmström, S. Radical-Initiated Formation of Organosulfates and Surfactants in Atmospheric Aerosols. *Geophys. Res. Lett.* **2010**, *37* (5).

(97) Howell, H.; Fisher, G. S. The Dissociation Constants of Some of the Terpene Acids. *J. Am. Chem. Soc.* **1958**, *80* (23), 6316–6319.

(98) Witkowski, B.; Al-sharafi, M.; Gierczak, T. Ozonolysis of β-Caryophyllonic and Limononic Acids in the Aqueous Phase: Kinetics, Product Yield, and Mechanism. *Environ. Sci. Technol.* **2019**, *53* (15), 8823–8832.

(99) Chen, J.; Griffin, R. J. Modeling Secondary Organic Aerosol Formation from Oxidation of α-Pinene, β-Pinene, and d-Limonene. *Atmos. Environ.* **2005**, *39* (40), 7731–7744.

(100) Mutzel, A.; Poulain, L.; Berndt, T.; Iinuma, Y.; Rodigast, M.; Böge, O.; Richters, S.; Spindler, G.; Sipilä, M.; Jokinen, T.; Kulmala, M.; Herrmann, H. Highly Oxidized Multifunctional Organic Compounds Observed in Tropospheric Particles: A Field and Laboratory Study. *Environ. Sci. Technol.* **2015**, *49* (13), 7754–7761.

(101) Kristensen, K.; Watne, Å. K.; Hammes, J.; Lutz, A.; Petäjä, T.; Hallquist, M.; Bilde, M.; Glasius, M. High-Molecular Weight Dimer Esters Are Major Products in Aerosols from α-Pinene Ozonolysis and the Boreal Forest. *Environ. Sci. Technol. Lett.* **2016**, *3* (8), 280–285.

(102) Kristensen, K.; Enggrob, K. L.; King, S. M.; Worton, D. R.; Platt, S. M.; Mortensen, R.; Rosenoern, T.; Surratt, J. D.; Bilde, M.; Goldstein, A. H.; Glasius, M. Formation and Occurrence of

Dimer Esters of Pinene Oxidation Products in Atmospheric Aerosols. *Atmos. Chem. Phys.* **2013**, *13* (7), 3763–3776.

(103) Zawadowicz, M. A.; Lee, B. H.; Shrivastava, M.; Zelenyuk, A.; Zaveri, R. A.; Flynn, C.; Thornton, J. A.; Shilling, J. E. Photolysis Controls Atmospheric Budgets of Biogenic Secondary Organic Aerosol. *Environ. Sci. Technol.* **2020**, *54* (7), 3861–3870.

(104) Surratt, J. D.; Murphy, S. M.; Kroll, J. H.; Ng, N. L.; Hildebrandt, L.; Sorooshian, A.; Szmigielski, R.; Vermeylen, R.; Maenhaut, W.; Claeys, M.; Flagan, R. C.; Seinfeld, J. H. Chemical Composition of Secondary Organic Aerosol Formed from the Photooxidation of Isoprene. *J. Phys. Chem. A* **2006**, *110* (31), 9665–9690.

(105) Pruppacher, H. R.; Jaenicke, R. The Processing of Water Vapor and Aerosols by Atmospheric Clouds, a Global Estimate. *Atmos. Res.* **1995**, *38* (1–4), 283–295.

(106) Griffith, E. C.; Carpenter, B. K.; Shoemaker, R. K.; Vaida, V. Photochemistry of Aqueous Pyruvic Acid. *Proc. Natl. Acad. Sci. U. S. A.* **2013**, *110* (29), 11714–11719.

(107) Carlton, A. G.; Turpin, B. J.; Lim, H.-J.; Altieri, K. E.; Seitzinger, S. Link between Isoprene and Secondary Organic Aerosol (SOA): Pyruvic Acid Oxidation Yields Low Volatility Organic Acids in Clouds. *Geophys. Res. Lett.* **2006**, *33* (6).

(108) Arakaki, T.; Anastasio, C.; Kuroki, Y.; Nakajima, H.; Okada, K.; Kotani, Y.; Handa, D.; Azechi, S.; Kimura, T.; Tsuhako, A.; others. A General Scavenging Rate Constant for Reaction of Hydroxyl Radical with Organic Carbon in Atmospheric Waters. *Environ. Sci. Technol.* **2013**, *47* (15), 8196–8203.

(109) Hoffmann, T.; Bandur, R.; Marggraf, U.; Linscheid, M. Molecular Composition of Organic Aerosols Formed in the α-Pinene/O_3 Reaction: Implications for New Particle Formation Processes. *J. Geophys. Res. Atmos.* **1998**, *103* (D19), 25569–25578.

(110) Ma, Y.; Luciani, T.; Porter, R. A.; Russell, A. T.; Johnson, D.; Marston, G. Organic Acid Formation in the Gas-Phase Ozonolysis of α-Pinene. *Phys. Chem. Chem. Phys.* **2007**, *9* (37), 5084.

(111) Holloway, F.; Anderson, H. J.; Rodin, W. Ozonolysis of α-Pinene. *Ind. Eng. Chem.* **1955**, *47* (10), 2111–2113.

(112) Yu, J.; Cocker, D. R.; Griffin, R. J.; Flagan, R. C.; Seinfeld, J. H. Gas-Phase Ozone Oxidation of Monoterpenes: Gaseous and Particulate Products. *J. Atmos. Chem.* **1999**, *34* (2), 207–258.

(113) Larsen, Bo. R.; Di Bella, D.; Glasius, M.; Winterhalter, R.; Jensen, N. R.; Hjorth, J. Gas-Phase OH Oxidation of Monoterpenes: Gaseous and Particulate Products. *J. Atmos. Chem.* **2001**, *38* (3), 231–276.

(114) Christoffersen, T. S.; Hjorth, J.; Horie, O.; Jensen, N. R.; Kotzias, D.; Molander, L. L.; Neeb, P.; Ruppert, L.; Winterhalter, R.; Virkkula, A.; Wirtz, K.; Larsen, B. R. Cis-Pinic Acid, a Possible Precursor for Organic Aerosol Formation from Ozonolysis of α-Pinene. *Atmos. Environ.* **1998**, *32* (10), 1657–1661.

(115) Jenkin, M. E.; Shallcross, D. E.; Harvey, J. N. Development and Application of a Possible Mechanism for the Generation of Cis-Pinic Acid from the Ozonolysis of α- and β-Pinene. *Atmos. Environ.* **2000**, *34* (18), 2837–2850.

(116) Glasius, M.; Calogirou, A.; Jensen, N. R.; Hjorth, J.; Nielsen, C. J. Kinetic Study of Gas-Phase Reactions of Pinonaldehyde and Structurally Related Compounds. *Int. J. Chem. Kinet.* **1997**, *29* (7), 527–533.

(117) Müller, L.; Reinnig, M.-C.; Naumann, K. H.; Saathoff, H.; Mentel, T. F.; Donahue, N. M.; Hoffmann, T. Formation of 3-Methyl-1,2,3-Butanetricarboxylic Acid via Gas Phase Oxidation of Pinonic Acid – a Mass Spectrometric Study of SOA Aging. *Atmos. Chem. Phys.* **2012**, *12* (3), 1483–1496.

(118) Bilde, M.; Pandis, S. N. Evaporation Rates and Vapor Pressures of Individual Aerosol Species Formed in the Atmospheric Oxidation of α- and β-Pinene. *Environ. Sci. Technol.* **2001**, *35* (16), 3344–3349.

(119) Kołodziejczyk, A.; Pyrcz, P.; Pobudkowska, A.; Błaziak, K.; Szmigielski, R. Physicochemical Properties of Pinic, Pinonic, Norpinic, and Norpinonic Acids as Relevant α-Pinene Oxidation Products. *J. Phys. Chem. B* **2019**, *123* (39), 8261–8267.

(120) Xu, Y.; Miyazaki, Y.; Tachibana, E.; Sato, K.; Ramasamy, S.; Mochizuki, T.; Sadanaga, Y.; Nakashima, Y.; Sakamoto, Y.; Matsuda, K.; Kajii, Y. Aerosol Liquid Water Promotes the Formation of Water-Soluble Organic Nitrogen in Submicrometer Aerosols in a Suburban Forest. *Environ. Sci. Technol.* **2020**, *54* (3), 1406–1414.

(121) Wonaschuetz, A.; Haller, T.; Sommer, E.; Witek, L.; Grothe, H.; Hitzenberger, R. Collection of Soot Particles into Aqueous Suspension Using a Particle-into-Liquid Sampler. *Aerosol Sci. Technol.* **2019**, *53* (1), 21–28.

(122) Clark, C. H.; Nakao, S.; Asa-Awuku, A.; Sato, K.; David R. Cocker, I. Real-Time Study of Particle-Phase Products from α-Pinene Ozonolysis and Isoprene Photooxidation Using Particle into Liquid Sampling Directly Coupled to a Time-of-Flight Mass Spectrometer (PILS-ToF). *Aerosol Sci. Technol.* **2013**, *47* (12), 1374–1382.

(123) Sorooshian, A.; Brechtel, F. J.; Ma, Y.; Weber, R. J.; Corless, A.; Flagan, R. C.; Seinfeld, J. H. Modeling and Characterization of a Particle-into-Liquid Sampler (PILS). *Aerosol Sci. Technol.* **2006**, *40* (6), 396–409.

(124) Weber, R. J.; Orsini, D.; Daun, Y.; Lee, Y.-N.; Klotz, P. J.; Brechtel, F. A Particle-into-Liquid Collector for Rapid Measurement of Aerosol Bulk Chemical Composition. *Aerosol Sci. Technol.* **2001**, *35* (3), 718–727.

(125) Waser, J. *Quantitative Chemistry*; W.A. Benjamin.

(126) Demarque, D. P.; Crotti, A. E. M.; Vessecchi, R.; Lopes, J. L. C.; Lopes, N. P. Fragmentation Reactions Using Electrospray Ionization Mass Spectrometry: An Important Tool for the Structural

Elucidation and Characterization of Synthetic and Natural Products. *Nat. Prod. Rep.* **2016**, *33* (3), 432–455.

(127) Claeys, M.; Iinuma, Y.; Szmigielski, R.; Surratt, J. D.; Blockhuys, F.; Van Alsenoy, C.; Böge, O.; Sierau, B.; Gómez-González, Y.; Vermeylen, R.; Van der Veken, P.; Shahgholi, M.; Chan, A. W. H.; Herrmann, H.; Seinfeld, J. H.; Maenhaut, W. Terpenylic Acid and Related Compounds from the Oxidation of α-Pinene: Implications for New Particle Formation and Growth above Forests. *Environ. Sci. Technol.* **2009**, *43* (18), 6976–6982.

(128) Szmigielski, R.; Surratt, J. D.; Gómez-González, Y.; Veken, P. V. der; Kourtchev, I.; Vermeylen, R.; Blockhuys, F.; Jaoui, M.; Kleindienst, T. E.; Lewandowski, M.; Offenberg, J. H.; Edney, E. O.; Seinfeld, J. H.; Maenhaut, W.; Claeys, M. 3-Methyl-1,2,3-Butanetricarboxylic Acid: An Atmospheric Tracer for Terpene Secondary Organic Aerosol. *Geophys. Res. Lett.* **2007**, *34* (24).

(129) Sander, R. Compilation of Henry's Law Constants (Version 4.0) for Water as Solvent. *Atmos. Chem. Phys.* **2015**, *15* (8), 4399–4981.

(130) Orlando, J. J.; Tyndall, G. S. Laboratory Studies of Organic Peroxy Radical Chemistry: An Overview with Emphasis on Recent Issues of Atmospheric Significance. *Chem. Soc. Rev.* **2012**, *41* (19), 6294–6317.

(131) Buszewski, B.; Noga, S. Hydrophilic Interaction Liquid Chromatography (HILIC)—a Powerful Separation Technique. *Anal. Bioanal. Chem.* **2012**, *402* (1), 231–247.